

## *PhD Dissertation 02/2015*

Development and application of quantification and visualization techniques to investigate the uptake of nanoparticles by cells and ecotoxicological test organisms.

Steffi Böhme

Development and application of quantification and  
visualization techniques to investigate  
the uptake of nanoparticles  
by cells and ecotoxicological test organisms

Der Fakultät für Chemie und Mineralogie  
der Universität Leipzig

vorgelegte

DISSERTATION

zur Erlangung des akademischen Grades

DOCTOR RERUM NATURALIUM

(Dr. rer. nat.)

von

Diplom Lebensmittelchemikerin Steffi Böhme  
geboren am 30.12.1988 in Schkeuditz.

Leipzig, den 08.07.2015



Durchgeführt am Helmholtz-Zentrum für Umweltforschung (UFZ), Leipzig  
Department für Bioanalytische Ökotoxikologie

Gutachter:

Prof. Dr. Thorsten Reemtsma, Universität Leipzig

Prof. Dr. Rolf Altenburger, RWTH Aachen

Tag der Verteidigung: 20.11.2015



## SUMMARY

Engineered nanoparticles (NPs) are widely applied for several consumer products. As a consequence, these materials are released into the air, soil or the aquatic environment. Within the mentioned environmental compartments, NPs are transported and may accumulate within plants or animals. In order to evaluate the toxicological behavior of NPs different *in vitro* and *in vivo* test models can be applied. However, for the detection, quantification, and visualization of NP amounts internalized within cells and organisms analytical techniques have to be developed further to be applicable to NPs. The presented dissertation addresses the emerging challenges for analytical chemists in the field of nanoparticle analysis.

On the one hand, analytical techniques were developed and validated to investigate the accumulation behavior of NPs within cells and organisms. Therefore, ICP-MS-based methods, flow cytometry, and electron microscopy techniques for the quantification and visualization were developed and successfully applied. Especially, LA-ICP-MS as a semi-quantitative imaging technique was established and validated for the investigation of biological samples and an occurring particle size effect was described for the first time.

On the other hand, the impact of the biological test system as well as specific NP characteristics on the time- and concentration dependent NP uptake were investigated. Both, quantification and visualization tools were combined to gain insight into the complex interaction between NPs and biological structures. For organisms such as the zebrafish (*Danio rerio*) embryo (ZFE) and *Daphnia magna*, the NP distribution patterns varied according to the applied particle type. In experiments involving the ZFE, the chorion was identified as main accumulation structure dependent on the exposure time. In contrast, daphnids actively ingest particles and accumulate them in the gut.

As shown for Ag-NPs, a correlation between the obtained quantitative results and the observed biological effects can be performed. Furthermore, a novel method combination of LA-ICP-MS and SP-ICP-MS able to distinguish between the internalization of particles or ionic fractions is presented.



## ZUSAMMENFASSUNG

Technisch hergestellte Nanopartikel (NP) werden vielfältig in verschiedenen Verbraucherprodukten eingesetzt, wodurch diese Materialien in die Luft, den Boden oder Gewässer freigesetzt werden. In den genannten Umweltkompartimenten werden die NP transportiert und reichern sich möglicherweise in Pflanzen und Tieren an. Um das toxikologische Verhalten von NP zu beurteilen, können verschiedene *in vitro* und *in vivo* Testmodelle angewendet werden. Dennoch müssen analytische Methoden zur Detektion, Quantifizierung und Visualisierung der Aufnahmemengen von Nanopartikeln in Zellen und Organismen weiterentwickelt werden, um für die Analytik von NP geeignet zu sein. Die hier präsentierte Arbeit thematisiert die aufkommenden Herausforderungen für analytische Chemiker im Bereich der Nanopartikelanalytik.

Einerseits wurden analytische Techniken entwickelt und validiert, um das Akkumulationsverhalten von NP in Zellen und Umweltorganismen zu untersuchen. Dafür wurden Methoden basierend auf der ICP-MS, der Durchflusszytometrie und elektronenmikroskopischen Techniken für die Quantifizierung und Visualisierung entwickelt und erfolgreich angewendet. Insbesondere die LA-ICP-MS als semi-quantitative Visualisierungstechnik wurde für die Untersuchung biologischer Proben etabliert und validiert, sowie ein auftretender Partikelgrößeneffekt zum ersten Mal beschrieben.

Zum anderen wurde der Einfluss des biologischen Testsystems sowie der Einfluss spezifischer NP Eigenschaften auf die zeit- und konzentrationsabhängige Aufnahme von NP untersucht. Sowohl Quantifizierungs- als auch Visualisierungsmethoden wurden kombiniert, um Einblick in die komplexe Interaktion zwischen NP und biologischen Strukturen zu gewinnen. Für Organismen, wie den Zebrafisch (*Danio rerio*) Embryo (ZFE) und *Daphnia magna*, konnten unterschiedliche NP Verteilungsmuster in Abhängigkeit des verwendeten Partikeltyps beobachtet werden. Die ZFE Experimente zeigten, dass die Chorionstruktur die wichtigste Akkumulationsstruktur in Abhängigkeit der Expositionszeit darstellt. Im Gegensatz dazu können Daphnien aktiv Partikel aufnehmen und sie im Darm akkumulieren.

Eine Korrelation zwischen den ermittelten quantitativen Ergebnissen und den beobachteten biologischen Effekten konnte anhand von Ag-NP gezeigt werden. Außerdem wurde eine neue Methodenkombination von LA-ICP-MS und SP-ICP-MS präsentiert, welche in der Lage ist, die Aufnahme von partikulären und ionischen Fraktionen zu unterscheiden.

## TABLE OF CONTENTS

Summary		
Zusammenfassung		
Abbreviations		
List of Figures		
List of tables		
Chapter 1	General introduction	10
Chapter 2	Quantification of Al <sub>2</sub> O <sub>3</sub> nanoparticles in human cell lines applying inductively coupled plasma mass spectrometry (neb-ICP-MS, LA-ICP-MS) and flow cytometry based methods	46
Chapter 3	Exploring LA-ICP-MS as a quantitative imaging technique to study nanoparticle uptake in <i>Daphnia magna</i> and zebrafish ( <i>Danio rerio</i> ) embryos	78
Chapter 4	The chorion of the zebrafish ( <i>Danio rerio</i> ) embryo as a biological barrier for nanoparticle uptake?	104
Chapter 5	Effect propagation after exposure silver nanoparticle exposure in zebrafish ( <i>Danio rerio</i> ) embryos: A correlation to internal concentration and distribution patterns	140
Chapter 6	First qualitative results of a novel Laser Ablation and Single Particle ICP-MS (LA-SP-ICP-MS) method combination	168
Acknowledgement		182
Curriculum vitae		183
Scientific contributions		184
Eidesstattliche Erklärung		188



## ABBREVIATIONS

BET	Brunauer-Emmet-Teller Effect (Specific Surface Area)
Cit	Sodium Citrate
DLS	Dynamic Light Scattering
EDX	Energy-dispersive X-ray Spectroscopy
EM	Electron Microscopy
EU	European Union
EC <sub>50</sub>	Effect Concentration (50 % of the population affected)
FET	Fish Embryo Acute Toxicity Test
FFF	Field Flow Fractionation
IC <sub>50</sub>	Immobilization Concentration (50% of the population affected)
ICP-MS	Inductively Coupled Plasma - Mass Spectrometry
ISO	International Organization for Standardization
LA-ICP-MS	Laser Ablation – ICP-MS
LC <sub>50</sub>	Lethal concentration (50% of the population affected)
MALS	Multi-Angle Light Scattering
NM	Nanomaterial
NP	Nanoparticle
OECD	Organization for Economic Co-operation and Development
PEC	Predicted Environmental Concentration
PIXE	Particle-induced X-ray Emission
PVP	Polyvinyl Pyrrolidone
ROS	Reactive Oxygen Species
SEM	Scanning Electron Microscopy
SHMP	Sodium Hexametaphosphate
SOP	Standard Operating Procedure
SP-ICP-MS	Single Particle – ICP-MS
TEM	Transmission Electron Microscopy
TSP	Tetrasodium Pyrophosphate
TXRF	Total-reflection XRF
XRF	X-ray Fluorescence
ZFE	Zebrafish ( <i>Danio rerio</i> ) embryo

## LIST OF FIGURES

Fig. 1	Release possibilities of NPs from consumer products and their fate in the environment	12
Fig. 2	Principle considerations regarding the toxicological testing and exposure of NPs	14
Fig. 3	Microscopic pictures of the ZFE and <i>Daphnia magna</i> which are applied as ecotoxicological test organisms	17

## LIST OF TABLES

Tab. 1	Characteristics of investigated nanoparticle powders	31
Tab. 2	Chemical and physical properties of investigated nanoparticle suspensions	31
Tab. 3	NP toxicity on an organism level	32
Tab. 4	Toxicity of ionic substances on an organism level	32

## **Chapter 1**

### **GENERAL INTRODUCTION**



## **NANOPARTICLE DEFINITION AND APPLICATIONS**

Nanoparticle research is a rapid developing and growing field due to the numerous applications of engineered nanomaterials, e.g., as ingredients of cosmetics, food, packaging material, electronics, or in medicine (Lowry et al. 2010).

Since 2011, the EU defines nanomaterials (NM) as “(...) *a natural, incidental or manufactured material containing particles, in an unbound state or as an aggregate or as an agglomerate and where, for 50 % or more of the particles in the number size distribution, one or more external dimensions is in the size range 1 nm-100 nm.*” (Commission 2011).

This definition includes all classes of nanoparticles (NPs) such as carbonaceous materials (e.g. SWCNTs, MWCNTs, C<sub>60</sub>), metal and metal oxide particles (e.g. Au-NPs, TiO<sub>2</sub>), semi-conductor nanocrystals (e.g. quantum dots), zero-valent metals (e.g. zero-valent iron), or polymers (e.g. dendrimers) (Bhatt and Tripathi 2011). However, other NP characteristics such as the chemical composition, the particle charge or surface area which may affect the hazardous potential of NPs are not regarded by this definition. As a consequence, the demand towards a new classification or grouping of NPs exists in the research community (Lynch et al. 2014).

Since the 1980s, researchers are interested in the manipulation of materials at the atomic and molecular level to create NPs with new advantageous characteristics (Klaine et al. 2012). These specific chemical and physical properties of NPs lead to their various applications. A yearly production of 2 000 tons was estimated for 2004 and is expected to increase up to 58 000 tons until 2020 (Maynard 2006). The most widely used materials are metal oxide NPs such as ZnO-NPs in sunscreens or TiO<sub>2</sub>-NPs as pigment or cosmetic additive (Nowack and Bucheli 2007). In sunscreens, TiO<sub>2</sub> and ZnO-NPs are applied since they are transparent and effectively absorb UV light (Klaine et al. 2012). The extraordinary properties of carbon nanotubes such as high electrical conductivity, being stronger than steel and harder than diamond result in the application of these materials for the construction of electronic devices or aircrafts and cars (Kumar and Ando 2010). The carrier capability of NPs was successful employed in the development of new

selective drug-delivery systems, especially in the field of cancer diagnosis and therapies (Davis 2008; Baker 2009). Additionally, the high adsorption rates of contaminants to NPs can be used for environmental remediation of contaminated water and soil as shown by first field studies (Zhang 2003; Quinn et al. 2005).

The above mentioned EU definition requires adequate analytical methods to detect and quantify NPs within consumer products, biological tissues or within environmental samples. Available analytical methods are often established for the analysis of chemical substances with known properties. NPs can behave completely different due to their unique chemical and physical characteristics and thus an improvement of existing or the development of new analytical measurement tools is required (Marquis et al. 2009). Especially, techniques able to analyze the internalization, modification, and localization of NPs with high (elemental) sensitivity and down to a single particle resolution level are needed.

### **IMPACT OF NANOPARTICLES ON THE ENVIRONMENT**

Despite the commercial benefits, the extensive use of NPs may lead to release, transport and accumulation of particles from nano-products into the environment. For example, industrial production sites, landfills or wastewater treatment plants can be mentioned as point sources of unintentional NP release. An overview on the fate of NPs in the environment, especially with regard to a potential accumulation in the food chain is shown in **Figure 1** (Böhme et al. 2014). In general, the potential hazard of NPs to the environment is mainly dependent on their mobility and bioavailability (Nowack and Bucheli 2007).

In order to establish a realistic and reliable risk assessment for NPs, knowledge on their environmental concentrations is necessary. Until now, modelled values of released NP amounts are used and vary dependent on the type of material (Sun et al. 2014). For example, Ag-NP and TiO<sub>2</sub>-NP were reported as the NPs with the highest predicted environmental concentrations (PEC) of 0.66 and 0.53 ng/l for surface water in the EU, respectively (Sun et al. 2014). One reason for the absence of measured environmental concentrations is the modification of NPs by various chemical reactions with biomolecules, aggregation, or dissolution within

the environmental compartments (Lowry et al. 2012). Often complex samples containing NPs, agglomerates generated by abrasion or combustion, dissolved ionic fractions, complexes, and natural or bulk-derived materials have to be analyzed (Gottschalk et al. 2013). Up to now, the analytical measurement of real environmental NP concentrations is limited due to the above mentioned reactions and the complexity of the analysis.

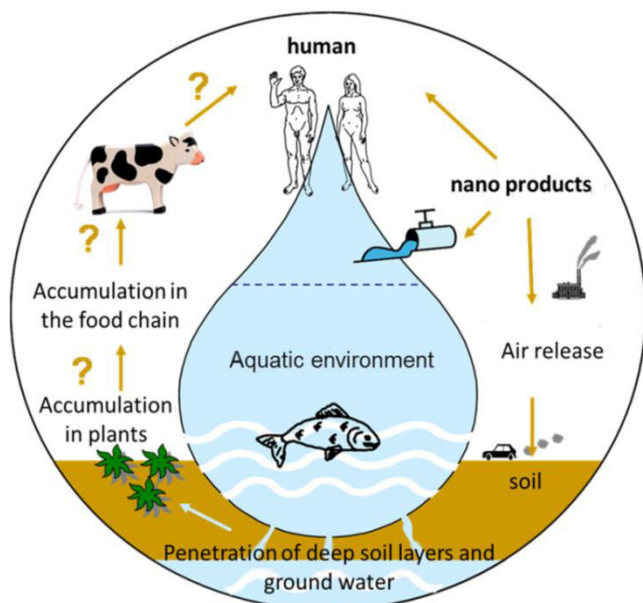


**Fig. 1:** Release possibilities of NPs from consumer products and their fate in the environment.

A few studies observed and detected NPs in different parts of the environment, e.g. in the effluents of waste water treatment plants, surface waters, water pipelines or bio-solids (Sanchis et al. 2011; Gondikas et al. 2014). For instance, Gondikas et al. (2014) measured increased  $\text{TiO}_2$ -NP amounts (potentially released by sunscreens) in the summer period in the suspended particulate matter of the Old Danube Lake using electron microscopy and ICP-MS-based techniques. Mitrano et al. (2012) applied SP-ICP-MS and detected and quantified Ag-NPs in effluents of wastewater treatment plants. Furthermore, Sanchis et al. (2011) detected a selection of fullerenes in the Mediterranean Sea atmosphere by LC-MS with median  $\text{C}_{60}$  and  $\text{C}_{70}$  concentrations of 0.06 and 0.48  $\text{ng/m}^3$ , respectively.

## NANOPARTICLE CHARACTERIZATION

Nanoparticles can be highly reactive with regard to their interaction with biological systems due to their small size, high surface area and the opportunity to modify their surface composition in a targeted manner (Hassellöv et al. 2008). For a detailed investigation on how NPs interact with the environment or with biological test systems, exact information on the chemical and physical properties of the NP under study are required. With knowledge on NP characteristics the stability, bioavailability and dissolution of NPs within biological media can be estimated and an adequate exposure design can be implemented (Hinderliter et al. 2010; Meißner et al. 2010). Different methods and protocols are established to characterize the chemical and physical properties of NPs. In general, one has to differentiate between the characterization of a particle powder, an aqueous particle suspension, or particles suspended in a relevant test media.

For particle powders, the morphology and primary particle size can be investigated by electron microscopic (EM) techniques, either scanning electron microscopy (SEM) or transmission electron microscopy (TEM) (Hassellöv et al. 2008). Therefore, a number of ~100-500 particles have to be measured and counted to ensure a statistical reliable result. The specific surface area of the individual NPs within the powder is usually obtained by gas adsorption measurements according to the Brunauer-Emmet-Teller (BET) method (Meißner et al. 2010).

Partly, the above mentioned techniques can be adopted for the particle characterization in suspension. The preparation of a NP suspension involves several dispersion methods, including energy input or use of stabilizing agents to ensure homogeneous and stable suspensions. Two principle considerations regarding the toxicological testing of NPs are possible: (1) the investigation of NP effects under environmentally relevant conditions, accepting potential agglomeration of NPs over time, or (2) the application of stabilized, mono-disperse NP suspensions, representing worst-case conditions (**Fig. 2**) (Kroll et al. 2013). For the biological testing of NPs in test media often the second option is chosen, assuming that stabilization is required to prevent the agglomeration and subsequently sedimentation of NPs. Therefore, the majority of NPs studied in this

thesis were stabilized or coated as listed in the results part (**Tab. 2**). However, an influence of the stabilizing substance on the outcome of the test needs to be excluded by choosing appropriate controls.

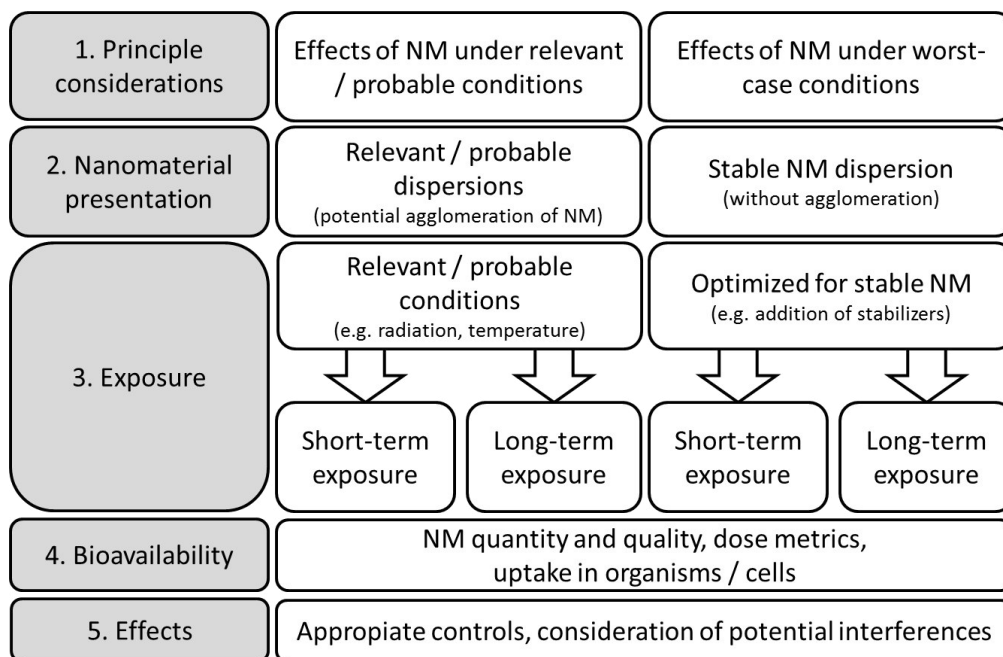


**Fig. 2:** Principle considerations regarding the toxicological testing and exposure of NPs.

Other important particle characteristics in suspension are e.g., the particle size distribution and the agglomeration behavior. Information on these parameters can be obtained by dynamic light scattering (DLS) (Hassellöv et al. 2008). In addition, DLS can be applied to determine the zeta potential of the NP suspensions. High absolute values of the zeta potential imply strong electrostatic repulsion forces, and indicate a stable particle suspension (Böhme et al. 2014).

Several NPs, such as Ag-, ZnO-, and CuO-NPs release ions over time. Hence the dissolved ionic fraction in the suspension or the test media has to be determined. The analytical determination of the dissolved ionic fraction, e.g., by ICP-MS requires a sufficient separation of the particular fraction beforehand by (ultra-)centrifugation, filtration or dialysis (Misra et al. 2012). The energy input during the particle suspension, the (fast) sedimentation and the complexation of NPs thin biological media are critical parameters of NP characterization. Other challenging tasks are the characterization of NPs composed of different substances/metals or particles of irregular shape.

## TOXICITY TESTING OF NANOPARTICLES

In order to investigate the toxicity and accumulation behavior of NPs under environmental relevant conditions, *in vivo* or *in vitro* test models are applied. For chemical substances validated standard operating procedures (SOPs) or guidelines for the biological testing are established by the Organization for Economic Co-operation and Development (OECD) or the International Organization for Standardization (ISO).

Using these guidelines for the testing of chemicals as basis, they can be applied for the toxicological assessment of NPs. However, adjustments have to be implemented with regard to NP specific effects such as adsorption, sedimentation or dissolution (Kühnel and Nickel 2014). Furthermore, additional quality assessment factors have to be considered e.g., the observation of the particle stability or the control of the exposure concentration at the beginning and the end of the exposure period. The handling of critical factors such as sedimentation of NPs by e.g., a stirring of the exposure system, the formation of a protein corona or other complexation reactions in exposure media are still under debate.

In order to estimate and compare the toxicity of individual chemical substances or NPs, dose-response curves are modelled and respective effect values are calculated. For cellular and organism test models often mortality or other specific endpoints (e.g. immobility for *Daphnia magna*) are used for effect correlations. Within this dissertation, the *in vitro* cell models (human lung epithelial cells (A549) and skin keratinocytes (HaCaT)) were applied as basis to establish the NP testing procedure and the analytical quantification methods. In a second step, more complex test organisms such as the zebrafish (*Danio rerio*) embryo (ZFE) and *Daphnia magna* were applied.

## TOXICITY OF NANOPARTICLES ON A CELLULAR LEVEL

For the toxicity testing on a cellular level both, immortalized or primary cell lines can be applied. However, the majority of studies on NPs used immortalized, continuously growing human cell lines (Lanone et al. 2009; Busch et al. 2011). As

endpoints metabolic changes or membrane integrity as parameters for viability were regarded and measured by fluorescence staining (Marquis et al. 2009). As reported by Monteiro-Riviere et al. (2009) interactions between NPs and the fluorescence markers can occur and thus the performance of more than one assay may be required for a reliable toxicity screening.

In order to determine the influence of the size or surface area of particles towards occurring biological effects or NP uptake amounts, different types of NPs should be investigated and compared as presented here in the exposure studies of chapter 2 to 4. Up to now, several studies tried to correlate the toxicity with particle specific properties such as particle size or surface area and often identified the mass concentration as not appropriate dose metric for NPs (Teeguarden et al. 2007; Bowman et al. 2012). Indeed, cellular transport processes are partly limited towards the mentioned particle parameters. For example, passive diffusion is possible for particles and ions which are smaller than 60 nm. In contrast, larger particles and particle agglomerates are internalized by various active phagocytotic or endocytotic mechanisms (Unfried et al. 2007). As a consequence, often a size-dependent interaction with smaller particles, as being more toxic, was reported (Pan et al. 2007). Furthermore, the chemical identity or a release of a dissolved ionic fraction from the particle surface plays an important role for cytotoxicity (Auffan et al. 2009; Kittler et al. 2010). The principle mechanisms underlying particle toxicity are still under investigation, but often refer to the formation of reactive oxygen species (ROS), damage of cell organelles, and a subsequent apoptosis reaction (Asharani et al. 2008; Hsin et al. 2008).

### TOXICITY ASSESSMENT ON ORGANISM LEVEL

The zebrafish embryo and *Daphnia magna* (**Fig. 3**) were applied as model organisms for the toxicological testing and accumulation studies of the work presented in chapter 3 to 5. Both organisms are established ecotoxicological test organisms representing the aquatic environment and the cultivation, handling, and exposure to chemicals are described in the respective OECD guideline 236 (OECD 2013) and 202 (OECD 2004). For both organism species a comprehensive

knowledge on the genome and organism behavior exists (Scholz et al. 2008) and they are easily to observe by light microscopy due to their transparency.

*Daphnia magna* is described as one of the most sensitive ecotoxicological test organism related to the testing of NPs (Kahru and Dubourguier 2010). According to the toxic potential of NPs the following classification can be applied: extremely toxic ( $EC_{50} < 0.1$  mg/l), very toxic ( $EC_{50}$ : 0.1-1 mg/l), toxic ( $EC_{50}$ : 1-10 mg/l), and harmful ( $EC_{50}$ : 10-100 mg/l) (Commission of the European Communities 1996).

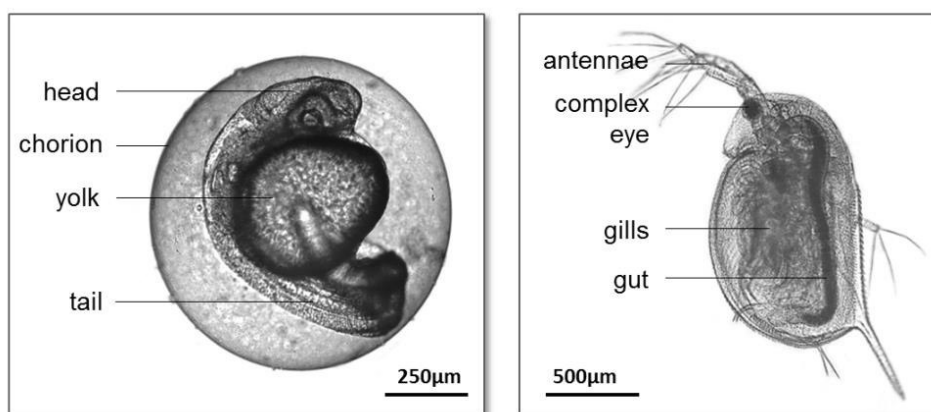


**Fig. 3:** Microscopic images of the ZFE and *Daphnia magna* which are applied as ecotoxicological test organisms

With respect to the toxicological effects of NPs to ecotoxicological organisms, an impact by toxic metal ions released from the particle surface was identified which can trigger toxic events (Misra et al. 2012; Wang and Wang 2014). Other particle specific (e.g. particle size or surface area) and environmental (e.g. pH, media composition) parameters were described as influencing factors on the toxicological outcome (Busch et al. 2011; Groh et al. 2015). However, the correlation of toxicological effects to internal NP concentrations would further improve the understanding of potential nano-specific organism interactions (Escher and Hermens 2004) and are missing for NPs.

## **ANALYTICAL METHODS FOR THE DETECTION, QUANTIFICATION, AND VISUALIZATION OF NANOPARTICLES WITHIN BIOLOGICAL SAMPLES**

Marginal experience on the detection and quantification of NPs in environmental samples (water, air, soil) as well as in consumer products (food, cosmetics) is available. In order to analyze the uptake and accumulation of NPs within these samples, a suitable sample preparation has to be developed and partial the combination of different analytical techniques is necessary (Fabricius et al. 2014). Furthermore, the general handling of NP containing samples can be critical due to adsorption of NPs to the walls of bottles or tubes connected to the analytical measurement (Hassellöv et al. 2008). With regard to environmental samples often low NP concentrations are expected and therefore (elemental) sensitive and selective analytical detection, quantification and visualization techniques are required. For the NP quantification, particle reference standards are needed which are only partly available, storable and payable up to now (Hassellöv et al. 2008). The choice of the here presented and discussed analytical techniques focus on the detection of metal or metal oxide composed NPs.

### **SAMPLE PREPARATION TECHNIQUES**

Dependent on the aim to measure total uptake amounts, to visualize the internalization and distribution, or to distinguish between particular and ionic fractions, different sample preparation techniques have to be applied.

For the measurement of whole uptake amounts, samples are often digested via an acid or enzymatic digestion to obtain a homogeneous solution. Nevertheless adjustments dependent on the type of NP have to be performed. For example, Ag-NPs are easily to digest under addition of nitric acid in an open digestion system. In contrast, metal oxide NPs such as Al<sub>2</sub>O<sub>3</sub>- or TiO<sub>2</sub> need an acid- or microwave-assisted digestion under high temperature and pressure to ensure the complete transfer of analytes into solution (Fabricius et al. 2014). After digestion the samples can be directly used for analysis or have to be diluted. The digestion of

the sample totally destroys the present NPs and therefore a distinction between particles or ions is no longer possible.

For the visualization of NPs within biological matrices such as cell layers or organisms, complex preparation techniques are necessary to ensure the complete detection and intactness of NPs. Therefore, cells or organisms treated with NPs are fixated to preserve the biological tissue and to avoid tissue destruction. Afterwards the samples can be embedded in paraffin or a cryo-section medium for the subsequent sectioning at room temperature or freezing temperatures around -20 °C, respectively (Böhme et al. 2015). With these techniques thin cell layers or organism sections can be produced for further analysis. However, the preparation of sections is time-consuming and several washing steps may lead to losses of NPs. Another method is the modification of NPs, e.g. by a fluorescent or radio-labelling or the specific synthesis of these kinds of NPs (Bertorelle et al. 2006; Gibson et al. 2011). However, it is unclear how these modifications influence the internalization process and if still mechanisms of particles under environmental relevant conditions are investigated. ZnO-NPs and Cd/Se-Quantum Dots often have an auto-fluorescence (Lin et al. 2003).

In order to analyze the respective NP fraction within an environmental sample, the particle fraction has to be separated and isolated prior to the analysis preferably without NP modification or destruction. The separation of NPs in environmental samples can be limited due to the presence of natural existing particles or the complexation of NPs with natural organic matter or other complexing agents (Hassellöv et al. 2008). The fractionation of liquid samples in different particle size classes can be performed by filtration, size exclusion chromatography, or field flow fractionation (FFF). Microfiltration (pore size  $>0.1 \mu\text{m}$ ) can be applied to isolate NPs from larger soil particles and other sample components and works also for larger volumes. In order to perform multi stage filtrations for crude size separations the filtration with membranes of various pore sizes is needed. Dependent on the membrane pore size and the type of NPs, interactions of the NPs of interest and the membrane material can occur such as collision, aggregation, or electrostatic interaction leading to the scavenging of NPs and a subsequent loss of NPs or change of NP size distribution (Hassellöv et al. 2008). By size exclusion

chromatography NPs can be fractionated by the application of a column with a porous packing material of the expected size distribution range. In contrast, FFF is a size-fractionating method working without a stationary phase (Hassellöv et al. 2008). The separation is based on the interaction of the cross flow build by an external field and the diffusion (Brownian motion) of the NPs. This interaction leads to a size-dependent NP separation with shorter retention times for smaller particles (Mitrano et al. 2012). FFF is an emerging NP fractionation technique with an effective separation range for particles of 1 - 1 000 nm and is often coupled to UV-, DLS-, MALS-detectors or an ICP-MS for an element sensitive analysis of mass concentrations.

### DETECTION OF NANOPARTICLES WITHIN BIOLOGICAL SAMPLES

There are different methods established to qualitatively detect NPs within biological samples such as cells or environmental organisms. In order to detect and analyze the particle internalization and distribution on a cellular level especially electron microscopic techniques (SEM, TEM) are applied (Busch et al. 2011; Heinlaan et al. 2011). These techniques allow a spatial resolution down to 1 nm (single particle detection) and in combination with energy-dispersive X-ray spectroscopy (EDX) information on the elemental composition can be obtained. The elemental detection limits by EDX are in the low percentage range related to the total sample amounts whereby higher sensitivities are obtained for heavier elements. However the general uncertainty of EDX measurements is ~20 % and therefore the technique is convenient for qualitative analysis (Hassellöv et al. 2008). In general, for biological samples a specific sample preparation is necessary due to the high vacuum working conditions which require low water contents of the samples. Furthermore, biological tissues are characterized by their poor conductivity. Therefore the sample has to be sputtered by a conductive metal target prior to EM analysis or the electron microscope has to be equipped with a nitrogen charge-compensator to avoid an electrostatic charging of the sample.

Another qualitative technique to investigate the NP uptake by cells and small organisms (algae) is flow cytometry. This method is based on the separation of single cells and the detection of scattered and fluorescent light signals after passage through the sample. The measured intensities of the forward scatter and the side scatter provide information on the size and the granularity of the investigated cells, respectively (Zucker et al. 2010). By the incorporation of NPs the granularity of the cell changes and can be measured for each individual cell by the change in side scatter signal (Busch et al. 2011). The method allows a rapid analysis of a high number of samples and is widely applied in medical quality control and research.

### ANALYTICAL METHODS TO QUANTIFY THE UPTAKE OF NANOPARTICLES

Different analytical techniques can be applied to detect and quantify the NP accumulation in biological and environmental samples. The methods discussed in the following are techniques which are largely applied and accessible.

X-ray based techniques such as X-ray fluorescence (XRF), total-reflection XRF (TXRF), synchrotron radiation methods, and particle-induced X-ray emission (PIXE) are characterized by their high sensitivity and low influence of matrix effects. However, the quantification by the addition internal standards or using fundamental physical parameters in combination with experimentally values can be difficult, the measurements can be expensive, and the sample throughput is low (Brown and Milton 2005). Therefore, X-ray methods are preferably applied for comparison and validation reasons.

An element specific and very sensitive technique is Inductively-Coupled Plasma Mass Spectrometry (ICP-MS) which is widely applied in routine analytical chemistry and which was already used for the detection and quantification of metal-based NPs (Au et al. 2009; Auffan et al. 2014; McTeer et al. 2014). As mass detectors, quadrupole-based or double-focusing sector field instruments are used. In order to reduce isobaric interferences, collision or reaction cells can be applied (Becker 2005). The samples have to be digested prior to the analytical

measurement and an external calibration is needed. The excitation source of ICP-MS instruments works under atmospheric working conditions what allows the combination with other fractionation and chromatographic techniques.

For example, the combination of an FFF with an ICP-MS, especially the analysis with SP-ICP-MS, enables a detection of single particle events to determine particle size distributions (Mitrano et al. 2012). This facilitates the differentiation between particular and ionic form within one sample and was firstly applied for colloids (Degueldre and Favarger 2003). For SP-ICP-MS measurements, an accurate and sufficient sample dilution down to a ppt-concentration range (corresponds to ~1 000 particles/ml) and knowledge on the NP density and shape are required. Currently, it is only possible to measure NPs composed of single elements or metal oxide NPs and therefore the identification of unknown NPs in a sample is difficult. The element intensities are measured in a time-resolved mode with low dwell times (10 - 20 ms) to ensure to distinguish single particle events from the background noise signal (Mitrano et al. 2012). The difference between NP specific intensities and the background signal represents the NP size and restricts the lower size detection limit (~15 nm for Au-NPs) (Lee et al. 2014). Therefore, the lower size detection limit is dependent on the instrument sensitivity, and the isotopic abundance and mass interferences of the respective element.

With the calculation of the particle size distribution and the measurement of quantitative sample concentrations, SP-ICP-MS is one of the promising techniques to adequately detect NPs within various sample matrices as claimed by the EU-definition. Recently, instrument developments in the direction of a multi-element detection were presented (Borovinskaya et al. 2013). However, improvements with regard to the development of suitable particle standards of known size, mass and number concentration for calibration and developments towards an adequate sample preparation for complex matrices such as sewage sludge are needed (Fabricius et al. 2014).

### VISUALIZATION TECHNIQUES FOR THE IMAGING OF NP INTERNALIZATION AND DISTRIBUTION

For a sensitive and selective imaging of NPs with low detection limits, often fluorescence microscopy is applied, especially in medicine and pharmacology (Salata 2004). However, the optical constants of the fluorescent NPs have to be known and the influence of the absorption by the surrounding matrix needs to be determined, limiting the general suitability of this method (Hassellöv et al. 2008). Furthermore, a real elemental based quantification is not possible.

The combination of electron microscopy with an EDX detector can be applied for elemental imaging whereby high spatial resolution can be achieved. Nevertheless, this technique is not sensitive enough to detect ions. In contrast, micro-PIXE can be applied as imaging technique with high sensitivity and high lateral resolution as shown by Tkalec et al. (2011).

Recently, ICP-MS-based methods were further developed to visualize the NP uptake on a cellular level with a spatial resolution down to 1  $\mu\text{m}$  by LA-ICP-MS (Drescher et al. 2012). The combination of ICP-MS with a laser was firstly introduced for the quantitative elemental analysis of solid samples such as rocks or archeological samples (Russo et al. 2002). During the last years the application towards the measurement of biological tissues as matrices increased (Böhme et al. 2015). The main advantage of LA-ICP-MS is a reduced risk of contamination due to a simple sample preparation. However, the calibration via matrix-matched or glass standards and the control of sample aliquots is difficult, leading to semi-quantitative results (Brown and Milton 2005). Furthermore, software tools to evaluate the collected data are not included in commercial ICP-MS software packages and therefore individual evaluation tools have to be developed.

In order to visualize the distribution of both, NPs and metal ions the combination of different methods is necessary until now. For example, SEM+EDX allows the detection of single particles, whereby LA-ICP-MS destroys the sample and measures the whole elemental concentrations. Future developments have to focus on techniques able to visualize, quantify and distinguish NP and ionic fractions in parallel.

## **ACCUMULATION ASSESSMENT OF NANOPARTICLES**

Especially the application of environmentally relevant, non-toxic NP concentrations should be strengthened here. These concentrations avoid the occurrence of non-specific accumulation effects related to an overload of the biological system with NPs. In addition, secondary, mechanical effects, e.g., the attachment of NPs at the cell or organism surface and a subsequent penetration are reduced (Ma and Lin 2013). Even if NPs found to be non-toxic, the internalization and distribution patterns can be of interest to obtain information on general biological mechanisms. Furthermore, the quantification of NP amounts within organisms and cells is necessary to understand toxico-kinetic mechanisms, since other interactions and conditions compared to chemicals occur for NPs (Praetorius et al. 2014).

## **INTERNALIZATION OF NANOPARTICLES BY HUMAN CELL LINES**

In order to investigate the particle uptake, distribution and elimination processes within cells, different visualization procedures such as fluorescence staining or an imaging by the application of analytical techniques can be performed. Furthermore, the quantification of uptake amounts is crucial to investigate the influence of different NP characteristics on the uptake processes.

Most accumulation studies describe a time and concentration-dependent particle internalization, independent of the examined type of nanomaterial (Chithrani et al. 2006; Zucker et al. 2010). In addition, an impact of the nanoparticle size was reported several times (Jiang et al. 2008; Powers et al. 2011). Jiang et al. (2008) showed that NPs with an approximate diameter of 50 nm seem to be taken up to a higher extent than other sizes due to preferential endocytosis. So far, the majority of studies identified no particle uptake by the cell nucleus (Bastian et al. 2009). In contrast, NPs were detected freely in the cytoplasm, in lysosomes and other cell organelles (Simon-Deckers et al. 2008). In this context, the formation of bigger agglomerates (Limbach et al. 2005) and perinuclear rings was observed (Zucker et al. 2010; Busch et al. 2011).

The NP uptake itself cannot only be attributed to the internalized mass. Especially, a correlation to particle specific characteristics such as particle size, shape, or surface area is useful (Limbach et al. 2005). With regard to the EU definition on nanomaterials, the expression of particle numbers is preferred.

### ACCUMULATION OF NANOPARTICLES WITHIN ECOTOXICOLOGICAL ORGANISMS

The internalization of NPs by ecotoxicological organisms is certainly based on the mechanisms described for the NP uptake on a cellular level. As a consequence, the developed and established quantification methods to determine the NP uptake by cells were taken as a basis and were applied for the analysis of organisms. However, dependent on the organism species, specific interactions between NPs and biological structures of invertebrates and fish can occur (Ma and Lin 2013). These nano-bio interactions mainly refer to the adsorption of NPs to outer and inner interfaces of the organism. For example, the adsorption of NPs at the exoskeleton or the setae of daphnids as well as the penetration of inner organs by the accumulation and transport of NPs through the gut were described (MA and Lin 2013).

The presented results in the following chapters focus on the uptake and distribution of NPs by two environmental organisms: the zebrafish embryo (ZFE) and *Daphnia magna*. Both organism species differ in their way of particle internalization and distribution. For example, the ZFE is surrounded by the chorion, a porous membrane, during the first 2-3 days of its development (Kimmel et al. 1995). The chorion can act as additional accumulation point for NPs or even as a biological barrier for several NPs (Fent et al. 2010; Lin et al. 2011). In contrast, *Daphnia magna*, as a filter-feeding organism can actively take up food and particles (Baun et al. 2008). The main accumulation of NPs was reported for the gut of these organisms as mentioned above (Rosenkranz et al. 2009). Especially the modification and fate of NPs once being internalized by the organisms is poorly understood and investigated until today.

## **OUTLINE OF THIS DISSERTATION**

The specific aim of this dissertation was the development, improvement, and application of analytical methods to quantify and visualize the accumulation of nanoparticles by cells and organisms. The results of this study were obtained within the framework of the EU-project NanoValid (Development of reference methods for hazard identification, risk assessment and LCA of engineered nanomaterials; grant no 263147). Different research questions are addressed by the manuscripts included in this thesis.

The main research questions of the thesis are the following:

1. Is the internalization of nanoparticles by human cells dependent on specific NP characteristics (e.g. particle size, surface area)?
2. What analytical techniques can be applied to investigate nanoparticle uptake and can comparable results be achieved with these techniques?
3. Is there an analytical technique which is able to quantify and visualize the accumulation of particles in parallel?
4. In which way is the particle accumulation and distribution within organisms dependent on the exposure time (kinetics), biological species or on particle characteristics?
5. What improvements in the exposure assessment and the measurement of the uptake of nanoparticles can be performed in future?

## LIST OF PUBLICATIONS AND AUTHORS CONTRIBUTION

### Chapter 2:

*Böhme S., Stärk H.-J., Meißner T., Springer A., Reemtsma T., Kühnel D., Busch W. (2014). Quantification of Al<sub>2</sub>O<sub>3</sub> nanoparticles in human cell lines applying inductively coupled plasma mass spectrometry (neb-ICP-MS, LA-ICP-MS) and flow cytometry-based methods. Journal of Nanoparticle Research 16(9): 2592.*

I am the first author of this publication. I performed the exposure and toxicity studies on the human cells, developed the calibration strategy for the flow cytometry and LA-ICP-MS measurements and achieved the uptake concentrations. Furthermore I was involved in the discussion and wrote the manuscript. The investigated particles were characterized by the IKTS in Dresden. In addition, the electron microscopy studies were performed by Armin Springer. The first experiments and the idea of the manuscript were implemented by Wibke Busch.

### Chapter 3:

*Böhme S., Stärk H.-J., Kühnel D., Reemtsma T. Exploring LA-ICP-MS as a quantitative imaging technique to study nanoparticle uptake in Daphnia magna and zebrafish (Danio rerio) embryos. Analytical Bioanalytical Chemistry 407(18): 5477-5485.*

I am the first author of this publication. I had the idea for the manuscript content, planned the experiments and wrote the manuscript. I performed the exposure experiments, analytical measurements, data evaluation, and developed the calibration strategy for the LA-ICP-MS method. The investigated particles were characterized by the IKTS in Dresden and NanoValid project partners. The discussion and structure of the manuscript was developed by the help of the co-authors.

### Chapter 4:

*Böhme S., Baccaro M., Schmidt M., Potthoff A., Stärk H.-J., Reemtsma T., Kühnel D. The chorion of the zebrafish (Danio rerio) embryo as a biological barrier for nanoparticle uptake?! Nanotoxicology (Submitted)*

I am the first author of this publication. I had the idea for the manuscript content, planned the experiments and wrote the manuscript. I performed parts of the exposure and measurements. The majority of experiments was performed by Marta Baccaro within her Master thesis. Furthermore, I proposed the sorption model and did all the calculations on the coverage, particle accumulation, and LA-ICP-MS evaluation. The investigated particles were characterized by the IKTS in Dresden and by other project partners of the EU project NanoValid. The discussion and structure of the manuscript was developed by the help of the co-authors.

Chapter 5:

*Böhme S., Stärk H.-J., Kühnel D. Occurrence of toxic effects by AgNP exposure of zebrafish (Danio rerio) embryo: a correlation to internal dose and distribution patterns. Environmental Science: Nano (Accepted)*

I am the first author of this publication. I had the idea for the manuscript content, planned the experiments and wrote the manuscript. I performed the exposure experiments, analytical measurements, and data evaluation. The investigated particles were characterized by the IKTS in Dresden and by other project partners of the EU project NanoValid. The discussion and structure of the manuscript was developed by the help of the co-authors.

Chapter 6:

*Böhme S., Stärk H.-J., Reemtsma T. Combination of LA-ICPMS and SP-ICPMS (LA-SP-ICPMS) as new analytical tool for NP-analysis of environmental samples. In preparation*

This manuscript is in preparation and experiments are still ongoing. Hans-Joachim Stärk and me are equal authors of this publication. Together we had the idea for the manuscript content and the combination of both methods. I performed the exposure experiments and wrote the first version of the manuscript. The ICP-MS measurements were mainly performed by Hans-Joachim Stärk. The investigated particles were characterized by the IKTS in Dresden and by other project partners of the EU project NanoValid. The presented version of this manuscript was partly edited by the authors.

Furthermore, I contributed to the following publications and manuscripts (not covered in this thesis):

Jemec A., Kühnel D., Potthoff A., Heinlaan M., Böhme S., Drobne D., Geppert M., Novak S., Schirmer K., Rohit R., Singh S., Aruoja V., Sihtmäe M., Juganson K., Käkinen A., Kahru A. Silver nanoparticles hazard study using multitrophic ecotoxicological test battery and characterisation of nanosilver: a FP7 Nanovalid interlaboratory exercise. Environmental International (accepted)

Böhme S., Stärk H.-J., Reemtsma T. Visualisierung der Aufnahme von Nanopartikeln in Umweltorganismen. GDCh Wochenschau 2014, Beitrag Woche 42, released: 02.11.2014

*<http://www.aktuelle-wochenschau.de/main-navi/archiv/wasserchemie-2014/kw42-visualisierung-der-aufnahme-von-nanopartikeln-in-umweltorganismen.html>*

Kühnel D., Böhme S., Stärk H.-J. Technische Nanomaterialien in der Umwelt – Analytischer Nachweis und mögliche Auswirkungen auf Organismen. Analytik News, Fachartikel, released: 03.07.2014

*<http://www.analytik-news.de/Fachartikel/Volltext/ufz3.pdf>*

Böhme S., Kühnel D. Environmental mixture toxicity of nanomaterials and chemicals: Is the trojan-horse a general occurring phenomenon? In preparation

## RESULTS

The presented dissertation addresses the emerging challenges for analytical chemists in the field of nanoparticle analysis. The specific aims were to develop, improve, and apply analytical methods to quantify and visualize the accumulation of NPs by cells and environmental test organisms. In the following, the results obtained within the individual studies are summarized.

On the one hand, established techniques were improved, validated, and further developed towards sensitive element detection techniques. Both, quantification and visualization tools were developed and combined to get overall information on the interaction between NPs and biological structures.

On the other hand, knowledge on the potential toxicity of the NPs of interest was obtained and an adequate exposure design for the accumulation assessment by cells and environmental organisms was developed. One focus was to determine the influence of specific NP or species characteristics on the NP uptake, distribution, and accumulation processes. Therefore, NPs of different sizes, surface charges, with different surface areas and chemical compositions as well as various biological species including human cell lines, the zebrafish embryo and *Daphnia magna* were investigated.

Furthermore, the suitability of the applied biological test systems were discussed and appropriate recommendations on the exposure design and analytical measurements are given in the following. The gained data on biological effects and internal NP concentrations were combined and a sorption and a correlation scheme were proposed within the chapter 4 and 5. With these information internal effect concentrations triggering biological responses can be obtained.

## CHARACTERIZATION OF NANOPARTICLE POWDERS AND SUSPENSIONS

The three  $\text{Al}_2\text{O}_3$  particles were purchased as powders from different manufacturers. They are named as Alu1 (AEROXIDE® Alu C), Alu2 (TAIMICRON®, TM-DAR) and Alu3 (NABALOX®, NO-625-10) and characterized

by the Fraunhofer Institute for Ceramic Technologies and Systems - IKTS (Dresden). The Ag-NP and Au-NP were provided as suspensions and the CuO-NPs and ZnO-NPs were delivered as powders by partners of the EU-project NanoValid. All nanomaterials were detailedly characterized by the project partners (**Tab. 1** and **2**).

For the Al<sub>2</sub>O<sub>3</sub> stock suspensions sodium hexametaphosphate (SHMP, 0.05 % (w/v)) is used as stabilizing agent. For the provided Ag-NP and Au-NP suspensions, polyvinylpyrrolidone (PVP) and sodium citrate (Cit) were used as coatings, respectively. The CuO-NPs were stabilized by the addition of tetrasodium pyrophosphate (TSPP, 0.1 % (w/v)). As for the ZnO-NPs no suitable stabilizer was found an alternative approach was chosen: a stock suspension of 10 g/l was sonicated and abandoned to sediment for 24 h. The ZnO-NP supernatant was taken as nanoscale fraction for the following characterization and biological experiments. The dissolved ionic fraction within the particle suspensions was measured after centrifugation by ICP-MS.

**Tab. 1:** Characteristics of investigated nanomaterial powders.

Nanomaterial	Crystal structure	BET (m <sup>2</sup> /g)	X <sub>BET</sub> (nm)	Polydispersity index	ρ (g/cm <sup>3</sup> )
Alu1	γ-Al <sub>2</sub> O <sub>3</sub> ; δ-Al <sub>2</sub> O <sub>3</sub>	117	14	0.19	3.3
Alu2	α-Al <sub>2</sub> O <sub>3</sub>	13.5	111	0.10	4.0
Alu3	α-Al <sub>2</sub> O <sub>3</sub>	2	750	-	4.0
CuO-NP	-	28	-	-	-
ZnO-NP	-	60	-	-	-

**Tab. 2:** Chemical and physical properties of investigated nanomaterial suspensions.

Nanomaterial	X <sub>TEM</sub> (nm)	X <sub>DLS</sub> (nm)	Zetapotential (mV)	Stabilizing agent	Coating	Dissolved fraction
Alu1	-	127	-58	SHMP	-	-
Alu2	-	186	-64	SHMP	-	-
Alu3	-	2500	-83	SHMP	-	-
Ag-NP	21 ± 8	117 ± 24	-19	-	PVP	48.3 ± 7.2
Au-NP	13 ± 1	18 ± 2	-38	-	Cit	-
CuO-NP	22-25	132 ± 2	-64	TSPP	-	9.8 ± 5.5
ZnO-NP	10-15	80 ± 1	+34	-	-	58.1 ± 2.6

## TOXICITY ASSESSMENT

The three different sized Al<sub>2</sub>O<sub>3</sub>-particles were used for toxicity and uptake studies on the cellular level and were found to be non-toxic (**chapter 2**).

In order to investigate the toxic potential of NPs on an organism level, two ecotoxicological test organisms, namely the zebrafish embryo and *Daphnia magna* were applied. The EC<sub>50</sub>-values were calculated for a 24 h exposure with NPs or the respective metal salts (**Tab. 3** and **4**).

**Tab. 3:** Results of the NP toxicity tests. Results are shown as EC<sub>50</sub>-values (LC<sub>50</sub> for *Danio rerio* and IC<sub>50</sub> for *Daphnia magna*) (n≥3).

Nanomaterial	<i>Danio rerio</i> (µg element/l)	<i>Daphnia magna</i> (µg element/l)
Al <sub>2</sub> O <sub>3</sub> -NP (Alu1/2/3)	non-toxic	non-toxic
Ag-NP	39.5	3.4
Au-NP	non-toxic	non-toxic
ZnO-NP	non-toxic	6 800
CuO-NP	non-toxic	69.8

**Tab. 4:** Results of the toxicity testing of the respective metal salts. Results are shown as EC<sub>50</sub>-values (LC<sub>50</sub> for *Danio rerio* and IC<sub>50</sub> for *Daphnia magna*) (n≥3).

Substance	<i>Danio rerio</i> (µg element/l)	<i>Daphnia magna</i> (µg element/l)
AgNO <sub>3</sub>	36.1	2.2
ZnSO <sub>4</sub> *7H <sub>2</sub> O	non-toxic	11 900
CuSO <sub>4</sub> *5H <sub>2</sub> O	non-toxic	96.4

## INTERNALIZATION OF NANOPARTICLES BY HUMAN CELLS

In **chapter 2** the internalization of nanoparticles by human culture cells (lung epithelial cells (A549) and skin keratinocytes (HaCaT)) was investigated. One question of this study was to determine the dependency of NP uptake on specific NP characteristics (e.g. particle size, surface area). Therefore, Al<sub>2</sub>O<sub>3</sub> particles of three different sizes (14, 111, 750 nm) and surface areas (117, 14, 2 m<sup>2</sup>/g) were applied. The particles were found to be non-toxic and the internalization by human

cells was verified with the help of electron microscopic techniques coupled to an energy-dispersive X-ray detector. For both, A549 and HaCaT cells, a concentration- and particle size-dependent uptake of  $\text{Al}_2\text{O}_3$  particles was observed, independent of the cell line. The results indicated that with decreasing particle diameter, a higher number of particles interacted with the cells and were internalized. The same is true regarding the particle surface area (**Fig. 1c**). However, related to the internalized aluminum amounts, higher concentrations were measured for cells exposed to larger particles in comparison to treatments with smaller particle sizes.

### APPLICATION AND COMPARISON OF ANALYTICAL TECHNIQUES TO QUANTIFY AND VISUALIZE NANOPARTICLE UPTAKE

Several studies applied standard metal quantification methods such as nebulization ICP-MS (neb-ICP-MS) after acid digestion of the sample to determine the NP internal concentrations within biological tissues. In order to improve existing or to develop new analytical methods, the comparison of obtained results with such standard methods is always necessary.

Both, flow cytometry and Laser Ablation ICP-MS (LA-ICP-MS) were improved and established as quantification methods for the investigation of the  $\text{Al}_2\text{O}_3$  particle uptake by cells in **chapter 2**. Since the two latter mentioned techniques were not used for quantification purposes before, calibration strategies were developed and the methods were established for the cellular test system. The obtained results were comparable to the concentration values measured by neb-ICP-MS after the digestion of cells. The same NP uptake in a concentration range of 2-8  $\mu\text{g Al}_2\text{O}_3/\text{cm}^2$  cell layer was determined by all of the above mentioned techniques, highlighting the suitability of the established methods for the quantification of NPs.

The advantages and disadvantages of the techniques regarding LOD, sample preparation, particle specific effects or data evaluation were discussed in this study. For example, LA-ICP-MS is a technique with a quick and easy sample preparation. Solid samples such as thin organic layers (e.g., a cell layer or

organism section) can be directly introduced to the system. In addition, LA-ICP-MS can be applied as imaging method as discussed later. Method disadvantages refer to the necessity of an external matrix-matched calibration and the complex data evaluation since no routine software is available. In contrast, flow cytometry analyzes the signal corresponding to single cell events and measures the signal difference occurring due to a change in the granularity of the cell, e.g., by the internalization of NPs. The method works on a single cell basis, with a high sample throughput and an established evaluation software. The irregular shape of cells, the detection limits regarding particle size and shape, and the optical properties of the scattering object (e.g., refractive index) are the critical points for the detection of NPs within cells using flow cytometry.

LA-ICP-MS was additionally used as a visualization technique for the investigation of the elemental (NP or ionic) distribution patterns within organisms in **chapter 3**. Furthermore, the LA-ICP-MS setup for the visualization of NPs was improved towards a quantification method and a data evaluation software was developed as part of this dissertation. For these experiments, the uptake of different NPs (Ag-, Au-, and Al<sub>2</sub>O<sub>3</sub>-NPs) by two ecotoxicological test organisms (*Danio rerio* and *Daphnia magna*) were studied. The investigations revealed a particle size effect leading to an intensity signal depression for particles >150 nm which was described for the first time by this study. In order to compensate for these effects, a matrix-matched calibration approach with NP-spiked agarose gels was developed and applied for the quantification. The quantitative LA-ICP-MS results from the visualization were compared to uptake concentrations obtained with neb-ICP-MS after digestion of whole organisms. Dependent on the applied organism, good recoveries were determined for zebrafish (*Danio rerio*) embryos (ZFE) and low recoveries for *Daphnia magna*. These recovery differences are a consequence of the different NP internalization mechanisms of the organisms, as *Daphnia magna* actively ingest particles. By the ingestion, the NPs may agglomerate and drop out of the detection limits related to the particle size.

## INFLUENCE OF THE BIOLOGICAL TEST SYSTEM OR NANOPARTICLE CHARACTERISTICS ON THE PARTICLE ACCUMULATION

As mentioned in **chapter 2**, the internalization and distribution of NPs within cells and environmental organisms was observed to be dependent on the biological processes but also on the NP specific characteristics. For NP-exposed cells a concentration- and particle size-dependent uptake of NPs was observed, independent of the cell type. In accordance to previous studies, higher internalized amounts of larger or middle-sized (~ 50 nm) particles were measured in comparison to the uptake of smaller NPs (Chithrani et al. 2006; Limbach et al. 2007). The sedimentation velocity is another parameter important to mention here since larger, faster settling particles lead to a higher penetration of cells.

The observed organism species differences described in **chapter 3** can be explained by NP modifications e.g., the agglomeration of NPs once being internalized in the gut of *Daphnia magna*. These NP modifications can occur by the uptake, deposition, or transportation of particles within the organism. As a result, a detailed investigation of the fate and modification of NPs within the applied organism is necessary to ensure reliable quantitative measurements by an adjusted external calibration.

Recent studies reported on the zebrafish embryo chorion as a potential biological barrier for NPs. In order to investigate this potential barrier function in more detail, the time-dependent accumulation patterns of four different NPs (Ag-, Au-, ZnO-, and CuO-NP) were compared. Therefore, the NP uptake was quantified by neb-ICP-MS and visualized by LA-ICP-MS in different ZFE compartments (whole egg, chorion, and embryo) in **chapter 4**. For Ag-, Au-, and CuO-NPs, the ZFE chorion was identified as main accumulation structure (54-75 % in relation to total uptake amounts). The NP enrichment at the ZFE chorion structure was verified by the calculation of the NP coverage of the chorion to be in a range of 21 % (Ag-NP) to 83 % (Au-NP). The agglomeration of particles in the media and at the chorion surface was detected by Dynamic light scattering and electron microscopy measurements, respectively. For ZFE exposed to ZnO-NPs low chorion coverage (11 %), but a high concentration for the embryo was measured. In addition,

a mechanistic sorption scheme illustrating the NP-organism interaction was proposed for the first time

### FUTURE IMPROVEMENTS IN EXPOSURE AND MEASUREMENT OF NANOPARTICLES

In the future, the combination of knowledge on potential toxicological effects by NPs and the internalization and distribution of NPs in the organism is important to better understand nano-bio interactions. A correlation between the occurrence of toxicological effects and the NP distribution in organisms was done for ZFEs exposed to AgNPs as presented in **chapter 5**. Therefore, both, a toxicological as well as an assessment of particle accumulation were performed. Differences between nominal and real exposure concentrations (55 % recovery) were measured prior to testing. The suppressed real concentrations can be explained by sorption to the walls of the test vessels and agglomeration processes of NPs within the test media. Hence the dose-response curves and subsequently effect values were corrected according to the measured exposure concentrations. Changes in the NP distribution and accumulation within the ZFE structures dependent on the developmental stage of the ZFE were observed in parallel to the occurrence of toxicological effects. However, it was not fully elucidated, whether those changes in silver distribution were the cause for toxicity or its effect. Finally, the correlation between internal concentration and toxicological effects revealed that particle toxicity may result from reaching of limit values of NPs associated to organisms which in turn trigger the toxic response.

Until now, the combination of an imaging technique to visualize the NP internalization and a quantification method determining the NP size in parallel is missing. In the last part of this dissertation (**chapter 6**), a novel method combination of LA-ICP-MS with SP-ICP-MS (LA-SP-ICP-MS) is introduced. Therefore, *Daphnia magna* were exposed to Ag-NPs, sectioned and analyzed by the application of the developed method protocol. Next to visualization information on the elemental distribution, the distinction of internalized NPs and the respective dissolved silver ions is possible without a complex sample preparation. However,

due to the received large data volumes, this approach is limited to small regions of interest. The obtained results show the first qualitative detection of single NPs after the ablation of a biological sample with SP-ICP-MS and indicate an internalization of both, a particle and ionic fraction. The improvement of instrumentation and data evaluation parameters would further move this method combination towards a reliable, quantitative single particle visualization technique.

## **DISCUSSION AND OUTLOOK**

In this dissertation, analytical techniques to detect, quantify, and visualize the distribution of nanoparticles within cells and environmental organisms were developed and successfully applied. Therefore, established methods for the detection of chemicals were adjusted to the analysis of NPs by improving the calibration setup, the sample preparation procedure, or the handling of novel types of samples. The analytical procedure was applied to a range of metal based nanoparticles by quantifying and visualizing their interaction with selected human cell lines and environmental organisms.

For example, flow cytometry was firstly improved towards the quantitative detection of NPs within cells. In comparison to standard analytical measurement techniques such as neb-ICP-MS, comparable results were obtained with flow cytometry indicating the suitability of the method. However, upper detection limits for nominal exposure concentrations above 50 mg/l were observed.

In addition, LA-ICP-MS was applied to quantify the NP uptake of exposed cell layers. As for flow cytometry, LA-ICP-MS measurements were in a comparable range with the standard neb-ICP-MS results. For the development of LA-ICP-MS as an imaging technique to visualize the NP internalization and distribution within organisms the sample preparation procedure was improved. The organisms were washed, fixated, and cut into thin sections after NP exposure within a time-frame of 30 min to avoid the modification and leaching of NPs. Furthermore, the LA-ICP-MS setup for the visualization of NPs was established at the institute, the visualization measurements were validated, and a data evaluation software was developed as part of this dissertation. The analytical measurements with LA-ICP-MS revealed a particle size effect observed by a signal intensity suppression for NP sizes >150 nm. In order to compensate for this effect, a matrix-matched calibration approach using NP spiked agarose gels was developed and validated based on an earlier study of Stärk and Wennrich (2011). The occurring particle size effect was firstly described within this dissertation and was not regarded in earlier LA-ICP-MS studies on NP measurements so far.

The suitability of the above mentioned techniques to quantitatively detect the NP uptake both, within a cell layer as well as in ecotoxicological organisms was demonstrated by the comparison with neb-ICP-MS results. The validation, preferably with established standard methods or material references is recommended for future studies in order to improve existing analytical techniques towards the NP-analysis within biological or environmental samples. In addition to the establishment of standard operating procedures (SOPs) for the sample preparation, NP characterization, and analytical measurements, the development of NP reference materials are highly needed to make upcoming studies more reliable and comparable. However, literature on method cross-validation, method comparison, or the performance of round robins in the field of analytical detection methods for NPs is scarce. Therefore, the improved analytical methods and presented results of this dissertation contribute to an improved NP-analysis with respect to biological samples. In the future, development towards a single cell and single particle analysis based on a quantification as well as a visualization level is needed to investigate interactions between nanoparticles and biological structures in more detail.

As a first step a detailed NP characterization is needed with regard to the adsorption behavior, the sedimentation velocity, or the dissolution rate of the NPs of interest. These parameters directly influence the real exposure concentration within the test system and the effective NP dose the biological sample is exposed to. The above mentioned NP characteristics can lead to a suppressed offered NP amount (adsorption, dissolution) whereby an enrichment of NPs at the target side such as the cell surface is possible for rapidly settling particles of high density. For traditional chemicals, the OECD guidance document on handling of difficult substances demands that the difference between nominal and real concentration should not exceed  $\pm 20\%$  (OECD 2000) otherwise corrective actions concerning exposure design or calculation of results should be applied. Whether this recommendation is also applicable to NP is currently under debate (Kühnel and Nickel 2014). However, the control of real exposure concentrations by analytical measurements, at least at the beginning and the end of exposure, is crucial.

The NP internalization, the passage through biological membranes, and the subsequent distribution and accumulation of NPs within the biological systems is of high interest. Nevertheless, these mechanisms are often followed unilateral by biological effect observations. With regard to the applied NPs, modifications within the media or the biological sample (cells, organisms) such as changes in the particle size, surface composition or charge have to be investigated to ensure a complete and sufficient determination of internal NP concentrations. Related to the applied biological test system, specific interactions of NPs with the biological test system (cells, organisms) were observed within this dissertation. For example, the zebrafish embryo chorion surrounding the embryo during the first 2-3 days of its development, lead to an enrichment of NPs as shown by the adsorption of NPs at the chorion surface by SEM+EDX measurements. Therefore, the ZFE dechoriation prior to NP exposure or before the analytical measurement is recommended to avoid uptake overestimations. With the information on internal NP concentrations within different organs of species, the occurring effects leading to the determined concentrations can be better understand. This relationship was firstly demonstrated within this dissertation by the development of a mechanistic sorption scheme describing the NP-organism interactions for different zebrafish embryo compartments.

Furthermore, the best way to investigate the internalization and transport of NPs is the visualization of the particles within the biological sample. In the future, the development of imaging techniques with spatial resolution limits down to 1  $\mu\text{m}$  or even down to a single particle resolution level would be important. Especially, techniques able to distinguish between the internalization of particles or ionic fractions are required to estimate the influence of dissolved ionic fractions on potentially observed toxicological effects. The presented combination of LA-ICP-MS and SP-ICP-MS can be suitable to solve this problem.

Finally, as shown for Ag-NPs, a correlation between the obtained analytical results and the observed biological effects can be performed what is the future step towards an improved risk assessment of nanomaterials.

### REFERENCES

- Asharani P., Low Kah Mun G., Hande M.P., et al. (2008). Cytotoxicity and genotoxicity of silver nanoparticles in human cells. *ACS nano*, 3(2): 279-290
- Au L., Zhang Q., Cobley C.M., et al. (2009). Quantifying the cellular uptake of antibody-conjugated Au nanocages by two-photon microscopy and inductively coupled plasma mass spectrometry. *ACS nano*, 4(1): 35-42
- Auffan M., Matson C.W., Rose J., et al. (2014). Salinity-dependent silver nanoparticle uptake and transformation by Atlantic killifish (*Fundulus heteroclitus*) embryos. *Nanotoxicology*, 8: 167-176
- Auffan M., Rose J., Wiesner M.R. and Bottero J.-Y. (2009). Chemical stability of metallic nanoparticles: a parameter controlling their potential cellular toxicity in vitro. *Environ Pollut*, 157(4): 1127-1133
- Baker J.R. (2009). Dendrimer-based nanoparticles for cancer therapy. *ASH Education Program Book*, 708-719
- Bastian S., Busch W., Kühnel D., et al. (2009). Toxicity of tungsten carbide and cobalt-doped tungsten carbide nanoparticles in mammalian cells *in vitro*. *Environ Health Perspect*, 117(4): 530-536
- Baun A., Hartmann N., Grieger K. and Kusk K.O. (2008). Ecotoxicity of engineered nanoparticles to aquatic invertebrates: a brief review and recommendations for future toxicity testing. *Ecotoxicology*, 17(5): 387-395
- Becker J. S. (2005). Trace and ultratrace analysis in liquids by atomic spectrometry. *TrAC-Trend Anal Chem*, 24(3): 243-254
- Bertorelle F., Wilhelm C., Roger J., et al. (2006). Fluorescence-modified superparamagnetic nanoparticles: intracellular uptake and use in cellular imaging. *Langmuir*, 22(12): 5385-5391
- Bhatt I. and Tripathi B.N. (2011). Interaction of engineered nanoparticles with various components of the environment and possible strategies for their risk assessment. *Chemosphere*, 82(3): 308-317
- Böhme S., Stärk H.-J. and Reemtsma T. (2014). Visualisierung der Aufnahme von Nanopartikeln in Umweltorganismen. *GDCh Wochenschau* ([www.aktuelle-wochenschau.de](http://www.aktuelle-wochenschau.de)), KW 42, released 02/11/2014
- Böhme S., Stärk H.-J., Kühnel D. and Reemtsma T. (2015). Exploring LA-ICP-MS as a quantitative imaging technique to study nanoparticle uptake in *Daphnia magna* and zebrafish (*Danio rerio*) embryos. *Anal Bioanal Chem*, 407(18): 5477-5485
- Böhme S., Stärk H.-J., Meißner T., et al. (2014). Quantification of Al<sub>2</sub>O<sub>3</sub> nanoparticles in human cell lines applying inductively coupled plasma mass spectrometry (neb-ICP-MS, LA-ICP-MS) and flow cytometry-based methods. *J Nanopart Res*, 16(9): 2592
- Borovinskaya O., Hattendorf B., Tanner M., et al. (2013). A prototype of a new inductively coupled plasma time-of-flight mass spectrometer providing temporally resolved, multi-element detection of short signals generated by single particles and droplets. *J Anal At Spectrom*, 28(2): 226-233

## 1. General introduction

---

- Bowman C.R., Bailey F.C., Elrod-Erickson M., et al. (2012). Effects of silver nanoparticles on zebrafish (*Danio rerio*) and *Escherichia coli* (ATCC 25922): A comparison of toxicity based on total surface area versus mass concentration of particles in a model eukaryotic and prokaryotic system. *Environ Toxicol Chem*, 31(8): 1793-1800
- Brown R.J. and Milton M.J. (2005). Analytical techniques for trace element analysis: an overview. *TrAC-Trend Anal Chem*, 24(3): 266-274
- Busch W., Bastian S., Trahorsch U., et al. (2011). Internalisation of engineered nanoparticles into mammalian cells *in vitro*: influence of cell type and particle properties. *J Nanopart Res*, 13(1): 293-310
- Commission of the European Communities CEC (1996). CEC technical guidance document in support of commission directive 93/67/EEC on risk assessment for new notified substances, *Office for official publications of the European Communities*, Luxembourg
- Chithrani B.D., Ghazani A.A. and Chan W.C. (2006). Determining the size and shape dependence of gold nanoparticle uptake into mammalian cells. *Nano Lett*, 6(4): 662-668
- Davis M. E. (2008). Nanoparticle therapeutics: an emerging treatment modality for cancer. *Nat Rev Drug Discov*, 7(9): 771-782
- Degueldre C. and Favarger P.-Y. (2003). Colloid analysis by single particle inductively coupled plasma-mass spectroscopy: a feasibility study. *Colloid Surface A*, 217(1): 137-142
- Drescher D., Giesen C., Traub H., et al. (2012). Quantitative imaging of gold and silver nanoparticles in single eukaryotic cells by laser ablation ICP-MS. *Anal Chem*, 84(22): 9684-9688
- Escher B.I. and Hermens J.L. (2004). Peer reviewed: internal exposure: linking bioavailability to effects. *Environ Sci Technol*, 38(23): 455A-462A
- European Commission (2011). Commission Recommendation of 18 October 2011 on the definition of nanomaterial. *Official J Eur Union*, 50: 38-40
- Fabricius A.-L., Duester L., Meermann B. and Ternes T.A. (2014). ICP-MS-based characterization of inorganic nanoparticles - sample preparation and off-line fractionation strategies. *Anal Bioanal Chem*, 406(2): 467-479
- Fent K., Weisbrod C.J., Wirth-Heller A. and Pieles U. (2010). Assessment of uptake and toxicity of fluorescent silica nanoparticles in zebrafish (*Danio rerio*) early life stages. *Aquat Toxicol*, 100(2): 218-228
- Gibson N., Holzwarth U., Abbas K., et al. (2011). Radiolabelling of engineered nanoparticles for *in vitro* and *in vivo* tracing applications using cyclotron accelerators. *Arch Toxicol*, 85(7): 751-773
- Gondikas A.P., von der Kammer F., Reed R.B., et al. (2014). Release of TiO<sub>2</sub> Nanoparticles from Sunscreens into Surface Waters: A One-Year Survey at the Old Danube Recreational Lake. *Environ Sci Technol*, 48(10): 5415-5422
- Gottschalk F., Sun T. and Nowack B. (2013). Environmental concentrations of engineered nanomaterials: review of modeling and analytical studies. *Environ Pollut*, 181: 287-300
- Groh K.J., Dalkvist T., Piccapietra F., et al. (2015). Critical influence of chloride ions on silver ion-mediated acute toxicity of silver nanoparticles to zebrafish embryos. *Nanotoxicology*, (9): 81-91
- Hassellöv M., Readman J.W., Ranville J.F. and Tiede K. (2008). Nanoparticle analysis and characterization methodologies in environmental risk assessment of engineered nanoparticles. *Ecotoxicology*, 17(5): 344-361

- Heinlaan M., Kahru A., Kasemets K., et al. (2011). Changes in the *Daphnia magna* midgut upon ingestion of copper oxide nanoparticles: A transmission electron microscopy study. *Water Res*, 45(1): 179-190
- Hinderliter P.M., Minard K.R., Orr G., et al. (2010). ISDD: a computational model of particle sedimentation, diffusion and target cell dosimetry for *in vitro* toxicity studies. *Part Fibre Toxicol*, 7(1): 36
- Hsin Y.-H., Chen C.-F., Huang S., et al. (2008). The apoptotic effect of nanosilver is mediated by a ROS-and JNK-dependent mechanism involving the mitochondrial pathway in NIH3T3 cells. *Toxicol Lett*, 179(3): 130-139
- Jiang W., Kim B.Y., Rutka J.T. and Chan W.C. (2008). Nanoparticle-mediated cellular response is size-dependent. *Nat Nanotechnology*, 3(3): 145-150
- Kahru A. and Dubourguier H.-C. (2010). From ecotoxicology to nanoecotoxicology. *Toxicology*, 269(2): 105-119
- Kimmel C. B., Ballard W.W., Kimmel S.R., et al. (1995). Stages of embryonic development of the zebrafish. *Dev Dynam*, 203(3): 253-310
- Kittler S., Greulich C., Diendorf J., et al. (2010). Toxicity of silver nanoparticles increases during storage because of slow dissolution under release of silver ions. *Chem Mater*, 22(16): 4548-4554
- Klaine S.J., Koelmans A.A., Horne N., et al. (2012). Paradigms to assess the environmental impact of manufactured nanomaterials. *Environ Toxicol Chem*, 31(1): 3-14
- Kroll A., Kühnel D. and Schirmer K. (2013). Testing Nanomaterial Toxicity in Unicellular Eukaryotic Algae and Fish Cell Lines. Oxidative Stress and Nanotechnology: Methods and Protocols in *Methods in Molecular Biology*, 1028: 165-195.
- Kühnel D. and Nickel C. (2014). The OECD expert meeting on ecotoxicology and environmental Fate - Towards the development of improved OECD guidelines for the testing of nanomaterials. *Sci Total Environ*, 472: 347-353
- Kumar M. and Ando Y. (2010). Chemical vapor deposition of carbon nanotubes: a review on growth mechanism and mass production. *J Nanosci Nanotechnol*, 10(6): 3739-3758
- Lanone S., Rogerieux F., Geys J., et al. (2009). Comparative toxicity of 24 manufactured nanoparticles in human alveolar epithelial and macrophage cell lines. *Part Fibre Toxicol*, 6(14): 455-460
- Lee S., Bi X., Reed R.B., et al. (2014). Nanoparticle size detection limits by single particle ICP-MS for 40 elements. *Environ Sci Technol*, 48(17): 10291-10300
- Limbach L.K., Li Y., Grass R.N., et al. (2005). Oxide nanoparticle uptake in human lung fibroblasts: effects of particle size, agglomeration, and diffusion at low concentrations. *Environ Sci Technol*, 39(23): 9370-9376
- Limbach L.K., Wick P., Manser P., et al. (2007). Exposure of engineered nanoparticles to human lung epithelial cells: influence of chemical composition and catalytic activity on oxidative stress. *Environ Sci Technol*, 41(11): 4158-4163
- Lin S., Zhao Y., Xia T., et al. (2011). High content screening in zebrafish speeds up hazard ranking of transition metal oxide nanoparticles. *ACS nano*, 5(9): 7284-7295
- Lin Y., Skaff H., Emrick T., et al. (2003). Nanoparticle assembly and transport at liquid-liquid interfaces. *Science*, 299(5604): 226-229

## 1. General introduction

---

- Lowry G.V., Gregory K.B., Apte S.C. and Lead J.R. (2012). Transformations of nanomaterials in the environment. *Environ Sci Technol*, 46(13): 6893-6899
- Lowry G.V., Hotze E.M., Bernhardt E.S., et al. (2010). Environmental occurrences, behavior, fate, and ecological effects of nanomaterials: an introduction to the special series. *J Environ Qual*, 39(6): 1867-1874
- Lynch I., Weiss C. and Valsami-Jones E. (2014). A strategy for grouping of nanomaterials based on key physico-chemical descriptors as a basis for safer-by-design NMs. *Nano Today*, 9(3): 266-270
- Ma S. and Lin D. (2013). The biophysicochemical interactions at the interfaces between nanoparticles and aquatic organisms: adsorption and internalization. *Environ Sci Process Impacts*, 15(1): 145-160
- Marquis B.J., Love S.A., Braun K.L. and Haynes C.L. (2009). Analytical methods to assess nanoparticle toxicity. *Analyst*, 134(3): 425-439
- Maynard A.D. (2006). Nanotechnology: A research strategy for addressing risk. Report, Woodrow Wilson International Center for Scholars
- McTeer J., Dean A.P., White K.N. and Pittman J.K. (2014). Bioaccumulation of silver nanoparticles into *Daphnia magna* from a freshwater algal diet and the impact of phosphate availability. *Nanotoxicology*, 8(3): 305-316
- Meißner T., Kühnel D., Busch W., et al. (2010). Physical-chemical characterization of tungsten carbide nanoparticles as a basis for toxicological investigations. *Nanotoxicology*, 4(2): 196-206
- Misra S.K., Dybowska A., Berhanu D., et al. (2012). The complexity of nanoparticle dissolution and its importance in nanotoxicological studies. *Sci Total Environ*, 438: 225-232
- Mitrano D.M., Leshner E.K., Bednar A., et al. (2012). Detecting nanoparticulate silver using single-particle inductively coupled plasma–mass spectrometry. *Environ Toxicol Chem*, 31(1): 115-121
- Monteiro-Riviere N.A., Inman A.O. and Zhang L. (2009). Limitations and relative utility of screening assays to assess engineered nanoparticle toxicity in a human cell line. *Toxicol Appl Pharmacol*, 234(2): 222-235
- Nowack B. and Bucheli T.D. (2007). Occurrence, behavior and effects of nanoparticles in the environment. *Environ Pollut*, 150(1): 5-22
- OECD (2000). Guidance Document on Aquatic Toxicity Testing of Difficult Substances and Mixtures. ([www.oecd.org](http://www.oecd.org))
- OECD (2013) Test No. 236: Fish embryo acute toxicity (FET) test. OECD Publishing ([www.oecd.org](http://www.oecd.org))
- OECD (2004) Test No. 202: *Daphnia sp.* acute immobilisation test. OECD Publishing ([www.oecd.org](http://www.oecd.org))
- Pan Y., Neuss S., Leifert A., et al. (2007). Size-dependent cytotoxicity of gold nanoparticles. *Small*, 3(11): 1941-1949
- Powers C.M., Slotkin T.A., Seidler F.J., et al. (2011). Silver nanoparticles alter zebrafish development and larval behavior: distinct roles for particle size, coating and composition. *Neurotoxicol Teratol*, 33(6): 708-714
- Praetorius A., Tufenkji N., Goss K.-U., et al. (2014). The road to nowhere: equilibrium partition coefficients for nanoparticles. *Environ Sci: Nano*, 1(4): 317-323

## 1. General introduction

---

- Quinn J., Geiger C., Clausen C., et al. (2005). Field demonstration of DNAPL dehalogenation using emulsified zero-valent iron. *Environ Sci Technol*, 39(5): 1309-1318
- Rosenkranz P., Chaudhry Q., Stone V. and Fernandes T.F. (2009). A comparison of nanoparticle and fine particle uptake by *Daphnia magna*. *Environ Toxicol Chem*, 28(10): 2142-2149
- Russo R.E., Mao X., Liu H., et al. (2002). Laser ablation in analytical chemistry - a review. *Talanta*, 57(3): 425-451
- Salata O.V. (2004). Applications of nanoparticles in biology and medicine. *J Nanobiotechnology*, 2(1): 3
- Sanchís J., Berrojalbiz N., Caballero G., et al. (2011). Occurrence of aerosol-bound fullerenes in the Mediterranean Sea atmosphere. *Environ Sci Technol*, 46(3): 1335-1343
- Scholz S., Fischer S., Gündel U., et al. (2008). The zebrafish embryo model in environmental risk Assessment - applications beyond acute toxicity testing. *Environ Sci Pollut Res*, 15(5): 394-404
- Simon-Deckers A., Gouget B., Mayne-L'Hermite M., et al. (2008). *In vitro* investigation of oxide nanoparticle and carbon nanotube toxicity and intracellular accumulation in A549 human pneumocytes. *Toxicology*, 253(1): 137-146
- Stärk H.-J. and Wennrich R. (2011). A new approach for calibration of laser ablation inductively coupled plasma mass spectrometry using thin layers of spiked agarose gels as references. *Anal Bioanal Chem*, 399(6): 2211-2217
- Sun T.Y., Gottschalk F., Hungerbühler K. and Nowack B. (2014). Comprehensive probabilistic modelling of environmental emissions of engineered nanomaterials. *Environ Pollut*, 185: 69-76
- Teeguarden J.G., Hinderliter P.M., Orr G., et al. (2007). Particokinetics *in vitro*: dosimetry considerations for in vitro nanoparticle toxicity assessments. *Toxicol Sci*, 95(2): 300-312
- Tkalec Ž.P., Drobne D., Vogel-Mikuš K., et al. (2011). Micro-PIXE study of Ag in digestive glands of a nano-Ag fed arthropod (*Porcellio scaber*, Isopoda, Crustacea). *Nucl Instrum Meth B*, 269(20): 2286-2291
- Unfried K., Albrecht C., Klotz L.-O., et al. (2007). Cellular responses to nanoparticles: target structures and mechanisms. *Nanotoxicology*, 1(1): 52-71
- Wang J. and Wang W.-x. (2014). Significance of physicochemical and uptake kinetics in controlling the toxicity of metallic nanomaterials to aquatic organisms. *J Zhejiang Univ-Sc A*, 15(8): 573-592
- Zhang W.-x. (2003). Nanoscale iron particles for environmental remediation: an overview. *J Nanopart Res*, 5(3-4): 323-332
- Zucker R., Massaro E., Sanders K., et al. (2010). Detection of TiO<sub>2</sub> nanoparticles in cells by flow cytometry. *Cytom Part A*, 77(7): 677-685

## Chapter 2

### **QUANTIFICATION OF Al<sub>2</sub>O<sub>3</sub> NANOPARTICLES IN HUMAN CELL LINES APPLYING INDUCTIVELY COUPLED PLASMA MASS SPECTROMETRY (NEB-ICP-MS, LA-ICP-MS) AND FLOW CYTOMETRY BASED METHODS**

Journal of Nanoparticle Research (2014), 16(9): 2592

Steffi Böhme<sup>1</sup>, Hans-Joachim Stärk<sup>2</sup>, Tobias Meißner<sup>3</sup>, Armin Springer<sup>4</sup>, Thorsten Reemtsma<sup>2</sup>, Dana Kühnel<sup>1</sup>, Wibke Busch<sup>1</sup>

<sup>1</sup> Helmholtz Centre for Environmental Research - UFZ, Department of Bioanalytical Ecotoxicology, Permoserstrasse 15, 04318 Leipzig (Germany)

<sup>2</sup> Helmholtz Centre for Environmental Research - UFZ, Department of Analytical Chemistry, Permoserstrasse 15, 04318 Leipzig (Germany)

<sup>3</sup> Fraunhofer Institute for Ceramic Technologies and Systems - IKTS, Department of Powder and Suspension Characterization, Winterbergstrasse 28, 01277 Dresden (Germany)

<sup>4</sup> Centre for Translational Bone, Joint and Soft Tissue Research, University Hospital Carl Gustav Carus, Technische Universität Dresden, Fetscherstrasse 74, 01307 Dresden, Germany



### ABSTRACT

In order to quantify and compare the uptake of aluminum oxide nanoparticles of three different sizes into two human cell lines (skin keratinocytes (HaCaT) and lung epithelial cells (A549)), three analytical methods were applied: digestion followed by nebulization inductively coupled plasma mass spectrometry (neb-ICP-MS), direct laser ablation ICP-MS (LA-ICP-MS), and flow cytometry. Light and electron microscopy revealed an accumulation and agglomeration of all particle types within the cell cytoplasm, whereas no particles were detected in the cell nuclei. The internalized Al<sub>2</sub>O<sub>3</sub> particles exerted no toxicity in the two cell lines after 24 h of exposure. The smallest particles with a primary particle size ( $x_{\text{BET}}$ ) of 14 nm (Alu1) showed the lowest sedimentation velocity within the cell culture media, but were calculated to have settled completely after 20 h. Alu2 ( $x_{\text{BET}} = 111$  nm) and Alu3 ( $x_{\text{BET}} = 750$  nm) were calculated to reach the cell surface after 7 h and 3 min, respectively. The internal concentrations determined with the different methods lay in a comparable range of 2-8  $\mu\text{g Al}_2\text{O}_3/\text{cm}^2$  cell layer, indicating the suitability of all methods to quantify the nanoparticle uptake. Nevertheless, particle size limitations of analytical methods using optical devices were demonstrated for LA-ICP-MS and flow cytometry. Furthermore, the consideration and comparison of particle properties as parameters for particle internalization revealed the particle size and the exposure concentration as determining factors for particle uptake.

### INTRODUCTION

The toxic potential of engineered nanoparticles toward human cell lines has been the subject of several *in vitro* studies (e.g., Bastian et al. (2009); Kühnel et al. (2012); Limbach et al. (2005); Simon-Deckers et al. (2008)). Besides the characterization of the toxic impact, these studies also documented and discussed the role of the internalization of particles into the cells. Techniques such as scanning electron microscopy (SEM) coupled with energy-dispersive X-ray spectroscopy (EDX) allow the determination of both the intracellular localization and the chemical identification of the nanomaterial but yield solely qualitative

information (Simon-Deckers et al. 2008; Busch et al. 2011). It has been shown that particles are primarily located in the cytoplasm, entrapped in vesicles or vacuoles (Simon-Deckers et al. 2008), or accumulated in mitochondria and lysosomes. Furthermore, the formation of perinuclear rings by internalized particles was described in several studies (e.g., Zucker et al. (2010) and Busch et al. (2011)). Especially in the fields of medicine and pharmacology, fluorescent or magnetic nanoparticles are used to allow an *in vivo* detection and direct quantification of internalized particles (Salata 2004). In line with that, the quantification of intracellular nanomaterials became an issue of high relevance for toxicological perspectives as well as for medical applications.

The cellular uptake processes are as diverse as the chemical and physical properties of nanoparticles. Most studies describe a time and concentration-dependent particle internalization, independent of the examined type of nanomaterial (e.g., Radziun et al. (2011); Zucker et al. (2010); Chithrani et al. (2006)). In general, passive diffusion is possible for particles and ions which are smaller than 60 nm. Larger particles and particle agglomerates are internalized by various active phagocytotic or endocytotic mechanisms (Unfried et al. 2007). Jiang et al. (2008) identified particles of a middle-size range (~50 nm) as preferentially taken up, compared to other size ranges. Besides the size of nanoparticles, additional chemical and physical characteristics, such as their surface area (Brown et al. 2001; Hussain et al. 2009), surface coating (Zhang et al. 2002), charge (Gratton et al. 2008), and shape (Chithrani et al. 2006; Gratton et al. 2008), are relevant for uptake and toxicity. These particle properties can be correlated to the appearance of biological effects or the selective accumulation of particles in the cells (Oberdörster et al. 2005; Stoeger et al. 2006; Wittmaack 2007; Waters et al. 2009). The correlation between specific nanoparticle properties and the quantitative amount of internalized nanomaterial were investigated in detail by Au et al. (2009); Chithrani et al. (2006); Limbach et al. (2005) and Zhu et al. (2013). For this goal, they applied inductively coupled plasma mass spectrometry (ICP-MS)-based approaches as well as electron microscopy.

Nebulization-ICP-MS (neb-ICP-MS) is an established and precise method with a detection limit in the ng/l concentration range. Additionally, new applications of

ICP-MS allow to gain information about the size distribution of particles (single-particle ICP-MS, e.g., Mitrano et al. (2012)) and the local distribution of particles (laser ablation ICP-MS, e.g., Drescher et al. (2012)). The laser ablation inductively coupled plasma mass spectrometry (LA-ICP-MS) system is an established method to investigate the element composition of geological and archeological samples (Russo et al. 2002). Furthermore, the applicability as a visualization method with a high spatial resolution has been described (Becker et al. 2007; Wang et al. 2013).

Another way to determine the internalization of nanoparticles into cells is the indirect measurement of the cellular granularity by flow cytometry methods (Palecanda and Kobzik 2000). As the incorporation of nanoparticles changes the granularity of living cells, the detection of the side scattered light in a flow cytometer can be used as an optical detection method to study nanoparticle uptake (Zucker et al. 2010; Busch et al. 2011). It is, however, of high interest whether the indirect flow cytometry measurements can be correlated directly to internal particle concentrations. In order to observe the behavior, destination, and distribution of nanomaterials in biological tissues, especially in cancer cells, flow cytometry has been applied in medical research (Suzuki et al. 2007).

In this study, we investigated the quantitative uptake of three differentially sized Al<sub>2</sub>O<sub>3</sub> particles in order to compare three different quantification methods. Al<sub>2</sub>O<sub>3</sub> particles were chosen because they are not toxic to human cells (Radziun et al. 2011), and they are commercially available in different sizes. In the first step, we investigated the uptake of the particles into the cells, and the distribution within cells qualitatively applying electron microscopy. The chemical and physical properties, the stability, and the behavior of the particles in the relevant media were characterized in detail, and the sedimentation velocity was calculated in order to determine the influence of a restricted bioavailability of nanomaterial to the cell monolayer. Second, three independent analytical methods (digestion combined with neb-ICP-MS, LA-ICP-MS, and flow cytometry) were used to determine the internal particle concentrations within the cell lines. The results were compared by normalizing the mass of the internalized aluminum oxide to the respective cell surface area. Finally, the relationship between the intracellular

concentrations and different particle properties was assessed by a direct comparison of different particle characteristics.

### **MATERIALS AND METHODS**

#### INITIAL AL<sub>2</sub>O<sub>3</sub> PARTICLE CHARACTERISTICS

The three Al<sub>2</sub>O<sub>3</sub> particles were purchased as powders from different manufacturers. They are named in the following as Alu1 (AEROXIDE® Alu C, Evonik Degussa GmbH), Alu2 (TAIMICRON®, TM-DAR, Taimei Chemicals Co., LTD.), and Alu3 (NABALOX®, NO-625-10, Nabaltec AG). The morphology of the particle powders was investigated by scanning electron microscopy (SEM, Zeiss Leo 982 FEG, Carl Zeiss SMTAG). The N<sub>2</sub>-BET-specific surface area was obtained by gas adsorption measurement according to the Brunauer-Emmet-Teller method (ASAP 2010 Analyzer, Micromeritics GmbH), and the crystalline structure of the powders was determined by X-ray diffraction (XRD7, Seifert-FPM). The powder density was determined using helium pycnometry (Penta Pycnometer, Quantachrome GmbH & Co. KG). Theoretical primary particle size ( $x_{\text{BET}}$ ) was calculated on the basis of the BET and density values obtained.

#### PREPARATION AND CHARACTERIZATION OF PARTICLE SUSPENSIONS

Particle suspensions in cell culture media were produced according to Meißner et al. (2010). Briefly, the stock suspensions of particles (500 mg/l) were prepared in pure water under addition of 0.05 % (w/v) sodium hexametaphosphate (SHMP, Merck KGaA) as stabilizing agent. SHMP is non-toxic in this concentration range and causes electrostatic repulsion between the particles. The suspensions were sonicated with an ultrasonic disintegrator equipped with a 14-mm sonotrode (UDS 751, Topas GmbH) for de-agglomeration. The particle size distribution and agglomeration behavior of the smallest (Alu1) and middle-sized particles (Alu2) in suspension were investigated by dynamic light scattering (DLS, Zetasizer Nano ZS, Malvern Instruments Ltd.), and the polydispersity index was determined. For the larger particles (Alu3), laser light diffraction (Mastersizer 2000, Malvern

Instruments Ltd.) was applied to measure the particle size in suspension, whereby different quantiles of the volume-weighted distribution help to gain information about the particle size distribution. The zeta potential of the stock suspensions was determined by measuring the electrophoretic mobility of the particles by means of electrophoresis. The Smoluchowski equation was taken to convert the electrophoretic mobility into the zeta potential. Stock suspensions were stored at 4 °C for a maximum of eight weeks. In order to estimate the influence of the sedimentation rate of the particles to the cell uptake, the sedimentation velocity ( $v_p$ ) was calculated for a spherical particle shape with the determined hydrodynamic particle diameters for a temperature of 37 °C according to Stoke's law:

$$v_p = \frac{2r^2 g * (\rho_p - \rho_f)}{9 * \eta}$$

Where  $r$  is the radius of the particle,  $g$  is the gravitational acceleration,  $\eta$  is the dynamic viscosity, and  $\rho_p$  and  $\rho_f$  describe the density of the particle and the surrounding media, respectively.

### HACAT AND A549 CELL CULTURE

Two different human cell lines were used, representing model cell lines for an inhalation-related (human lung epithelial cells, A549) and a dermal-related uptake pathway (human skin keratinocytes, HaCaT, Boukamp et al. (1988)) both with a cell diameter of approximately 10  $\mu\text{m}$ . Both cell lines were cultivated in RPMI medium (RPMI 1640, Biochrom AG) supplemented with 10 % fetal bovine serum (FBS, (v/v), Sigma Aldrich) in 75 cm<sup>2</sup> flasks at 37 °C in a humidified and 5 % CO<sub>2</sub> atmosphere. A sub-cultivation was done every 3-4 days. The cell monolayer was washed two times with Versene (0.48 mM EDTA/PBS buffer solution, Gibco®, Invitrogen), detached with trypsin (0.25 % (v/v) in phosphate-buffered saline (PBS)), and the cells were counted with a hemocytometer.

## EXPOSURE OF CELLS

Cells were seeded in different densities, depending on the plate format used in the actual experiment (**Tab. 1**). By microscopic inspections it was guaranteed that subsequent experiments were performed exclusively on complete closed cell monolayers. Independent of the exposure setup, the medium height for all experiment was 2 mm. Before usage, particle stock suspensions were re-dispersed by shaking and sonication in an ultrasound bath (Eurolab USR 30H, Merck KGaA) for 5 min before they were diluted in cell culture media and subsequently applied to the cells. For all experiments, concentrations of 10, 20, 30, 40 and 50 mg/l were used. By dividing the total offered particle amount through the cell surface area, the exposure was expressed as  $\mu\text{g Al}_2\text{O}_3/\text{cm}^2$  cell layer in the following text. After 24 h of exposure, cells were washed twice with Versene to remove particles loosely bound to the cell surface, which was controlled by light microscopy. Controls of water and water with 0.05 % SHMP were included in all experiments. All results represent a minimum of three biological replicates.

**Tab. 1** Exposure designs for the cell viability tests and the different exposure experiments

experiment	plate format	cell density	exposure volume
cell viability test	24-well plates, 1.9 cm <sup>2</sup>	5 x 10 <sup>4</sup> cells/ml	1 ml
flow cytometry	6-well plates, 9.6 cm <sup>2</sup>	20 x 10 <sup>4</sup> cells/ml	2 ml
neb-ICP MS	6-well plates, 9.6 cm <sup>2</sup>	20 x 10 <sup>4</sup> cells/ml	2 ml
LA-ICP MS	glass slides, 12.95 cm <sup>2</sup>	17 x 10 <sup>4</sup> cells/ml	3 ml

## ANALYSIS OF CELLULAR PARTICLE UPTAKE BY LIGHT AND ELECTRON MICROSCOPY

The particle distribution within the cells was investigated after 24 h of exposure to the highest concentration of 50 mg/l. Particle-treated cells were observed by an inverse microscope (Leica DMI 4000B, magnification 200x) connected to a Leica DFC 290 HD camera. Detailed analyses of the localization of particles inside the cells were performed by scanning electron microscopy (SEM, Philips ESEM XL 30 FEG) coupled with energy-dispersive X-ray spectroscopy (EDX with EDAX

detecting unit, EDAX Inc.) for element analysis. Therefore, cell pellets containing  $\sim 10 \times 10^5$  cells were fixated with 2.5 % glutaraldehyde in PBS after exposure. After washing with PBS, the samples were stained with osmium tetroxide, washed with deionized water, dehydrated with a graduated acetone series, including an additional staining step with uranyl acetate, and finally embedded in epoxy resin. In the last step, samples were cut by a microtome (Leica EM UC6, Leica Microsystems GmbH) and measured by SEM-coupled EDX to determine the element distribution (Bastian et al. 2009; Kühnel et al. 2012).

### ICP-MS ANALYSIS

Two approaches for the ICP-MS-based quantification of particle uptake into human cells were developed. First, an acid digestion followed by analysis with a standard neb-ICP-MS measurement and second, a laser ablation system coupled with ICP-MS (ELAN DRC II, Perkin Elmer Sclex.) to analyze thin films or cell monolayers. For both experimental setups, cells were exposed for 24 h to all types of particles in a concentration range between 10-50 mg/l and washed twice with PBS to remove particles loosely bound to the cell surface. Scandium (standard solution 1 g/l, Merck KGaA) with a concentration of 10 µg/l was measured as an internal standard element for all samples. Raw aluminum data of ICP-MS measurements were corrected by multiplication with the Al<sub>2</sub>O<sub>3</sub>/Al mass ratio factor of 1.89. Finally, all received results of the neb-ICP-MS and LA-ICP-MS experiments were extrapolated to the amount of particles per cm<sup>2</sup> cell layer.

### DIGESTION FOR NEBULIZATION-ICP-MS

The complete destruction of cells and dissolution of aluminum oxide nanoparticles was achieved by acid digestion. After the exposure period, cells were washed, detached with trypsin and centrifuged. The cell pellet was stored at -20 °C and re-suspended in water for the digestion process. An acid digestion method with addition of 10 ml hydrochloric acid (30 %, suprapur, Merck KGaA) and 500 mg potassium chlorate (for analysis, Merck KGaA) in separate reaction vessels inside the digestion system (HPA-S, AntonPaar GmbH) was developed. During the

reaction, elemental chlorine was formed at a temperature of 250 °C, a pressure of 100 bar and a reaction time of 2 h for small Al<sub>2</sub>O<sub>3</sub> particles (Alu1, Alu2) and 4 h for micron-sized particles (Alu3). These long reaction conditions are necessary to gain the best recovery rates ( $\sim 99 \pm 5 \%$ ). After digestion and appropriate dilution, all samples and controls were analyzed by neb-ICP-MS connected to an auto sampler (Perkin Elmer SC-2 DX). An external calibration was performed by analyzing an aluminum standard solution (standard solution 1 g/l, Merck KGaA).

### LASER ABLATION ICP-MS

The amount of aluminum in cells grown on glass slides was measured by LA-ICP-MS. After exposure the cell layer was carefully washed several times with PBS and allowed to dry under a laminar flow. An external calibration was performed by application of 30  $\mu\text{m}$  thick agarose gels, according to an earlier protocol (Stärk and Wennrich 2011). The external calibration curve was generated by spiking agarose gel slides with the individual particle type. Gels were prepared by dissolving 100 mg agarose (for electrophoresis, Merck KGaA) in water. After addition of 5 ml ammonium acetate buffer (for analysis, 2 mol/l, Merck KGaA) and scandium as internal standard (scandium standard solution, 1 g/l, Merck KGaA), the gel solution was filled up to 10 ml with water. The gel solution was heated to 90 °C and homogenized by carefully shaking. Before pouring the gel (4 ml of gel solution), a defined particle amount was added to the solution. Gel slides were allowed to dry and were measured by a laser ablation (LSX 500, Nd:YAG, CETAC) coupled with an ICP-MS system. The laser was adjusted to 50 % energy, 200  $\mu\text{m}$  spot size, 100  $\mu\text{m}/\text{sec}$  scan rate and 20 Hz pulse repetition rate. The nebulizer was used in parallel to merge the laser aerosol with a blank solution, guarantying constant wet plasma conditions over all experiments. Therefore, the laser gas stream was laterally connected via a tube to the spray chamber (Scott type rython, Perkin Elmer Sclex.). For an easier evaluation a line of 5000  $\mu\text{m}$  length was ablated, leading to a total ablation area of 1 mm<sup>2</sup> which represents a cell number of  $\sim 39\,000$  cells. A minimum of three lines was ablated for each gel slide. The amount of aluminum measured for each slide was then corrected by a factor of 1.141 according to the concentration gradient at the boundary of the slide (Stärk

and Wennrich 2011). Finally, the concentration of aluminum was extrapolated to the whole slide area of 1295.16 mm<sup>2</sup> and transformed into concentration values of µg Al<sub>2</sub>O<sub>3</sub>/cm<sup>2</sup> cell layer.

### FLOW CYTOMETRY

For flow cytometry measurements, cells were exposed for 24 h to particles in a concentration range of 10-50 mg/l, washed twice with PBS and detached with accutase (PAA Laboratories). Detached cells were washed again in PBS and centrifuged. The cell pellets were re-suspended in PBS, stored on ice and immediately measured by a flow cytometer (FACS Calibur, Becton-Dickinson). The flow cytometer contains a 488 nm air-cooled argon-ion laser and a FSC diode detector. A flow rate of 35 µl/min was chosen. For each experiment, 10 x 10<sup>4</sup> viable cells were counted and the median side scatter (SSC) and forward scatter (FSC) values were measured. The SSC-values represent the granularity of the cells (Zucker et al. 2010). The SSC-values were converted into the particle concentration per sample by using the individual particle suspensions in a concentration range from 2-80 mg/l without cell matrix for calibration. Flow cytometry data were analyzed using CellQuest Pro software (Becton-Dickinson) and the FlowJo Software (version 7.2.2; Tree Star Inc.). Finally, all received results were extrapolated to the amount of particles per cm<sup>2</sup> cell layer. This allows a direct comparison of the results with those achieved by neb-ICP-MS and LA-ICP-MS, independent of the exposure volume, the total cell number, or the exposure format.

### RESULTS

The aim of this study was the appropriate quantification of particle concentrations within human cells, by the application of three different analytical techniques. First, the chemical and physical particle properties were characterized in detail and the toxic potential of the investigated nanomaterials was determined. The second step comprised the detection of the internalized particles within the cells, prior to a quantification which was the third and major aim of the study.

## CHARACTERISTICS OF ALUMINUM OXIDE POWDERS AND SUSPENSIONS

The parameters determined for the particle powders and suspensions are summarized in **Tab. 2**. SEM pictures show a spherical to irregular shape of the particles, with larger agglomerates or aggregates observed for the small (Alu1) and middle-sized material (Alu2) (**Fig. 1**). The particle surface area (BET) for the particle powders ranges between 117 m<sup>2</sup>/g (Alu1), 13.5 m<sup>2</sup>/g (Alu2), and 2 m<sup>2</sup>/g (Alu3). Under inclusion of the density (3.6 g/cm<sup>3</sup> for Alu1, 4.0 g/cm<sup>3</sup> for Alu2 and Alu3) and the BET values, a primary particle size ( $x_{\text{BET}}$ ) of 14 nm (Alu1), 111 nm (Alu2), and 750 nm (Alu3) was calculated. The diameter of the particles in suspension ranges between 127 nm (Alu1) and 2.5 μm (Alu3) (**Tab. 2**). The high absolute values of the zeta potential imply strong electrostatic repulsion forces, indicating a stable particle suspension. Fetal bovine serum was supplemented to the medium and is known as an additional particle stabilizing agent under physiological conditions (e.g., Meißner et al. (2010)). However, agglomeration in cell culture media and increasing particle diameters were observed by DLS during the exposure period. The sedimentation velocity after the exposure period was calculated to be 2.5, 7, and 1 270 mm/24 h for Alu1, Alu2, and Alu3, respectively. Considering the media height of 2 mm in the cell culture vessels, the micron-sized (Alu3), middle-sized (Alu2), and smallest (Alu1) particles were expected to be settled completely after 3 min, 7 h, and 20 h, respectively. The micron-sized particles (Alu3) settled most rapidly. For the smallest particles (Alu1), it is assumed that the majority of particles had reached the cell surface during the exposure time of 24 h.

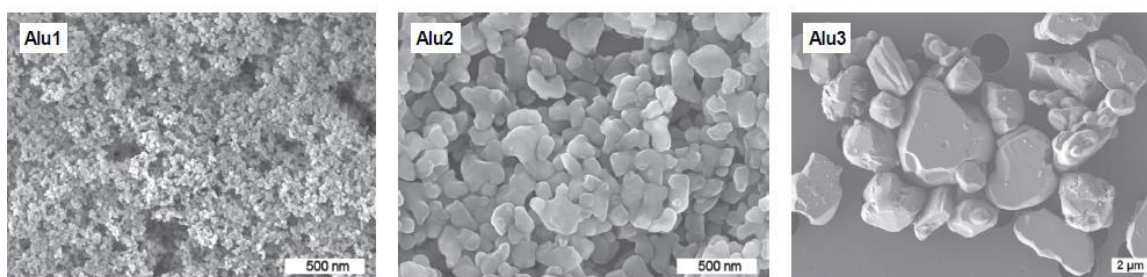


**Fig. 1** SEM images of aluminum oxide powders (Alu1-AEROXIDE® Alu C, Alu2-TAIMICRON®, Alu3-NABALOX®)

## 2. Quantification of Al<sub>2</sub>O<sub>3</sub> particles in human cells

**Tab. 2** Chemical and physical characteristics of the investigated aluminum oxide powders and suspensions

	Alu1	Alu2	Alu3
product name	Alu C	TM-DAR	NO 625-10
powder characteristics			
crystal structure	γ-Al <sub>2</sub> O <sub>3</sub> ; δ-Al <sub>2</sub> O <sub>3</sub>	α-Al <sub>2</sub> O <sub>3</sub>	α-Al <sub>2</sub> O <sub>3</sub>
BET (m <sup>2</sup> /g) <sup>a</sup>	117	13.5	2
X <sub>BET</sub> (nm) <sup>b</sup>	14	111	750
ρ (g/cm <sup>3</sup> )	3.3	4.0	4.0
suspension characteristics			
x (nm)	127 <sup>c</sup>	186 <sup>c</sup>	2500 (X <sub>50,3</sub> ) <sup>d</sup>
X <sub>10,3</sub> ; X <sub>90,3</sub>	-	-	1200; 4900 <sup>d</sup>
polydispersity index	0.19	0.10	-
zeta potential (mV)	-58	-64	-83

<sup>a</sup> – specific surface area      <sup>b</sup> – primary particle size      <sup>c</sup> – hydrodynamic diameter X<sub>DLS</sub> (DLS)

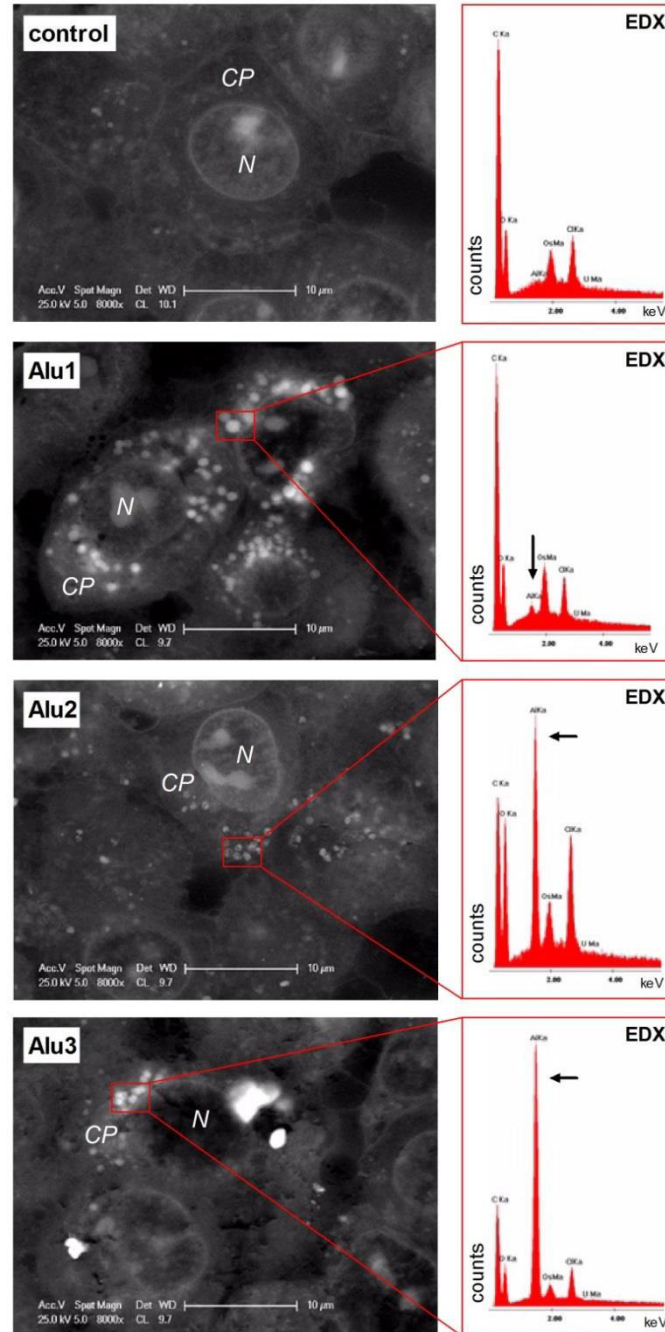
<sup>d</sup> – particle size in suspension measured by laser light diffraction

### PARTICLE INTERNALIZATION, DISTRIBUTION AND TOXICITY TO CELLS

Observations performed with light microscopy clearly showed that particles became associated to cells upon 24 h of exposure (see Supplemental Material, **Fig. S1**). For the three particle types investigated, distinct differences of the particle distribution in the cell cytoplasm were observed, with a homogenous distribution of the small particles (Alu1) and a heterogeneous, random localization of the micron-sized particles (Alu3). In contrast, the middle-sized particles (Alu2) exhibit the formation of ring patterns around the cell nuclei, described by Zucker et al. (2010) as perinuclear rings for titanium dioxide particles. To confirm the internalization of particles in cells, SEM coupled with an element detection unit (SEM/EDX) was performed (**Fig. 2**). In the cytoplasm of both cell lines, electron dense material was detected after the exposure with aluminum oxide particles (the results for the HaCaT cells are provided in the supplemental material (**Fig. S2**)). No such material was observed in control cells and in the cell nucleus of all treatments. Electron dense material in the cells was identified as aluminum, showed by the presence of an aluminum peak in the spectra measured by EDX,

and exemplarily shown for single A549 cells in **Fig. 2**. The internalized particles formed agglomerates inside the cells.

**Fig. 2** SEM micrographs of sections of embedded human lung epithelial cells (A549) exposed to 10.4 µg Al<sub>2</sub>O<sub>3</sub>/cm<sup>2</sup> cell layer and medium without particles (control) for 24 h. The area subjected to EDX analysis is marked with a red rectangle. Heavy elements (e.g., aluminum) appear as light electron dense areas. No aluminum was detected in control cells. All three types of particles were incorporated by the cells and were located in the cell cytoplasm (CP). No particles were detected in the cell nucleus (N)



The toxicity of the different aluminum oxide particles was investigated prior to the measurements of internal concentrations. All details and results are presented in the supplemental material. For this purpose, a combined cell viability assay, using AlamarBlue and CFDA-AM as fluorescence indicator dyes for metabolic activity

and membrane integrity, respectively, was performed. For all types of particles and both cell lines, no toxicity was observed, including the highest test concentration of 50 mg/l, which equals 26.3 µg Al<sub>2</sub>O<sub>3</sub>/cm<sup>2</sup> cell layer (**Fig. S3**). By the selection of those non-toxic Al<sub>2</sub>O<sub>3</sub> particle concentrations for the internal concentration measurements, the investigation of vital cells was ensured.

### QUANTIFICATION OF NANOPARTICLE UPTAKE BY NEBULIZATION-ICP-MS

A quantification of the aluminum concentration inside the cells was achieved by an adjusted acid digestion method followed by neb-ICP-MS measurement. After calibration with an aluminum standard solution, the aluminum oxide content was calculated in correspondence to the area of the exposed cell monolayer. In general, a particle type-dependent increase in the uptake concentrations from the smallest (Alu1) to the micron-sized particles (Alu3) was observed (**Fig. 3**). For example, the highest aluminum oxide amounts were detected for the cells exposed to 10.4 µg Al<sub>2</sub>O<sub>3</sub>/cm<sup>2</sup> cell layer of micron-sized particles (Alu3). Further, a clear exposure concentration-dependent increase of particle amounts within cells was detected for all treatments. Additionally, the internal concentration of the middle-sized Al<sub>2</sub>O<sub>3</sub> particles (Alu2) is significantly different between the two cell lines. A twofold higher amount of aluminum oxide was measured in the lung epithelial cells compared to the skin keratinocytes after exposure to 8.3 and 10.4 µg Al<sub>2</sub>O<sub>3</sub>/cm<sup>2</sup> cell layer, respectively. This is also observed in cells exposed to the smallest particles (Alu1), whereas the difference between the internal concentrations in the two cell types is marginal and only significant for the highest exposure concentration. The relative uptake rates (% uptake) of particle internalizing cells were constant over the tested concentration range and vary between 8 (Alu1), 16-21 (Alu2), and 38-39 % (Alu3) of the totally offered material (**Fig. S4**).

## 2. Quantification of Al<sub>2</sub>O<sub>3</sub> particles in human cells

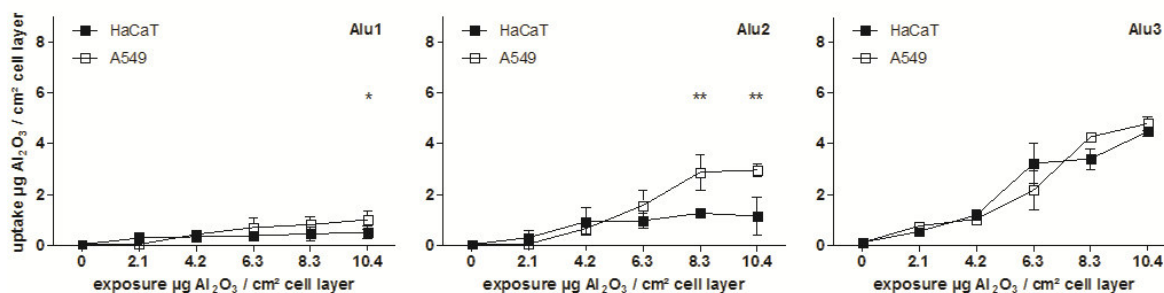


**Fig. 3** Internal concentrations of Al<sub>2</sub>O<sub>3</sub>-NP over various exposure concentrations as obtained by digestion combined with nebulization-ICP-MS measurements after 24 h of exposure. Results are presented for each particle type and cell line in one diagram. Data are shown as mean  $\pm$  standard deviation of at least three independent replicates. Significant differences between the cell lines were tested with two-way ANOVA (\* $p < 0.05$ , \*\* $p < 0.01$ )

### QUANTIFICATION OF NANOPARTICLE UPTAKE BY LA-ICP-MS

A LA-ICP-MS method was developed to quantify the amount of aluminum within cells grown on glass slides. The experimental setup was designed with the aim to avoid any further sample preparation. Since the laser ablation system is limited due to its optical properties and the quality of the plasma plume, which derives from the laser-sample-ablation process, a particle size correlated effect can be detected with this method, independent of the inserted laser energy. This results from an incomplete destruction of large particles and leads to an underestimation of signal intensities. To compensate for the occurrence of the observed particle size effects, an external calibration was performed by spiking agarose gels with the individual particle suspensions. For all particle exposed cells, a concentration-dependent increase in aluminum oxide concentration was observed (**Fig. 4**). The highest particle concentrations were measured in the cells exposed to the middle-sized particles (Alu2). A significant difference between the two cell lines was only observed for Alu1, which was taken up to a higher extent by A549 cells. Furthermore, a high variability between the replicates was observed. Regarding the obtained results for the micron-sized particles (Alu3), uptake concentrations lower than  $2.5 \mu\text{g Al}_2\text{O}_3/\text{cm}^2$  cell layer were measured. This value is 45 % lower than determined by digestion combined with neb-ICPMS experiments.

## 2. Quantification of Al<sub>2</sub>O<sub>3</sub> particles in human cells

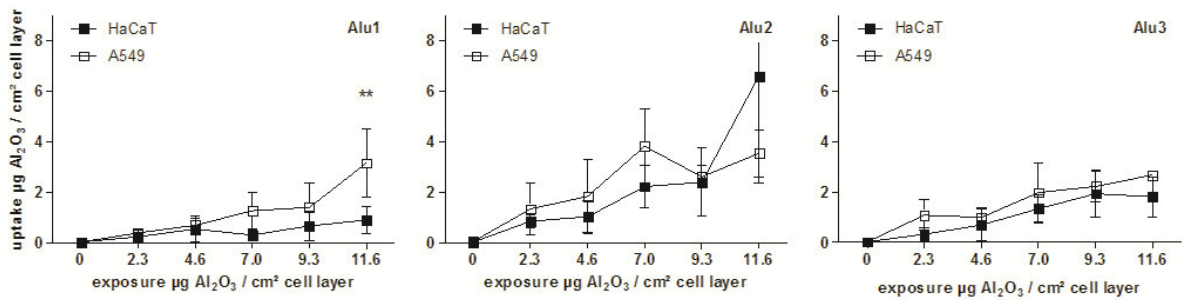


**Fig. 4** Internal concentrations of Al<sub>2</sub>O<sub>3</sub>-NP over various exposure concentrations as obtained by LA-ICP-MS measurements after 24 h of exposure. Results are presented for each particle type and cell line in one diagram. Data are shown as mean ± standard deviation of at least three independent replicates. The obtained LA-ICP-MS values are converted into the internalized particle mass by external calibration using individually spiked agarose gels. Significant differences between the cell lines were tested with two-way ANOVA (\*\*p < 0.01)

### QUANTITATIVE FLOW CYTOMETRY STUDIES

Cells treated with nanoparticles show an increase in granularity and consequently in the SSC-signal intensity, which is measurable by flow cytometry. In the first step, we established calibration curves for the three aluminum oxide particle types in a concentration range from 2 to 80 mg/l, without cells as matrices. A concentration-dependent increase in the SSC value was observed, and a linear correlation between the SSC values and the particle concentrations could be determined between 0 and 50 mg/l for all particle types. With the help of these calibration curves and by the subtraction of the SSC values for the control cells, the obtained SSC values for the exposed cells were converted into uptake concentrations of particles. Only a minor concentration-dependent increase in the signal intensity could be observed for the smallest Al<sub>2</sub>O<sub>3</sub> particles (Alu1). In contrast, the uptake concentrations detected for the middle (Alu2) and micron-sized particles (Alu3) show a clear concentration dependency (**Fig. 5**). A high variability between the replicates was observed for the micron-sized particles (Alu3). Compared to the results of neb-ICP-MS, the flow cytometry measurements are based on the unspecific optical detection of changes in the granularity of the cellular system and could not indicate significant differences between the cell lines.

## 2. Quantification of Al<sub>2</sub>O<sub>3</sub> particles in human cells

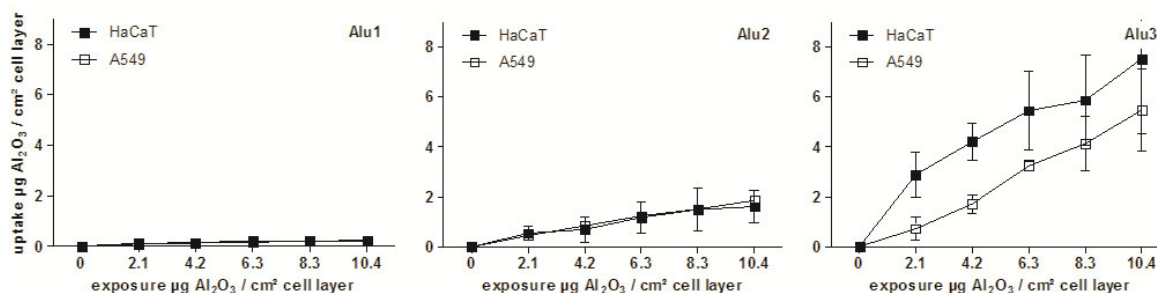


**Fig. 5** Internal concentrations of Al<sub>2</sub>O<sub>3</sub>-NP over various exposure concentrations as obtained by flow cytometry measurements after 24 h of exposure. Results are presented for each particle type and cell line in one diagram. Data are shown as mean  $\pm$  standard deviation of at least three independent replicates. The obtained SSC values are converted into the internalized particle mass by external calibration curves. Two-way ANOVA revealed no significant differences between the cell lines

## DISCUSSION

In this study, two human cell lines were exposed to three different types of aluminum oxide particles, with primary particle size medians of 14, 111, and 750 nm, respectively. The observed instability of aluminum oxide particles within cell culture media containing serum albumin by DLS measurements is in accordance with findings of Radziun et al. (2011) and Simon-Deckers et al. (2008) who showed the agglomeration and sedimentation of aluminum oxide nanoparticles in cell culture medium irrespective of the presence of fetal bovine serum. This seems to be an aluminum oxide-specific phenomenon, as serum albumin was described to stabilize, e.g., titanium dioxide or tungsten carbide nanoparticles within the relevant culture media (e.g., Ji et al. (2010) and Meißner et al. (2010)). The instability of aluminum oxide particles in cell culture medium could be due to the positive particle surface charge under physiological conditions. In our experiments, SHMP with negative binding sites was introduced as additional stabilizing agent, what could shield the particle surface by preventing an additional binding of serum albumin. By calculating the sedimentation velocity of all particles, it was estimated that all types of particles had settled completely during the exposure time of 24 h. Especially, the micron-sized particles (Alu3) settled extremely rapid with a sedimentation velocity of more than 1 m/24 h. The low sedimentation velocity of 2.5 mm/24 h for the smallest particles (Alu1) could lead

to a reduced bioavailability. This has to be considered when interpreting the uptake data.

The internalization and localization of particles in the cell cytoplasm were investigated by light and electron microscopy. Both methods revealed an accumulation and agglomeration of all types of particles in the cell cytoplasm, whereas no particles were found to be located in the cell nuclei. The homogenous distribution of the smallest (Alu1) in contrast to a heterogeneous, random localization of the micron-sized particles (Alu3) in the cell cytoplasm may be due to the size and agglomeration behavior of the particles. Furthermore, in particular, the middle-sized particles (Alu2) formed perinuclear rings, as described previously for polymer, titanium dioxide, and tungsten carbide nanoparticles (Gratton et al. 2008; Zucker et al. 2010; Busch et al. 2011). With this data we show that the same material can behave qualitatively different within cells depending on physical properties such as particle size. We also conclude that this is cell type independent, at least in our study, as the different patterns of particle distribution are similar in lung and skin cells.

Although the particles were internalized into the cells, no acute toxic effects up to a concentration of 50 mg/l and an exposure duration of 24 h were detected. Simon-Deckers et al. (2008) also described non-toxic effects of Alu1 (AEROXIDE® Alu C) toward A549 cells after 72 h of exposure to a maximum concentration of 100 µg/ml. One reason for the low toxicity is the low solubility of aluminum oxide particles, preventing the occurrence of toxic effects caused by dissolved ions which leach out of the particle surface once inside the medium or the cell. However, as an export of particles out of cells has not yet been described, no predictions for long-term or chronic effects can be derived from acute cell toxicity assays.

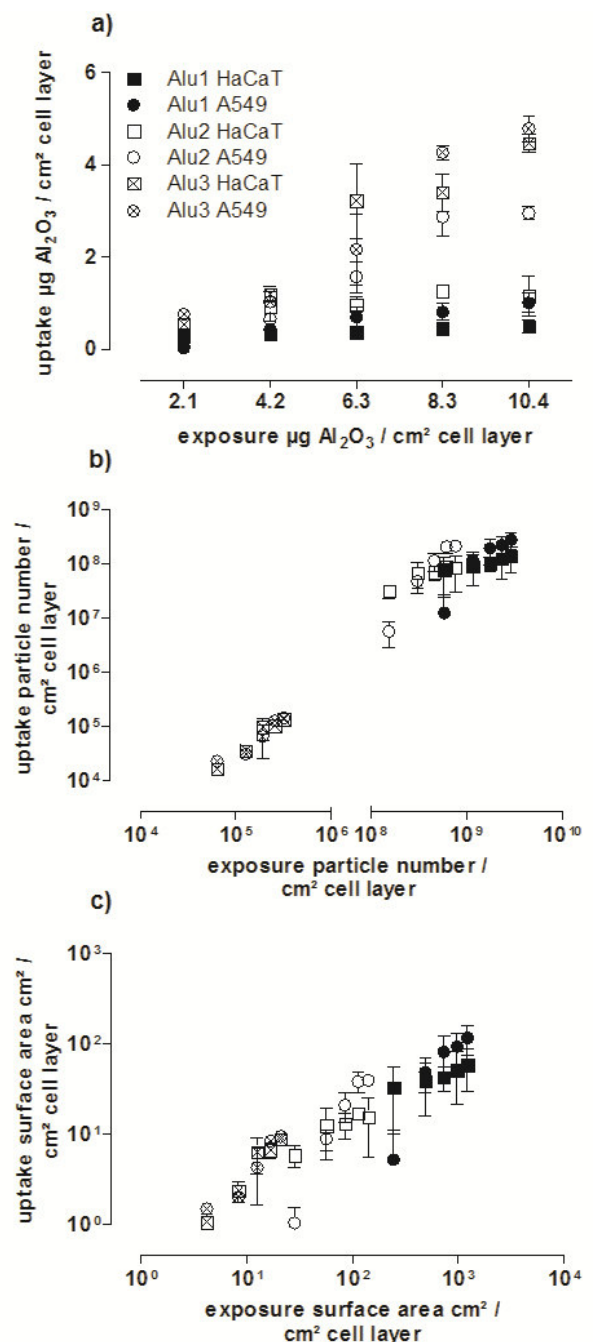
The uptake amounts of incorporated particles were quantified by digestion combined with neb-ICP-MS, LA-ICP-MS, and flow cytometry measurements. The results of all three methods confirmed a concentration-dependent particle internalization, with minor significant differences between the lung and the skin cell lines. A concentration-dependent uptake of Al<sub>2</sub>O<sub>3</sub> particles into murine and human skin fibroblasts was measured previously by Radziun et al. (2011) using ICP-OES.

In their study, only one type of a self-synthesized Al<sub>2</sub>O<sub>3</sub> particle with a median particle size of 50–80 nm and an exposure duration of 24 h was applied. The quantity of uptake reported by Radziun et al. (2011) cannot be compared with our results because they normalized it to the protein content rather than to the cell surface. In our study, additionally, a size dependency with respect to particle internalization was observed (**Fig. 6a**). Higher aluminum amounts in the cells exposed to larger particles (Alu2/3) were measured. The influence of particle size on the particle uptake may be related to the size and density-dependent sedimentation velocity. Several studies have already discussed the influences of gravitation, diffusion, and agglomeration on the bioavailability of particles to the cell monolayer (Teeguarden et al. 2007; Hinderliter et al. 2010). According to these particokinetic dosimetry considerations, it is necessary to measure the offered material to the cell surface, to calculate the effective dose, which could be magnitudes below the nominal exposure concentration. Principally, large and dense particles with a diameter >100 nm are most affected by gravitation forces, whereas particles below 100 nm are stronger influenced by diffusion processes (Teeguarden et al. 2007). Future studies should elucidate the influence of sedimentation on internal concentrations by extending the exposure times for smaller particles. In general, the cellular internalization of nanoparticles seems not to be limited by the particle size, the quantity of uptake events, or the nominal mass, as no kind of saturation effect with respect to the intracellular Al<sub>2</sub>O<sub>3</sub> amounts was detected within an exposure duration of 24 h. These observations were in contrast to the findings of Davda and Labhasetwar (2002) who described a higher efficiency of polymer nanoparticle uptake at low exposure concentrations and the achievement of a cell saturation capacity. In this case, the particle composition might have influenced the uptake behavior of the cells. In addition, another cell type was used in their study which could lead to different uptake mechanisms and uptake behavior.

In addition to the size and concentration-dependent internalization, the correlation of the internal aluminum oxide amounts and the applied particle numbers or particle surface area were analyzed (**Fig. 6b** and **6c**). The correlation of the obtained results with particle properties was performed, according to the

knowledge of measured particle characteristics, such as particle density and size. Our results indicate that with decreasing particle diameter, a larger number of particles were offered and also internalized. The same is true regarding the particle surface area. Previous studies correlated biological effects to different particle dose metrics (Oberdörster et al. 2005; Waters et al. 2009). Especially, biological responses, such as lung inflammatory responses, have been correlated with the dose metrics of mass concentration, particle number, and particle surface area in order to find the measure that is directly related to effects (Nel et al. 2006).

**Fig. 6** Correlation between the nominal exposure and measured uptake concentrations by digestion combined with neb-ICP-MS expressed by **a** particle mass, **b** particle number calculated with the hydrodynamic particle diameter, and **c** particle surface area. These comparisons included all results for both cell lines after 24 h of exposure for all test concentrations. Data are shown as mean  $\pm$  standard deviation of at least three independent replicates



So far, most studies indicate that the particle surface area could be the main influencing factor for biological effects (Oberdörster et al. 2005; Stoeger et al. 2006; Waters et al. 2009). In order to validate this correlation between offered and internalized concentrations, measured as particle surface area, additional experiments are necessary applying same concentrations of different particles. Chithrani et al. (2006) and Limbach et al. (2005) directly compared the intracellular mass concentrations with particle characteristics. In line with our study, they described a dependency of particle mass uptake on the particle size with increased internal concentrations for larger particles.

The major aim of our study was the quantification of incorporated nanomaterial applying different quantification methods. We found that the three methods show similar uptake results in a concentration range of 2-8 µg Al<sub>2</sub>O<sub>3</sub>/cm<sup>2</sup> cell layer. In **Tab. 3**, the advantages and disadvantages, also with regard to the applicability of the methods, are summarized, considering the sensitivity, precision, the efforts which are necessary for sample preparation and data evaluation, occurring detection limits and resolution capabilities. The acid digestion followed by neb-ICP-MS analysis provides reliable quantification results, a high sensitivity, and precision. Nevertheless, the required acid digestion has to be adjusted to the element composition of the investigated metal or metal-containing particles before the introduction of the sample to the measurement system. For certain dense metals or metal oxides, high temperatures and pressures are essential to avoid false negative results and to guarantee a homogenous sample after digestion. Furthermore, no spatial resolution within cells or distinction of dissolved and particulate metals is possible. This leads to reliable results regarding the concentration in a complete exposed cell monolayer but yields no information about the particle distribution inside individual cells and across the monolayer.

In addition to digestion combined with neb-ICPMS analysis, another element-specific technique was applied in this study. The LA-ICP-MS method is already well established for the element analysis of geological and archeological samples, by the application of available standard references for calibration (Russo et al. 2002).

## 2. Quantification of Al<sub>2</sub>O<sub>3</sub> particles in human cells

**Tab. 3** Method comparison of digestion combined with nebulization-ICP-MS, LA-ICP-MS, and flow cytometry considering obtained data of this study and literature data

parameter	neb-ICP-MS	LA-ICP-MS	flow cytometry
sample preparation	washing, cell counting, adjusted acid digestion	washing	washing
sensitivity	ppt-range	ppm-range	ppm-range
precision	+++	++	+
element specificity	yes	yes	none
particle size limits	none	yes	yes
calibration	solution standards	spiked agarose gels	particle slurries
measurement speed	high	low	high
data evaluation	established	complex	medium
spatial resolution	none homogenous sample	potentially high down to low $\mu\text{m}$ -range (intracellular level)	high single cells are investigated

During our experiments, the measurement system was adapted to biological samples; especially, the laser ablation of thin organic layers has been further developed. Therefore, spiked agarose gels for an external calibration approach according to earlier studies (Stärk and Wennrich 2011) were applied. The measurement of these particle spiked gels revealed a particle size effect. This effect was identified by element intensity suppression, which led to a concentration underestimation for larger particles (**Fig. 4**, Alu<sub>3</sub>). Such particle size limits have already been described in other studies (Thompson et al. 1990; Guillong and Günther 2002). The LA-ICPMS method has the advantage to require no further sample preparation. It allows the measurement of a cell layer grown and exposed on glass slides. Further developments with respect to the optical resolution promise, a direct investigation of the particle internalization on the cellular level was down to a resolution of 1  $\mu\text{m}$ , as already shown to operate by Drescher et al. (2012) and Wang et al. (2013). The method disadvantages refer to the instrumentation setup, the particle properties, and the data evaluation. Especially, particle size limits, transport efficiency of particles by the aerosol, or limits according to optical particle properties are important and have to be considered (Durrant 1999; Guillong and Günther 2002).

In comparison to the ICP-MS-based methods, the flow cytometry technique provides a rapid method that does not require a complex sample preparation and data evaluation. It is already implemented for the detection of nanoparticles in cells in a qualitative way, especially in the field of medicine (Suzuki et al. 2007; Zucker et al. 2010; Busch et al. 2011). The feasibility of this method for quantification of internalized nanomaterial has not yet been systematically investigated. In this study, it is shown that the results of this indirect method lay in a comparable range to direct element-specific analytical measurements. However, the method poses the disadvantage that the linear calibration curves can only be obtained up to a nominal concentration of 50 mg/l for all three particles, due to the interaction of the optical particle properties and the detection system. As the investigated particle concentrations within cells are much lower, these limitations did not influence the results of this study but have to be considered separately for each nanomaterial in future studies. The difficulty of the measurement of particle solutions by flow cytometry over a broad concentration range has already been described by Chandler et al. (2011). The irregular shape of cells, the detection limits regarding particle size and shape, and the optical properties of the scattering object (e.g., refractive index) were mentioned as critical points for the detection of nanoparticles within cells using flow cytometry (e.g., Chandler et al. (2011); Zucker et al. (2010); Stringer et al. (1995)). Additionally, Palecanda and Kobzik (2000) described the problem of a missing capability to distinguish between surface bound and incorporated particles. An advantage of flow cytometry is the potential combination with other biological investigations (e.g., fluorescent staining of specific proteins of interest or stress-related biomarkers). Additionally, cells are separated and measured individually, which offers a high resolution, in order to investigate single cells or e.g., the variability in the particle uptake behavior between cells. Furthermore, this method can be applied to non-metal-containing particles, such as carbon-based materials which are not accessible using ICP-MS-based methods. The optimization to correlate SSC values to typical distribution patterns or the agglomeration behavior of particles could be the task of future developments. In summary, particle size limitations of analytical methods using optical devices were demonstrated for LA-ICP-MS and flow cytometry. In addition, the results obtained with the semi-quantitative method of flow cytometry allow

conclusions about the internalization of particles within cells and concentration-dependent trends.

### ACKNOWLEDGMENTS

This research was funded by the EU FP7 project NanoValid (Development of reference methods for hazard identification, risk assessment, and LCA of engineered nanomaterials; Grant No 263147) and the German Federal Ministry for Education and Research (BMBF) project INOS (Identification and Evaluation of Health and Environmental Effects of Technical Particles at the Nanoscale; Grant #03X0013C). Additionally, S.B. was kindly supported by the Helmholtz Impulse and Networking Fund through the Helmholtz Interdisciplinary Graduate School for Environmental Research (HIGRADE).

### REFERENCES

- Au L., Zhang Q., Cobley C.M., et al. (2009). Quantifying the cellular uptake of antibody-conjugated Au nanocages by two-photon microscopy and inductively coupled plasma mass spectrometry. *ACS Nano*, 4(1): 35-42
- Bastian S., Busch W., Kühnel D., et al. (2009). Toxicity of tungsten carbide and cobalt-doped tungsten carbide nanoparticles in mammalian cells *in vitro*. *Environ Health Perspect*, 117(4): 530-536
- Becker J.S., Zoriy M., Becker J.S., et al. (2007). Laser ablation inductively coupled plasma mass spectrometry (LA-ICP-MS) in elemental imaging of biological tissues and in proteomics. *J Anal At Spectrom*, 22(7): 736-744
- Boukamp P., Petrussevska R.T., Breitkreutz D., et al. (1988). Normal keratinization in a spontaneously immortalized aneuploid human keratinocyte cell line. *J Cell Biol*, 106(3): 761-771
- Brown D.M., Wilson M.R., MacNee W., et al. (2001). Size-dependent proinflammatory effects of ultrafine polystyrene particles: a role for surface area and oxidative stress in the enhanced activity of ultrafines. *Toxicol Appl Pharmacol*, 175(3): 191-199
- Busch W., Bastian S., Trahorsch U., et al. (2011). Internalisation of engineered nanoparticles into mammalian cells *in vitro*: influence of cell type and particle properties. *J Nanopart Res*, 13(1): 293-310
- Chandler W., Yeung W., Tait J. (2011). A new microparticle size calibration standard for use in measuring smaller microparticles using a new flow cytometer. *J Thromb Haemost*, 9(6): 1216-1224
- Chithrani B.D., Ghazani A.A., Chan W.C. (2006). Determining the size and shape dependence of gold nanoparticle uptake into mammalian cells. *Nano Lett*, 6(4): 662-668

- Davda J., Labhassetwar V. (2002). Characterization of nanoparticle uptake by endothelial cells. *Int J Pharm*, 233(1): 51-59
- Drescher D., Giesen C., Traub H., et al. (2012). Quantitative imaging of gold and silver nanoparticles in single eukaryotic cells by laser ablation ICP-MS. *Anal Chem*, 84(22): 9684-9688
- Durrant S.F. (1999). Laser ablation inductively coupled plasma mass spectrometry: achievements, problems, prospects. *J Anal At Spectrom*, 14(9): 1385-1403
- Gratton S.E., Ropp P.A., Pohlhaus P.D., et al. (2008). The effect of particle design on cellular internalization pathways. *Proc Natl Acad Sci*, 105(33): 11613-11618
- Guillong M., Günther D. (2002). Effect of particle size distribution on ICP-induced elemental fractionation in laser ablation-inductively coupled plasma-mass spectrometry. *J Anal At Spectrom*, 17(8): 831-837
- Hinderliter P.M., Minard K.R., Orr G., et al. (2010). ISDD: a computational model of particle sedimentation, diffusion and target cell dosimetry for *in vitro* toxicity studies. *Part Fibre Toxicol*, 7(1): 36
- Hussain S., Boland S., Baeza-Squiban A., et al. (2009). Oxidative stress and proinflammatory effects of carbon black and titanium dioxide nanoparticles: role of particle surface area and internalized amount. *Toxicology*, 260(1): 142-149
- Ji Z., Jin X., George S., et al. (2010). Dispersion and stability optimization of TiO<sub>2</sub> nanoparticles in cell culture media. *Environ Sci Technol*, 44(19): 7309-7314
- Jiang W., Kim B.Y., Rutka J.T., and Chan W.C. (2008). Nanoparticle mediated cellular response is size-dependent. *Nat Nanotechnol*, 3(3): 145-150
- Kühnel D., Scheffler K., Wellner P., et al. (2012). Comparative evaluation of particle properties, formation of reactive oxygen species and genotoxic potential of tungsten carbide based nanoparticles *in vitro*. *J Hazard Mater*, 227: 418-426
- Limbach L.K., Li Y., Grass R.N., et al. (2005). Oxide nanoparticle uptake in human lung fibroblasts: effects of particle size, agglomeration, and diffusion at low concentrations. *Environ Sci Technol*, 39(23): 9370-9376
- Meißner T., Kühnel D., Busch W., et al. (2010). Physical-chemical characterization of tungsten carbide nanoparticles as a basis for toxicological investigations. *Nanotoxicology*, 4(2): 196-206
- Mitrano D.M., Leshner E.K., Bednar A., et al. (2012). Detecting nanoparticulate silver using single-particle inductively coupled plasma-mass spectrometry. *Environ Toxicol Chem*, 31(1): 115-121
- Nel A., Xia T., Mädler L., Li N. (2006) Toxic potential of materials at the nanolevel. *Science*, 311(5761): 622-627
- Oberdörster G., Oberdörster E., Oberdörster J. (2005). Nanotoxicology: an emerging discipline evolving from studies of ultrafine particles. *Environ Health Perspect*, 113(7): 823-839
- Palecanda A., Kobzik L. (2000). Alveolar macrophage-environmental particle interaction: analysis by flow cytometry. *Methods*, 21(3): 241-247
- Radziun E., Dudkiewicz Wilczynska J., Książek, I., et al. (2011). Assessment of the cytotoxicity of aluminium oxide nanoparticles on selected mammalian cells. *Toxicol In Vitro*, 25(8): 1694-1700

- Russo R.E., Mao X., Liu H., et al. (2002). Laser ablation in analytical chemistry - a review. *Talanta*, 57(3): 425-451
- Salata O.V. (2004). Applications of nanoparticles in biology and medicine. *J Nanobiotechnol*, 2(3)
- Simon-Deckers A., Gouget B., Mayne-L'Hermite M., et al. (2008). *In vitro* investigation of oxide nanoparticle and carbon nanotube toxicity and intracellular accumulation in A549 human pneumocytes. *Toxicology*, 253(1): 137-146
- Stärk H.-J., Wennrich R. (2011). A new approach for calibration of laser ablation inductively coupled plasma mass spectrometry using thin layers of spiked agarose gels as references. *Anal Bioanal Chem*, 399(6): 2211-2217
- Stoeger T., Reinhard C., Takenaka S., et al. (2006). Instillation of six different ultrafine carbon particles indicates a surface area threshold dose for acute lung inflammation in mice. *Environ Health Perspect*, 114(3): 328-333
- Stringer B., Imrich A., Kobzik L. (1995). Flow cytometric assay of lung macrophage uptake of environmental particulates. *Cytometry*, 20(1): 23-32
- Suzuki H., Toyooka T., Ibuki Y. (2007). Simple and easy method to evaluate uptake potential of nanoparticles in mammalian cells using a flow cytometric light scatter analysis. *Environ Sci Technol*, 41(8): 3018-3024
- Teeguarden J.G., Hinderliter P.M., Orr G., et al. (2007). Particokinetics *in vitro*: dosimetry considerations for in vitro nanoparticle toxicity assessments. *Toxicol Sci*, 95(2): 300-312
- Thompson M., Chenery S., Brett L. (1990). Nature of particulate matter produced by laser ablation-implications for tandem analytical systems. *J Anal At Spectrom*, 5(1): 49-55
- Unfried K., Albrecht C., Klotz L.-O., et al. (2007). Cellular responses to nanoparticles: target structures and mechanisms. *Nanotoxicology*, 1(1): 52-71
- Wang H., Grolimund D., Giesen C., et al. (2013). Fast chemical imaging at high spatial resolution by laser ablation inductively coupled plasma mass spectrometry. *Anal Chem*, 85(21): 10107-10116
- Waters K.M., Masiello L.M., Zangar R.C., et al. (2009). Macrophage responses to silica nanoparticles are highly conserved across particle sizes. *Toxicol Sci*, 107(2): 553-569
- Wittmaack K. (2007). In search of the most relevant parameter for quantifying lung inflammatory response to nanoparticle exposure: particle number, surface area, or what? *Environ Health Perspect*, 115(2): 187-194
- Zhang Y., Kohler N., Zhang M. (2002). Surface modification of superparamagnetic magnetite nanoparticles and their intracellular uptake. *Biomaterials*, 23(7): 1553-1561
- Zhu J., Liao L., Zhu L., et al. (2013). Size-dependent cellular uptake efficiency, mechanism, and cytotoxicity of silica nanoparticles toward HeLa cells. *Talanta*, 107: 408-415
- Zucker R., Massaro E., Sanders K., et al. (2010). Detection of TiO<sub>2</sub> nanoparticles in cells by flow cytometry. *Cytom Part A*, 77(7): 677-685

**SUPPLEMENTAL MATERIAL****Particle internalization and distribution within cells****RESULTS**

Using light microscopy particle agglomeration and sedimentation on the cell surface was observed. Particles were found to be localized inside the cells. These observations gave first evidence that particles were internalized by both cell lines. A homogenous distribution of the smallest- (Alu1) and a heterogeneous, random localization of the micron-sized particles (Alu3) was observed (**Fig. S1**). Additionally, the formation of perinuclear rings by the middle-sized particles (Alu2) occurred.

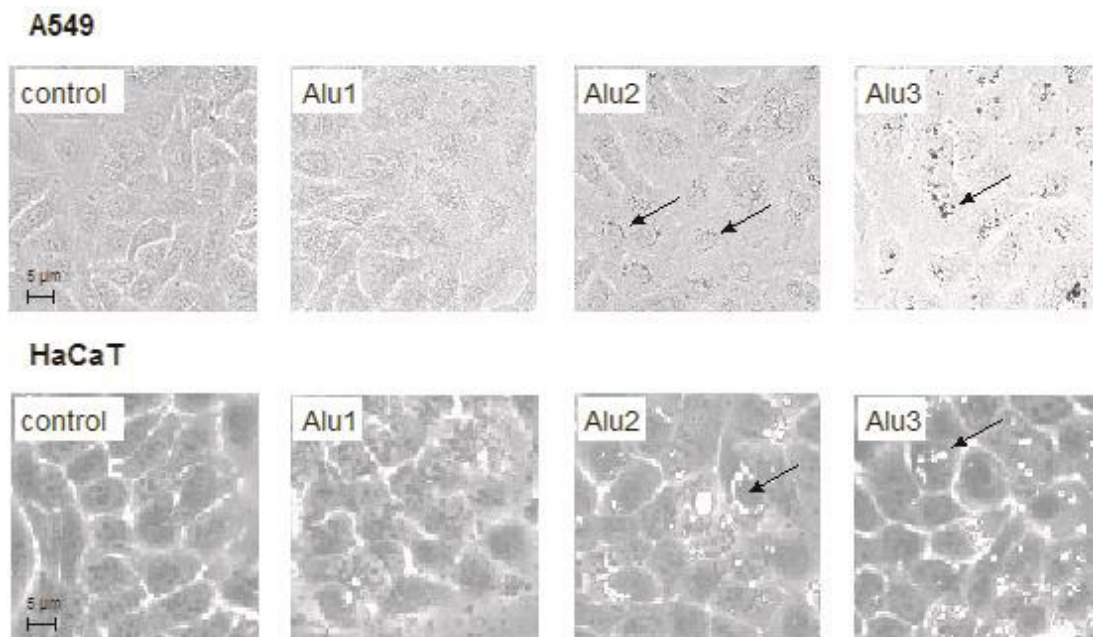
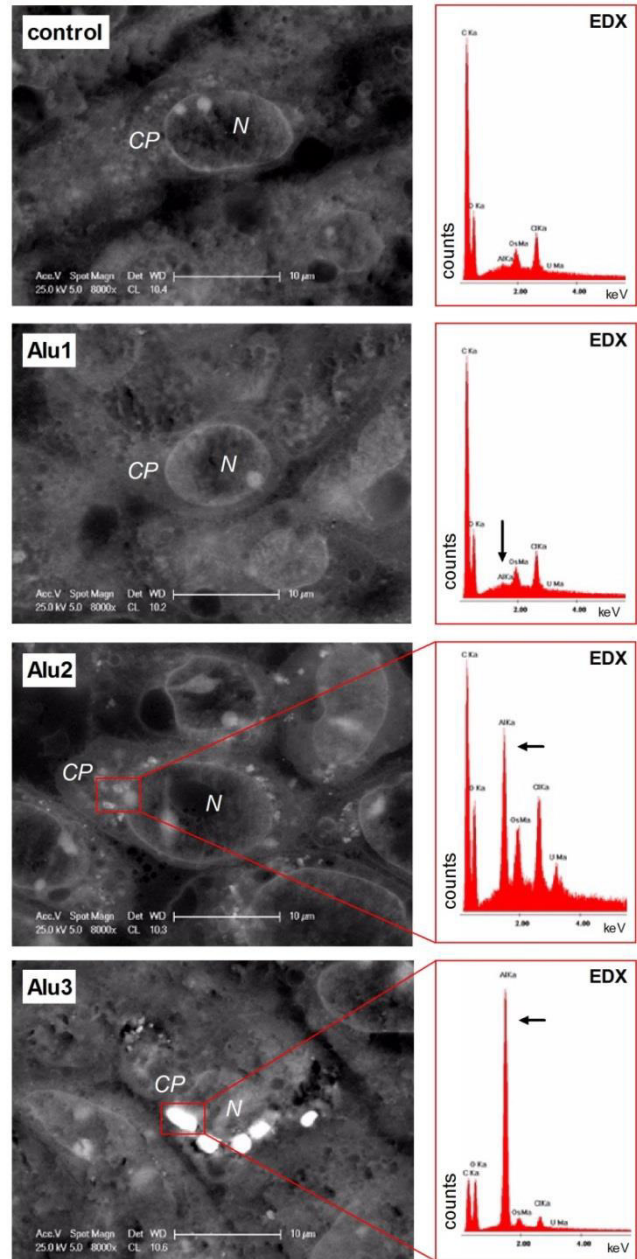


**Fig. S1** Light microscopy images of both cell lines exposed for 24 h to the three types of aluminum oxide particles at the highest test concentration (10.4 µg Al<sub>2</sub>O<sub>3</sub> / cm<sup>2</sup> cell layer). Light microscopy images were obtained with the transmission mode (A549) or the inverse mode (HaCaT). The formation of ring patterns (Alu2) or agglomerates (Alu3) within the cytoplasm is marked by an arrow

To prove the internalization of the particles into the cells, scanning electron microscopy coupled with an element detection unit (SEM / EDX) was performed with fixated and sectioned samples as described. The micrographs of the human keratinocytes (HaCaT) are shown in **Fig. S2** in addition to the results obtained for the human lung epithelial cells (A549) that are included in the article. In contrast to

the A549 cells, the internalization of the smallest particles (Alu1) in HaCaT cells could not be clearly confirmed by this method.

**Fig. S2** SEM micrographs of sections of embedded human keratinocytes (HaCaT) after 24h exposure with 10.4 µg Al<sub>2</sub>O<sub>3</sub>/cm<sup>2</sup> cell layer and medium without particles (control). Heavy elements (e.g., aluminum) appear as light areas, which were used for EDX measurements (red rectangles). Alu2 and Alu3 particles were incorporated by the cells and were located in the cell cytoplasm (CP). No particles were detected in the cell nucleus (N)



### Cell viability assays

#### MATERIALS AND METHODS

Potential toxic effects of aluminum oxide particles were investigated using a combined fluorescence cell viability test. Two different fluorescent indicator dyes were used: AlamarBlue (Biosource) to measure the cellular metabolic activity, and

5-carboxyfluorescein diacetate, acetoxymethyl ester (CFDA-AM, Molecular Probes, Eugene) to investigate changes in the cell membrane integrity. Assays were performed according to earlier protocols of Schirmer et al. (1997), which have already been successfully applied for the toxicity testing of nanoparticles in mammalian cell lines (Bastian et al. 2009; Kühnel et al. 2012). After the exposure with the particles for 24 h, cells were incubated for 30 min in the dark with the combined solution of both dyes (5 % (v/v) of AlamarBlue and 4 M CFDA-AM in PBS). Finally, the fluorescence was analyzed with a fluorescence plate reader (GENios Plus, Tecan). The wavelengths for excitation/emission were 530/595 nm for AlamarBlue and 493/541 nm for CFDA-AM. All results were related to 100 % viability concerning to water control.

## RESULTS

For all types of particles and both cell lines no toxicity could be observed even at the highest test concentration of 50 mg/l, which equals 26.3 µg Al<sub>2</sub>O<sub>3</sub>/cm<sup>2</sup> cell layer (**Fig. S3**). A slight, but not significant, decrease of the metabolic activity was observed for HaCaT cells after the exposure to the middle-sized particles (Alu2) in four of five applied concentrations.

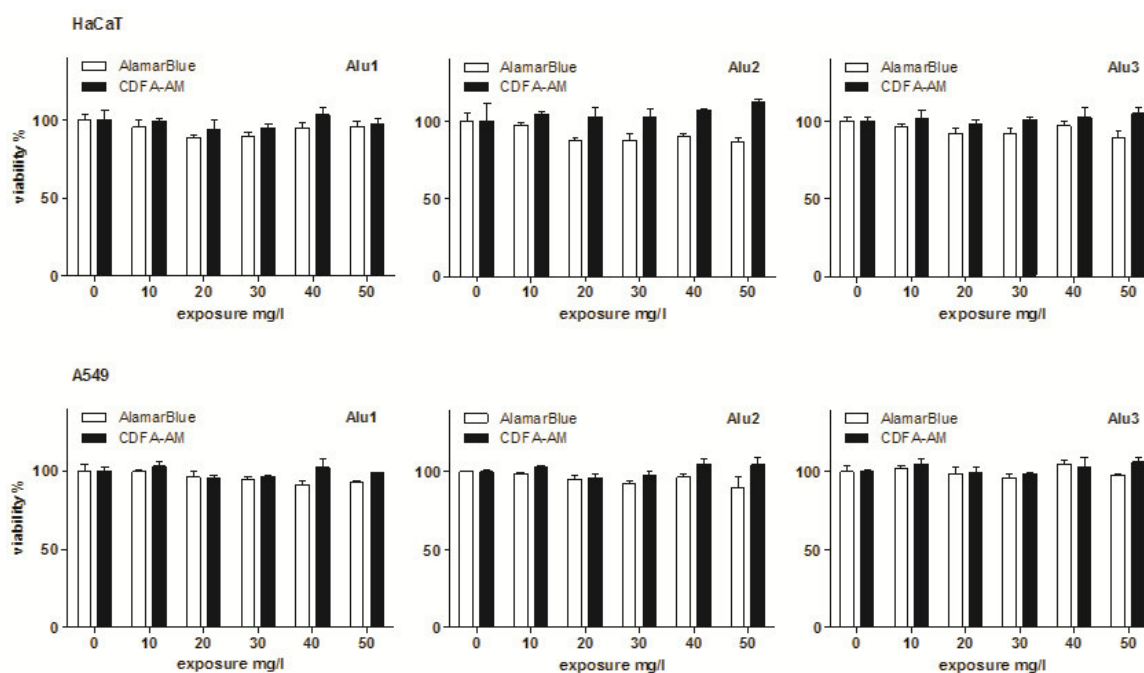


**Fig. S3** Cell viability tests after 24 h of exposure. The results measured with the two different dyes are presented in one diagram for each particle type and each cell line. Data are shown as the mean ± standard deviation of three independent biological replicates

## Quantification of nanoparticle uptake by nebulization-ICP-MS

### RESULTS

The results of the quantification of particle uptake by the cells were converted into percent of initial exposure concentrations (relative uptake rate) and are shown in **Fig. S4**.

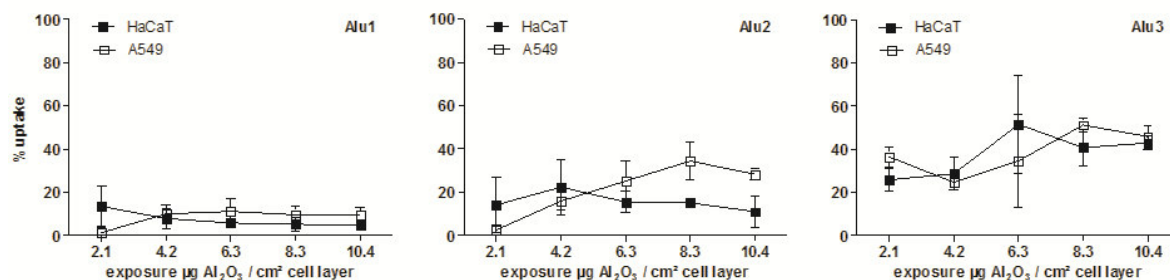


**Fig. S4** Relative uptake rates compared to initial exposure concentrations. The results are calculated by conversion of the neb-ICP-MS results. Results are presented for each particle type, both cell lines, which were exposed for 24 h, in one diagram. Data are shown as mean  $\pm$  standard deviation of at least 3 independent replicates

### References

- Bastian S., Busch W., Kühnel D., et al. (2009). Toxicity of tungsten carbide and cobalt-doped tungsten carbide nanoparticles in mammalian cells *in vitro*. *Environ Health Perspect*, 117(4): 530-536
- Kühnel D., Scheffler K., Wellner P., et al. (2012). Comparative evaluation of particle properties, formation of reactive oxygen species and genotoxic potential of tungsten carbide based nanoparticles *in vitro*. *J Hazard Mater*, 227: 418-426
- Schirmer K., Chan A., Greenberg B., et al. (1997). Methodology for demonstrating and measuring the photocytotoxicity of fluoranthene to fish cells in culture. *Toxicology in vitro*, 11(1): 107-119.



## Chapter 3

### **EXPLORING LA-ICP-MS AS A QUANTITATIVE IMAGING TECHNIQUE TO STUDY NANOPARTICLE UPTAKE IN *DAPHNIA MAGNA* AND ZEBRAFISH (*DANIO RERIO*) EMBRYOS**

Analytical Bioanalytical Chemistry (2015), 407(18): 5477-5485

Steffi Böhme<sup>1</sup>, Hans-Joachim Stärk<sup>2</sup>, Dana Kühnel<sup>1</sup>, Thorsten Reemtsma<sup>2</sup>

<sup>1</sup> Helmholtz Centre for Environmental Research - UFZ, Department of Bioanalytical Ecotoxicology, Permoserstrasse 15, 04318 Leipzig (Germany)

<sup>2</sup> Helmholtz Centre for Environmental Research - UFZ, Department of Analytical Chemistry, Permoserstrasse 15, 04318 Leipzig (Germany)



#### **ABSTRACT**

The extent and the mechanisms by which engineered nanoparticles (ENPs) are incorporated into biological tissues are a matter of intensive research. Therefore, laser ablation coupled to inductively coupled plasma mass spectrometry (LA-ICP-MS) is presented for the detection and visualization of engineered nanoparticles ( $\text{Al}_2\text{O}_3$ , Ag, and Au) in ecotoxicological test organisms (*Danio rerio* and *Daphnia magna*). While ENPs are not taken up by the zebrafish embryo but attach to its chorion, incorporation into the gut of *D. magna* is clearly visible by a 50- $\mu\text{m}$  spot ablation of 40- $\mu\text{m}$ -thick organism sections. During laser ablation of the soft organic matrix, the hard ENPs are mobilized without a significant change in their size, leading to decreasing sensitivity with increasing size of ENPs. To compensate for these effects, a matrix-matched calibration with ENPs of the same size embedded in agarose gels is proposed. Based on such a calibration, the mass of ENPs within one organism section was calculated and used to estimate the total mass of ENPs per organism. Compared to the amount determined after acid digestion of the test organisms, recoveries of 20-100 % (zebrafish embryo (ZFE)) and of 4-230 % (*D. magna*) were obtained with LODs in the low ppm range. It is likely that these differences are primarily due to an inhomogeneous particle distribution in the organisms and to shifts in the particle size distribution from the initial ENPs to those present in the organism. It appears that quantitative imaging of ENPs with LA-ICP-MS requires knowledge of the particle sizes in the biological tissue under study.

#### **INTRODUCTION**

Engineered nanoparticles (ENPs) have a huge variety of applications, while their behavior and effects in the environment are poorly known and a matter of ongoing research. Analytical methods for the determination in all environmental compartments are being developed and have to be improved as a prerequisite for studies on the fate, the uptake, and the bioaccumulation behavior of ENPs in the environment and environmental organisms, respectively.

For the determination of nanoparticle distribution in organisms or cells, visualization with optical devices is advantageous. Until now, methods such as micro-particle-induced X-ray emission (micro-PIXE) or magnetic resonance imaging (MRI) have been used [1, 2]. Other techniques often apply magnetic, fluorescent, or radio-labeled particles which may require a modification of the physical or chemical properties of the ENPs under study. For metal or metal oxide ENPs, the combination of laser ablation with element-specific detection by laser ablation coupled to inductively coupled plasma mass spectrometry (LA-ICP MS) allows their determination without the need for labeling. ICP-MS systems offer a high-sensitivity, high-precision, and wide dynamic range of up to 6 orders of magnitude [3]. LA-ICP-MS was initially established for the element detection in geological and archeological samples [4] and was later applied to determine metalloproteins and metalloenzymes after separation by gel electrophoresis [5] and to record the elemental distributions in biological tissues [6–8]. In these reports, the area studied was in the square micrometer-to-centimeter range. In order to increase the spatial resolution to a range suitable to detect single ENP and their uptake and distribution on a cellular level, the equipment as well as the software had to be improved [9–11].

When LA-ICP-MS is used not only to study the spatial distribution of elements but also to quantify their amounts, suitable calibration approaches are required. For hard geological samples, solid reference materials like glass, ceramic, and metals are available for calibration [4].

Quantification becomes more challenging from soft matrices such as biological tissues because laser ablation from such materials is less controlled [12]. A calibration approach suitable for metal ions is the use of matrix-matched standards. For example, Becker et al. [6] quantified uranium cations in rat brain sections by LA-ICP-MS using spiked rat brain tissue homogenates for calibration. The selection of a suitable matrix depends on the ablated mass and instrumental drifts during the long ablation periods (often several hours) [13]. Especially, the application of carbon as an internal standard is questionable since Frick and Günther [14] proved the separate transport of carbon in the gaseous phase and of trace elements in the particle phase. Konz et al. [13] presented an internal

standard correction methodology by the application of homogenous thin gold films on the tissue surface which can enhance the optical structure definition and increase the ablation efficiency.

While strategies for the quantification of metal ions from soft tissue by LA-ICP-MS have been developed, it is not clear, yet, how quantification works in the case that hard metal ENPs are ablated from soft tissue matrices. For the reasons given above, it appears unlikely that external calibration as for solid materials or by liquid metal standards is suitable. Often studies applied LA-ICP-MS solely as a visualization technique to gain information on the ENP distribution [15–17]. In contrast, Drescher et al. [9] deposited ENPs on a nitrocellulose membrane and analyzed the spiked material for calibration of ENPs in cells by LA-ICP-MS to obtain semi-quantitative data. Koelmel et al. [18] applied AuNP-spiked cellulose pellets as standards, and Wang et al. [19] performed quantification by the ablation of droplet residues on glass slides containing Au standards. Another way is the spiking of the respective sample material with a range of NP concentrations as presented by Judy et al. [20] for tobacco plant leaves. Recently, Böhme et al. [21] spiked agarose gels with Al<sub>2</sub>O<sub>3</sub> nanoparticles for calibration of LA-ICP-MS analysis of whole cell layers. That study showed that ENPs of different sizes may exhibit a different response. This indicates that the processes taking place during the ablation of ENPs from soft matrices and their size dependence require further investigation. If quantitative imaging by LA-ICP-MS was feasible, it would allow determining internal concentrations for specific regions or organs of small organisms and thus improve (a) to study the kinetics of uptake and internal transport and (b) to link biological effects to internal concentrations in the sensitive organ.

Therefore, this study explores the suitability of LA-ICPMS for the quantitative imaging of ENP uptake by ecotoxicological test organisms like *Daphnia magna* and zebrafish (*Danio rerio*) embryos. For methodical investigations, agarose gels as a model for soft matrices are spiked with ENPs of different qualities (Al<sub>2</sub>O<sub>3</sub>, Ag, Au) and different particle sizes and the sensitivity of detection by LA-ICP-MS is studied. In addition, we aim to investigate the potential of this calibration approach by applying it to real organisms exposed to ENPs in lab studies and comparing the

ENP concentrations determined by LA-ICP-MS with the data gathered after acid digestion of whole organisms.

## MATERIALS AND METHODS

### CHARACTERIZATION OF NANOPARTICLE SUSPENSIONS

The investigated silver and gold nanoparticle suspensions were provided and characterized in detail by partners of the EU project NanoValid (see Electronic Supplementary Material (ESM) **Tab. S1**). The silver particles are characterized by a primary particle size (PPZ) of  $21\pm 8$  nm, a polyvinylpyrrolidone (PVP) coating, and a dissolved silver fraction of 48 %. In contrast, the gold particles are stabilized by sodium citrate to prevent agglomeration processes within the suspension and have a PPZ of  $13\pm 1$  nm. The three aluminum oxide nanomaterials ( $\text{Al}_2\text{O}_3$ -NPs) were purchased as powders from industrial partners and were characterized in detail within the study of Böhme et al. [21]. Sodium hexametaphosphate (SHMP, 0.05 % (w/v); Merck KGaA) is used as a stabilizing agent for the  $\text{Al}_2\text{O}_3$  stock suspensions. In the case of  $\text{Al}_2\text{O}_3$ -NPs, the specific surface area was used to calculate the mean particle sizes of 14, 111, and 750 nm, respectively. Furthermore, dynamic light scattering (DLS) was applied to determine the particle size distribution and the zeta potential of the ENPs in the stock suspensions.

### ORGANISM CULTIVATION AND SAMPLE PREPARATION

Zebrafish embryos (*D. rerio*) were cultivated and exposed to the respective ENPs according to the OECD test guideline 236 [22]. The organisms were cultured at  $26\pm 1$  °C at a 14:10-h light/dark cycle. Fish were fed daily with *Artemia sp. ad libitum*. For the egg collection, spawn traps were placed into the fish tanks on the day prior to spawning. After selection of fertilized eggs, exposure experiments were started at a time point of 2 h post fertilization (hpf) in ISO water for 24 h with an ENP concentration of 100 µg element/L which is below the respective  $\text{EC}_{50}$  values (data not shown). The exposure of *D. magna* was performed according to the OECD test guideline 202 [23]. The crustaceans were cultivated under

controlled conditions at 20 °C at a 16:8-h light/dark cycle. Daphnids were fed three times a week with algae, and the individuals aged less than 24 h (neonates) were exposed to the respective nanomaterial in Aachener Daphnien Medium (ADaM) for 48 h with an ENP concentration of 10 µg element/L (non-toxic). After exposure, only living, healthy organisms were collected and washed twice with a medium.

For the acid digestion of whole organisms, 10 individuals of each species were collected for one sample and a minimum of three biological replicates was performed.

For the visualization by LA-ICP-MS, whole organisms were fixated with a paraformaldehyde phosphate-buffered solution, embedded with frozen section medium (Neg-50; Richard Allen Scientific), and cut in 40-µm sections using a microtome (Microm CryoStar, HM 560; Thermo Scientific) at -20 °C. The sections were placed on glass slides, and the number of sections needed for one individual organism was noted. A minimum of three independent biological replicates was performed, and one section of each individual was analyzed.

#### DETERMINATION OF THE TOTAL ELEMENT CONCENTRATIONS

A quadrupole ICP-MS (ELAN DRC-e; PerkinElmer SCIEX) was applied to analyze the element concentrations of the exposed organisms, either from solution after acid digestion or from the aerosol generated by laser ablation (see below). The acid digestion of organisms exposed to Al<sub>2</sub>O<sub>3</sub>-NPs was performed with hydrochloric acid (30 %, Suprapur; Merck) and the addition of 500 mg potassium chlorate (for analysis; Merck) in separate reaction vessels for 4 h (HPA-S, Anton Paar; temperature 250 °C, pressure 100 bar) [21]. Ag and AuNPs were solubilized by digestion in an open system (DigiPrep, S-Prep) with nitric acid (65 %, Suprapur; Merck) or *aqua regia* (3:1 HCl:HNO<sub>3</sub>), respectively. An external calibration was performed by analyzing the respective element standard reference solutions (1 g/L; Merck).

#### ENP VISUALIZATION BY LA-ICP-MS AND EXTERNAL CALIBRATION

The exposed organism sections were ablated using a Nd:YAG laser with a wavelength of 266 nm (LSX 500; CETAC, USA) (ESM **Tab. S2**). The laser energy was adjusted to 60 % ( $\sim 6 \text{ J/cm}^2$ ) to ensure a complete ablation of the organic layer. The nebulizer was used in parallel to mix the laser aerosol with a blank solution and to have constant wet plasma conditions. Due to instrument limitations (ablation chamber with long washout times), a 50- $\mu\text{m}$  spot diameter as spot size for the spot ablation was selected to avoid measurement times above 4 h for one organism section.

An external calibration was performed with individually spiked agarose gels of 40  $\mu\text{m}$  in thickness [24]. Instead of dissolved metal cations, the ENPs under study were spiked to the agarose solutions after heating (90 °C) [21]. Then, 4 ml of the agarose solution was carefully pivoted and immediately deposited on the glass slide. The gel slides were allowed to dry and analyzed by LA-ICP-MS with the same laser ablation parameters as the organism sections. Both organism sections and agarose gels had a thickness of 40  $\mu\text{m}$  (z-direction), and thus, a mass of  $\sim 100 \text{ ng}$  per spot was ablated. The measured element intensities for the ablated gel slides were corrected by a factor of 1.141 according to the concentration gradient at the boundary of the slide [24]. The transient signals for the individual spots were collected in a data matrix. By application of the external calibration curves, the intensities were transformed to concentration values. The concentration for the scale bar of the colored contour plots was determined as a particle concentration in picograms per ablated spot. In addition, LODs of the applied method can be found in ESM **Tab. S3**.

#### AEROSOL PARTICLE ANALYSIS

To determine the particle size distribution of the aerosol particles generated by laser ablation, the aerosol was collected on an adhesive carbon film placed on a SEM sample carrier for 30 s. To avoid a charge-up of the sample, the surface was sputtered with gold for 20 s. The carrier was then introduced into a scanning

electron microscope equipped with a field emission cathode (SEM, JEOL JSM-6300F). A voltage of 1.5 kV, a working distance of 8 mm, and a secondary electron image (SEI) mode were applied to gain the SEM images. To determine the particle size distribution, the mean was calculated over the measured particle sizes of ~50 particles.

#### DATA EVALUATION

The complex data received by LA-ICP-MS measurements were evaluated by self-written software obtained with MATLAB 13a (MathWorks, USA). Different parameters, like the number of measured elements, data offset, spot number, or the time between spots, can be adjusted. In detail, for each spot, a mean over the three largest values is obtained and the background is subtracted. Due to the knowledge on the total number of ablated spots and the number of spots in *x*- and *y*-direction a data matrix can be built. Finally, the data matrix containing all spot-related values, a first contour plot, and an overview of the measurement parameters was displayed by the software. The final contour plots were generated by OriginPro 9.1G (OriginLab Corporations, USA) due to a higher image quality. Therefore, the element intensities were transformed into concentration data using the matrix-matched calibration. The LA-ICP-MS contour plot was overlaid with a sample image taken before the analysis using an installed microscopic camera. For the comparison with the total element concentrations of whole organisms determined by digestion and subsequent ICP-MS measurement, the concentration determined from one section by LA-ICP-MS has to be extrapolated. Due to the fact that the organism section is completely ablated by the laser, all individual spot concentration values can be added and multiplied by the number of sections. For this purpose, the number of sections for one individual organism was noted before (18-20 sections).

## RESULTS AND DISCUSSION

### VISUALIZATION OF ENP DISTRIBUTION BY LA-ICP-MS

Within this study, a LA-ICP-MS method to visualize the ENP uptake and the distribution in the biological tissues of environmental organisms, like the zebrafish (*D. rerio*) embryo and a crustacean (*D. magna*), was developed. These organisms are established model systems for the toxicological testing of chemicals, and the available exposure protocols [22, 23] were adapted for nanomaterials. To visualize the uptake and to locate the regions of ENP accumulation within the organisms, a 50- $\mu\text{m}$  spot size provided sufficient spatial resolution and reduced the time required for data recording compared to a smaller spot size. Moreover, larger spot sizes lead to higher sensitivity because more materials per spot are ablated (ESM **Tab. S3**). From the LA-ICP-MS data of one organism section, a 2D color plot was generated and overlaid with a visual image of the same section before ablation. These overlays clearly show an inhomogeneous ENP distribution for both organisms and all studied nanomaterials (AgNPs, AuNPs, and Al<sub>2</sub>O<sub>3</sub>-NPs), with characteristic differences (**Fig. 1**, ESM **Fig. S1**).

For zebrafish embryo (ZFE), most of the particles were accumulated at the chorion, an envelope surrounding the embryo for the first days of its development (**Fig. 1**). ZFE is solely nourished from the yolk within these first days of development and cannot actively take up nutrients and, even less so, particles. This particle barrier function of the chorion is already described in the literature [25, 26].

On the contrary, the ENP distribution in *D. magna* clearly indicates active uptake, since metal signals are elevated in the gut of the organisms and minor amounts are visualized to be accumulated in the gill and eye tissues (**Fig. 1**). This finding is in agreement to other studies where the gut uptake of fluorescent polystyrene beads [27] and CuO-NPs [28] in *D. magna* was investigated by confocal and electron microscopy.

### 3. LA-ICP-MS as quantitative imaging technique

Visualization by LA-ICP-MS, indeed, shows the regions of the test organisms where different ENPs are accumulated. In addition, LA-ICP-MS parameters were optimized to limit the analysis time with sufficient spatial resolution.

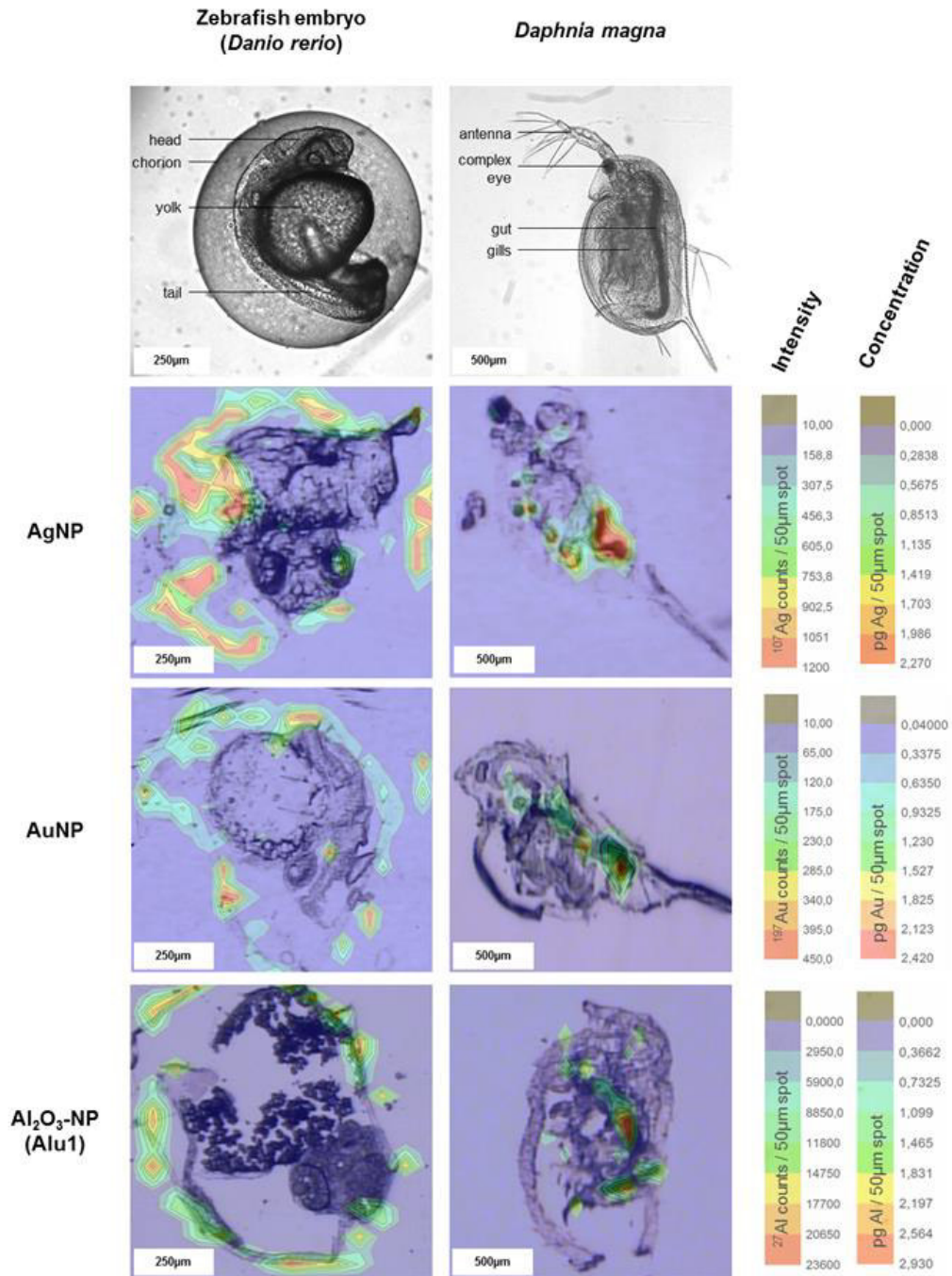


**Fig. 1** Overlay of visual images and the signal intensity for the respective element as recorded by LA-ICP-MS of ZFE (left) and *Daphnia magna* (right)

#### MATRIX-MATCHED CALIBRATION APPROACH

It appeared useful to elucidate the potential of LA-ICP-MS not only to visualize but also to quantify ENPs in biological tissues. To study the sensitivity of detection for different ENP materials as well as possible size-dependent effects, defined amounts of ENPs of Al<sub>2</sub>O<sub>3</sub>, Au, or Ag of different particle sizes were embedded in agarose gels to simulate the biological objects under study.

The response obtained by spot ablation of the ENPs from agarose gels was compared with the results determined under the same instrumental conditions for agarose gels spiked with the dissolved metal cations. For all the particles under study, linear calibration curves were obtained with low standard deviation (**Fig. 2**). The high precision indicates that an even distribution of the ENPs in the agarose gels was achieved, which is a prerequisite for this calibration approach. For all the materials, the sensitivity of detection was lower for the ENPs compared to the respective metal cation dissolved in agarose gel. This effect was weakest for Au (**Fig. 2(b)**) and more pronounced for Ag (**Fig. 2(c)**) and Al<sub>2</sub>O<sub>3</sub> (**Fig. 2(a)**). For the Al<sub>2</sub>O<sub>3</sub>-NPs, for which three particle sizes were available (mean primary particle size of 14, 110, and 750 nm), strongly decreasing signal intensities with increasing particle size were observed (**Fig. 2(a)**). For the largest particle size (750 nm), the signal intensity decreased to about 20 % of the Al<sup>3+</sup> standard.

For the three materials under investigation, the decrease in signal intensity with increasing particle size does not seem to depend so much on the respective material (**Fig. 2(d)**). Up to a particle size of approx. 100 nm, the response of the ENPs remained in the range of 50-75 % and no strong size dependency is visible. Above that size, however, the sensitivity strongly decreased. This trend could not be weakened by improved tuning of the instrument, e.g., by increasing the laser energy (data not shown).

Several processes may contribute to this size-dependent sensitivity, such as (a) a size-dependent degree of evaporation of particle material out of the soft biological matrix, (b) a variable degree of formation of small aerosol particles upon ablation, (c) a size-dependent transport efficiency for the aerosol particles from the site of

### 3. LA-ICP-MS as quantitative imaging technique

ablation to the plasma, and eventually, (d) a size-dependent extent of evaporation and ion formation from the aerosol particles in the plasma.

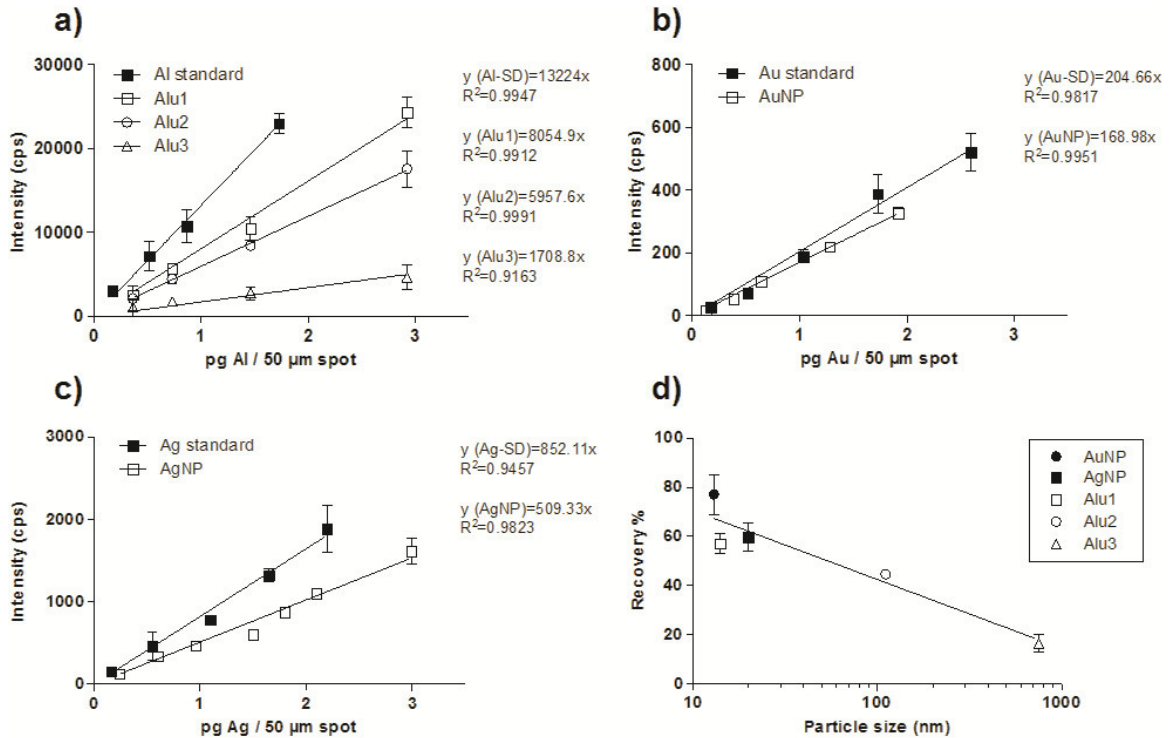


**Fig. 2** Signal intensity recorded by LA-ICP-MS for different ENPs and for metal cations (element standards) from agarose gels versus concentration of (a) Al<sub>2</sub>O<sub>3</sub>, (b) Au, and (c) Ag (n $\geq$ 3). Signal intensity for ENP relative to the respective metal cation (recovery) versus the ENP size is shown in (d)

To study this in more detail, aerosol particles generated by LA-ICP-MS from Al<sub>2</sub>O<sub>3</sub>-NPs of all the three sizes from the agarose matrix were collected on an adhesive carbon film placed on a SEM sample carrier approximately half the way between the ablation chamber and the plasma. The particle size distributions of the collected aerosols measured by SEM were in a comparable range as the initial sizes of the ENPs in suspension as determined using the BET method ( $x_{BET}$ ) (ESM **Tab. S4**). Furthermore, particle agglomerates or aggregates in the aerosol were observed which even exceeded the size of the original particles (ESM **Tab. S4**). These data suggest that, in the case of the soft tissue matrix studied here, the mobilization of ENPs occurs largely by the interaction of the laser with the organic material surrounding the ENPs and that the embedded ENPs are transferred into the gas stream with only minor reduction in size. In cases where a part of the laser energy is taken up by ENPs, this may lead to their superficial melting, allowing for

their agglomeration to even larger particles during the evaporation process. Such agglomeration has been described upon incomplete ablation from a hard material [29].

It has been shown before that an increasing diameter of the particles in the aerosol may lead to decreasing transport speed and transport efficiency towards the plasma by the gas stream [3, 30]. While, for the analysis of ENPs from suspension, their incorporation into aqueous droplets can increase the transport efficiency to almost 100 % [31], this approach is not feasible for LA-ICP-MS of soft biological matrices. Eventually, in the plasma, small particles may completely evaporate during their residence time, whereas larger particles (>150 nm) may evaporate only incompletely, leading to decreasing efficacy of evaporation and ionization in the plasma with increasing particle size [32, 30]. Therefore, in the case of ENP determination from soft tissue ablation, transport and ionization may be size dependent, all contributing to decreasing sensitivity for ENPs of increasing size.

More data of ENPs of different compositions and over a larger size range would be needed to assess whether the decrease of sensitivity with size compared to the dissolve metal cations is independent of the ENP material and whether a suitable equation can be derived to describe the relationship between particle size and the relative response obtained by LA-ICP-MS.

Based on the above findings, a quantification of ENPs from soft biological tissues by LA-ICP-MS requires a matrix-matched calibration with ENPs of similar size distribution as in the samples analyzed. The agarose gel matrix can be considered similar to the biological material in organic carbon and element composition as well as in water content. Moreover, the ENPs are embedded into the biopolymer rather than deposited only on its surface, similar to what one expects for the exposed organisms. This is different to the analysis of ENPs from thin cell layers, where ENPs deposited on the surface of glass [19] or filters [9] have been employed for matrix-matched calibration.

## QUANTIFICATION OF ENP IN ZFE AND *D. MAGNA* BY MATRIX-MATCHED CALIBRATION

The calibration graphs obtained from the ENPs embedded in agarose gels (**Fig. 2**) were used to convert the signal intensities of the LA-ICP-MS analysis of ZFE and *Daphnia* sections to the respective concentration scale (pg element/50- $\mu$ m spot). From these data, the mass of ENPs per section was calculated, and from that, the total mass of ENPs per organism was estimated by multiplying it by the number of sections per organism. To test the validity of these data, the mass of ENPs in the test organism was independently determined by acid digestion and neb-ICP-MS analysis of 10 individuals (ZFE and *D. magna*). This second approach should provide information on the true ENP concentration, provided that the ENPs are fully digested (**Tab. 1**).

**Tab. 1** Concentration of ENP in ZFE and *Daphnia magna* determined by acid digestion with neb-ICP-MS and calculated from the LA-ICP-MS data (n $\geq$ 3)

Nanomaterial	ZFE ( <i>Danio rerio</i> )			<i>Daphnia magna</i>		
	neb-ICP-MS ng / individual	LA-ICP-MS	% of digestion	neb-ICP-MS ng / individual	LA-ICP-MS	% of digestion
AgNP	5.4 $\pm$ 3.1	5.4 $\pm$ 2.9	100	0.9 $\pm$ 0.6	2.1 $\pm$ 0.5	233
AuNP	41.6 $\pm$ 18.0	8.3 $\pm$ 2.4	20	132.4 $\pm$ 33.1	5.5 $\pm$ 1.8	4
Al <sub>2</sub> O <sub>3</sub> (Alu1)	72.5 $\pm$ 8.6	27.2 $\pm$ 3.1	38	122.9 $\pm$ 43.7	4.6 $\pm$ 2.9	4
Al <sub>2</sub> O <sub>3</sub> (Alu2)	84.3 $\pm$ 29.1	81.3 $\pm$ 23.1	96	96.1 $\pm$ 36.2	6.9 $\pm$ 4.3	7
Al <sub>2</sub> O <sub>3</sub> (Alu3)	92.7 $\pm$ 26.3	64.6 $\pm$ 17.4	70	92.1 $\pm$ 33.1	6.7 $\pm$ 1.8	7

The ENP concentration for the two test organisms as determined after acidic digestion by neb-ICP-MS varies from 5 to 130 ng/individual (**Tab. 1**). Such concentrations are within the range reported in the literature, where 150 ng of Al was found in *D. magna* exposed to 20 mg/L Al<sub>2</sub>O<sub>3</sub>-NPs [33] and 30 ng of Au at an exposure concentration of 0.5 mg/L AuNPs [34]. In addition, Auffan et al. [25] showed total silver concentrations of 60-140 ng/fish embryo after the exposure to 5 mg/L AgNPs.

The validity of the quantitative imaging by LA-ICP-MS with the external matrix-matched calibration using agarose gels strongly differs for the two kinds of test organisms (**Tab. 1**). For ZFE, this approach shows a median recovery of 70 % for all the materials and particle sizes, which is an acceptable result. The variability is, however, high with lowest recovery for Au (20 %) and highest for Ag (100%). The recoveries for Al<sub>2</sub>O<sub>3</sub> were between these two extremes. However, also here, the recovery varied from 38 to 96 %, without an obvious size dependency (**Tab. 1**). These variable recoveries can, in part, be explained by the fact that (a) not the same individual was used for either analysis and that (b) for digestion and neb-ICP-MS analysis, 10 whole organisms were measured, whereas in the case of LA-ICP-MS, the data for one organism section were extrapolated to the (one) whole organism. Thus, inhomogeneous ENP distribution will contribute to different ENP concentrations determined by neb-ICP-MS and LA-ICP-MS.

The results were much worse for *D. magna*, however, with a median recovery of only 7 % (**Tab. 1**) and a difference between 4 % for Au and 233 % for Ag. Recoveries for AgNPs of >100 % for both test organisms may be explained by the fact that Ag was partially dissolved from the ENP surface and that this part experienced much better efficiency of ablation, transport, and ionization compared to the particulate Ag. For Au and Al<sub>2</sub>O<sub>3</sub>-ENP, the recovery by LA-ICP-MS in *D. magna* was extremely poor (4-7 %). Obviously, the imaging for ENPs in *D. magna* by LA-ICP-MS did not deliver valid quantitative information with the applied matrix-matched calibration.

Some of the variability in both ZFE and *D. magna* may originate from the variability of the tissue matrix as such, which may influence the ablation process. This variability cannot be compensated by internal standardization [35], but why is the analytical approach leading to reasonable data for ZFE not suited for *Daphnia*?

In the case of ZFE, the ENPs were evenly distributed over the chorion surface (**Fig. 1**); this increases the probability that the amount of ENPs determined in one section is representative for and comparable to the amount of the other sections of the organism. Moreover, it is reasonable to assume that the particles adsorbed to the chorion are mostly unchanged in size. Under these conditions, the matrix-matched calibration can sufficiently compensate the size-dependent sensitivity of

LA-ICP-MS (**Fig. 2**). As a consequence, the quantitative imaging of ENPs by LA-ICP-MS for one section is correct and the extrapolation to the whole organism provides a reasonable estimate of the amount of ENPs per ZFE organism (**Tab. 1**).

For *D. magna*, however, the images provided by LA-ICPMS clearly show that the ENPs were ingested (**Fig. 1**). Since the intestine is not evenly distributed over the whole organism, the amount of ENPs in one section may significantly differ from their amount in another section. This would explain a higher variability of the concentration data gathered for the *Daphnia* organisms. Besides that, in the gastrointestinal tract of the *D. magna*, ENPs may change their shape and size by agglomeration due to the influence of enzymes or proteins within the digestion fluid. Indeed, an enhanced agglomeration of TiO<sub>2</sub>-NPs [36] and an active in vivo biomodification of lipid-coated carbon nanotubes through digestion by *D. magna* were already reported [37]. If these processes lead to a significant particle agglomeration and thus to increasing particle sizes compared to the original ENPs, the calibration with the initial ENP size would clearly underestimate the amount of ENPs in the tissue (**Fig. 2**). This would explain the poor recovery of ENPs from *D. magna* by LA-ICP-MS (**Tab. 1**).

Due to the abovementioned difficulties of ENP quantification within *D. magna*, it appears that quantitative imaging by LA-ICP-MS requires knowledge of the particle size distribution within the organism under study. This knowledge may be gathered by electron microscopy or using other analytical methods, requiring separate sample preparation and analysis. In case that the final particle size distribution in the organism significantly differs from the initial distribution of the ENP size, a matrix-matched calibration with this final particle sizes has to be performed for valid quantitative imaging.

## CONCLUSION

As shown here for Ag, Au, and Al<sub>2</sub>O<sub>3</sub> nanoparticles, imaging by LA-ICP-MS allows to visualize ENP accumulation in *D. rerio* embryos and in *D. magna*. If combined with a visual image of the respective organism, the organ in which accumulation occurs can be determined. The increasing size of the ENPs leads to decreasing sensitivity of detection by LA-ICP-MS from soft biological tissue. As shown for sections of *D. rerio*, quantitative imaging by LA-ICP-MS is possible, when an external matrix-matched calibration is performed with the ENPs of similar size embedded in agarose gels. In this way, the extent of uptake of ENPs into organisms can be determined, internal exposure concentrations can be measured, and toxicological points of action can be identified. If the size distribution of ENPs in an organism differs from that of the initial ENP taken up by the organism, quantitative imaging becomes erroneous. It is then necessary to determine the size of ENPs in the organism for an adequate calibration and a subsequent quantification of the internal concentration of the ENP.

## ACKNOWLEDGMENTS

The authors thank Dr. Petra Göring and Monika Lelonek of the SmartMembranes GmbH for their technical support and permission to use the SEM for the investigation of the collected nanoparticle aerosol. In addition, the authors thank Sarah Reithel and Josefine Müller of the Department of Bioanalytical Ecotoxicology (UFZ) for their help in the laboratory and Wolfgang Larisch of the Department of Analytical Environmental Chemistry (UFZ) for the development of the software tool. This research was supported by EU FP7 grant (NanoValid) no. 263147. Additionally, S.B. was kindly supported by Helmholtz Impulse and Networking Fund through Helmholtz Interdisciplinary Graduate School for Environmental Research (HIGRADE).

## REFERENCES

1. Mulder W.J., Griffioen A.W., Strijkers G.J., et al. (2007). Magnetic and fluorescent nanoparticles for multimodality imaging. *Nanomedicine (Lond)*, 2: 307-324
2. Novak S., Drobne D., Valant J., and Pelicon P. (2012). Internalization of consumed TiO<sub>2</sub> nanoparticles by a model invertebrate organism. *J Nanomater*, 2012: 1-8
3. Durrant S.F. (1999). Laser ablation inductively coupled plasma mass spectrometry: achievements, problems, prospects. *J Anal At Spectrom*, 14(9): 1385-1403
4. Russo R.E., Mao X., Liu H., et al. (2002). Laser ablation in analytical chemistry - a review. *Talanta*, 57(3): 425-451
5. Becker J.S., Mounicou S., Zoriy M.V., et al. (2008). Analysis of metal-binding proteins separated by non-denaturing gel electrophoresis using matrix-assisted laser desorption/ionization mass spectrometry (MALDI-MS) and laser ablation inductively coupled plasma mass spectrometry (LA-ICP-MS). *Talanta*, 76(5): 1183-1188
6. Becker J.S., Dobrowolska J., Zoriy M., and Matusch A. (2008). Imaging of uranium on rat brain sections using laser ablation inductively coupled plasma mass spectrometry: a new tool for the study of critical substructures affined to heavy metals in tissues. *Rapid Commun Mass Spectrom*, 22(18): 2768-2772
7. Niehoff A.-C., Moosmann A., Söbbing J., et al. (2014). A palladium label to monitor nanoparticle-assisted drug delivery of a photosensitizer into tumor spheroids by elemental bioimaging. *Metallomics*, 6(1): 77-81
8. Wu B., Zoriy M., Chen Y., and Becker J.S. (2009). Imaging of nutrient elements in the leaves of *Elsholtzia splendens* by laser ablation inductively coupled plasma mass spectrometry (LA-ICP-MS). *Talanta*, 78(1): 132-137
9. Drescher D., Giesen C., Traub H., et al. (2012). Quantitative imaging of gold and silver nanoparticles in single eukaryotic cells by laser ablation ICP-MS. *Anal Chem*, 84(22): 9684-9688
10. Mueller L., Traub H., Jakubowski N., et al. (2014). Trends in single-cell analysis by use of ICP-MS. *Anal Bioanal Chem*, 406(27): 6963-6977
11. Wang H.A.O., Grolimund D., Giesen C., et al. (2013). Fast chemical imaging at high spatial resolution by laser ablation inductively coupled plasma mass spectrometry. *Anal Chem*, 85(21): 10107-10116
12. Pozebon D., Scheffler G.L., Dressler V.L., and Nunes M.A. (2014). Review of the applications of laser ablation inductively coupled plasma mass spectrometry (LA-ICP-MS) to the analysis of biological samples. *J Anal At Spectrom*, 29(12): 2204-2228
13. Konz I., Fernández B., Fernández M.L., et al. (2013). Gold internal standard correction for elemental imaging of soft tissue sections by LA-ICP-MS: element distribution in eye microstructures. *Anal Bioanal Chem*, 405(10): 3091-3096
14. Frick D.A., Günther D. (2012) Fundamental studies on the ablation behaviour of carbon in LA-ICP-MS with respect to the suitability as internal standard. *J Anal At Spectrom*, 27(8): 1294-1303
15. Büchner T., Drescher D., Traub H., et al. (2014). Relating surface-enhanced Raman scattering signals of cells to gold nanoparticle aggregation as determined by LA-ICP-MS micromapping. *Anal Bioanal Chem*, 406(27): 7003-7014

### 3. LA-ICP-MS as quantitative imaging technique

---

16. Judy J.D., Unrine J.M., Bertsch P.M. (2011). Evidence for biomagnification of gold nanoparticles within a terrestrial food chain. *Environ Sci Technol*, 45(2): 776-781
17. Wang T., Hsieh H., Hsieh Y., et al. (2012). The *in vivo* biodistribution and fate of CdSe Quantum dots in the murine model: a laser ablation inductively coupled plasma mass spectrometry study. *Anal Bioanal Chem*, 404(10): 3025-3036
18. Koelmel J., Leland T., Wang H., et al. (2013). Investigation of gold nanoparticles uptake and their tissue level distribution in rice plants by laser ablation-inductively coupled mass spectrometry. *Environ Pollut*, 174: 222-228
19. Wang M., Zheng L.-N., Wang B., et al. (2014). Quantitative analysis of gold nanoparticles in single cells by laser ablation inductively coupled plasma-mass spectrometry. *Anal Chem*, 86(20): 10252-10256
20. Judy J., Unrine J., Rao W., et al. (2012). Bioavailability of gold nanomaterials to plants: importance of particle size and surface coating. *Environ Sci Technol*, 46(15): 8467-8474
21. Böhme S., Stärk H.-J., Meißner T., et al. (2014). Quantification of Al<sub>2</sub>O<sub>3</sub> nanoparticles in human cell lines applying inductively coupled plasma mass spectrometry (neb-ICP-MS, LA-ICP-MS) and flow cytometry-based methods. *J Nanoparticle Res*, 16(9): 2592
22. OECD (2013) Test No. 236: Fish embryo acute toxicity (FET) test. OECD Publishing ([www.oecd.org](http://www.oecd.org))
23. OECD (2004) Test No. 202: *Daphnia sp.* acute immobilisation test. OECD Publishing ([www.oecd.org](http://www.oecd.org))
24. Stärk H.-J., Wennrich R. (2011). A new approach for calibration of laser ablation inductively coupled plasma mass spectrometry using thin layers of spiked agarose gels as references. *Anal Bioanal Chem*, 399(6): 2211-2217
25. Auffan M., Matson C.W., Rose J., et al. (2014). Salinity-dependent silver nanoparticle uptake and transformation by Atlantic killifish (*Fundulus heteroclitus*) embryos. *Nanotoxicology*, 8(S1): 167-176
26. Osborne O.J., Johnston B.D., Moger J., et al. (2013). Effects of particle size and coating on nanoscale Ag and TiO<sub>2</sub> exposure in zebrafish (*Danio rerio*) embryos. *Nanotoxicology*, 7(8): 1315-1324
27. Rosenkranz P., Chaudhry Q., Stone V., and Fernandes T.F. (2009). A comparison of nanoparticle and fine particle uptake by *Daphnia magna*. *Environ Toxicol Chem*, 28(10): 2142-2149
28. Heinlaan M., Kahru A., Kasemets K., et al. (2011). Changes in the *Daphnia magna* midgut upon ingestion of copper oxide nanoparticles: a transmission electron microscopy study. *Water Res*, 45(1): 179-190
29. Thompson M., Chenery S., Brett L. (1990). Nature of particulate matter produced by laser Ablation - implications for tandem analytical systems. *J Anal At Spectrom*, 5(1): 49-55
30. Guillong M., Günther D. (2002). Effect of particle size distribution on ICP-induced elemental fractionation in laser ablation-inductively coupled plasma-mass spectrometry. *J Anal At Spectrom*, 17(8): 831-837
31. Gschwind S., Hagedorfer H., Frick D.A., and Günther D. (2013). Mass quantification of nanoparticles by single droplet calibration using inductively coupled plasma mass spectrometry. *Anal Chem*, 85(12): 5875-5883

### 3. LA-ICP-MS as quantitative imaging technique

---

32. Bergum S. (2013). Combined effects of titanium dioxide nanoparticles (TiO<sub>2</sub>NPs) and benzo(a)pyrene (B(a)P) on hemocyte cells and NADPH cytochrome C reductase activity in blue mussels (*Mytilus edulis*). *Master thesis*, Norwegian University of Science and Technology
33. Hu J., Wang D., Forthaus B.E., and Wang J. (2012). Quantifying the effect of nanoparticles on As(V) ecotoxicity exemplified by nano-Fe<sub>2</sub>O<sub>3</sub> (magnetic) and nano-Al<sub>2</sub>O<sub>3</sub>. *Environ Toxicol Chem*, 31(12): 2870-2876
34. Skjolding L.M., Kern K., Hjorth R., et al. (2014). Uptake and depuration of gold nanoparticles in *Daphnia magna*. *Ecotoxicology*, 23(7): 1172-1183
35. Ellis S.R., Bruinen A.L., Heeren R.M. (2014). A critical evaluation of the current state-of-the-art in quantitative imaging mass spectrometry. *Anal Bioanal Chem*, 406(5): 1275-1289
36. Wang D., Hu J., Forthaus B.E., and Wang J. (2011). Synergistic toxic effect of nano-Al<sub>2</sub>O<sub>3</sub> and As(V) on *Ceriodaphnia dubia*. *Environ Pollut*, 159(10): 3003-3008
37. Roberts A.P., Mount A.S., Seda B., et al. (2007). *In vivo* biomodification of lipid-coated carbon nanotubes by *Daphnia magna*. *Environ Sci Technol*, 41(8): 3025-3029

## SUPPLEMENTARY INFORMATION

### Materials and methods

#### CHARACTERIZATION OF NANOPARTICLE SUSPENSIONS

The investigated silver and gold nanoparticle suspensions were provided and characterised in detail by partners of the EU-project NanoValid (**Tab. S1**). The three aluminum oxide nanomaterials ( $\text{Al}_2\text{O}_3$ -NPs) were purchased as powders from different industrial partners. These particles are named in the following as Alu1 (AEROXIDE<sup>®</sup>, Alu C, Evonik Degussa GmbH), Alu2 (TAIMICRON<sup>®</sup>, TM-DAR, Taimei Chemicals Co., LTD.) and Alu3 (NABALOX<sup>®</sup>, NO-625-10, Nabaltec AG) and were already characterized in detail by the study of Böhme et al. [1].

**Tab. S1** Chemical and physical properties of investigated nanomaterials

Nano-material	Coating	Characterization of powders			Characterization of suspensions			
		BET (m <sup>2</sup> /g)	X <sub>BET</sub> (nm)	ρ (g/cm <sup>3</sup> )	X <sub>TEM</sub> (nm)	X <sub>DLS</sub> (nm)	Zeta-potential (mV)	Stabilizing agent
AgNP	PVP	-	-	10.49	21 ± 8	117 ± 24	-19	-
AuNP	Sodium citrate	-	-	19.3	13 ± 1	18 ± 2	-38	-
Alu1 [1]	-	117	14	3.6	-	127	-58	SHMP
Alu2 [1]	-	13.5	111	3.99	-	186	-64	SHMP
Alu3 [1]	-	2	752	3.99	-	2500	-83	SHMP

#### ENP VISUALIZATION AND QUANTIFICATION BY NEB-ICP-MS AND LA-ICP-MS

A quadrupole ICP-MS (ELAN DRCE, Perkin Elmer Sclex.) was applied to analyze the element concentrations of the exposed organisms, either from solution after acid digestion or from the aerosol generated by laser ablation. The exposed organism sections were ablated by a Nd:YAG laser (LSX 500, CETAC, USA). The laser ablation parameters can be found in the **Tab. S2**. The laser energy was adjusted to 60 % to ensure a complete ablation of the organic layer and a spot

### 3. LA-ICP-MS as quantitative imaging technique

diameter of 50  $\mu\text{m}$  was applied. The nebulizer was used in parallel to mix the laser aerosol with a blank solution and to have constant wet plasma conditions.

**Tab. S2** Laser and ICP-MS parameters for the quantification and visualization of organism sections

Neb-ICP-MS		LA-ICP-MS	
ICP-MS parameters		ICP-MS parameters	
RF power (kW)	1.2	RF power (kW)	1.1
Lens voltage (V)	9.0	Lens voltage (V)	6.0
Argon nebulizer flow rate (L min <sup>-1</sup> )	0.9	Argon nebulizer flow rate (L min <sup>-1</sup> )	0.5
Argon auxiliary flow rate (L min <sup>-1</sup> )	1.2	Argon auxiliary flow rate (L min <sup>-1</sup> )	1.2
Argon makeup gas flow rate (L min <sup>-1</sup> )	0	Argon makeup gas flow rate (L min <sup>-1</sup> )	0.4
Dwell time (ms)	200	Dwell time (ms)	200
Measured isotopes (m/z)	<sup>45</sup> Sc, <sup>35</sup> Cl, <sup>66</sup> Zn, <sup>103</sup> Rh, <sup>27</sup> Al, <sup>107</sup> Ag, <sup>197</sup> Au	Measured isotopes (m/z)	<sup>13</sup> C, <sup>27</sup> Al, <sup>107</sup> Ag, <sup>197</sup> Au
Laser parameters			
		Laser energy (%)	60
		Repetition rate (Hz)	20
		Laser spot size ( $\mu\text{m}$ )	50
		Distance between spots ( $\mu\text{m}$ )	50
		Delay between spots (sec)	35
		Scanning mode	spot raster
		Analysis time	3-4 h

## Results and discussion

### VISUALIZATION OF ENP DISTRIBUTION BY LA-ICP-MS

Within this study, a LA-ICP-MS method to visualize the nanoparticle uptake and the distribution in the biological tissues of environmental organisms, like the zebrafish (*Danio rerio*) embryo and *Daphnia magna* was developed. The 2D-color plots for Alu2 and Alu3 are shown in **Fig. S1**. For ZFE most of the particles were accumulated at the chorion. On the contrary, the ENP distribution in *Daphnia magna* clearly indicates active uptake, since metal signals are elevated in the gut

### 3. LA-ICP-MS as quantitative imaging technique

of the organisms and minor amounts are visualized to be accumulated in the gill and eye tissues. The limit of detection (LOD) depends on the type of the introduced particle and the spot diameter which is used for the laser ablation itself (**Tab. S3**). In this context, an increasing spot diameter leads to an increase in the ablated area, a larger produced and evaporated volume and thus a higher detection limit. The LODs for silver and gold are lower when comparing them with the ones for aluminum, what is a result of the natural abundance of these elements which is higher for aluminum.

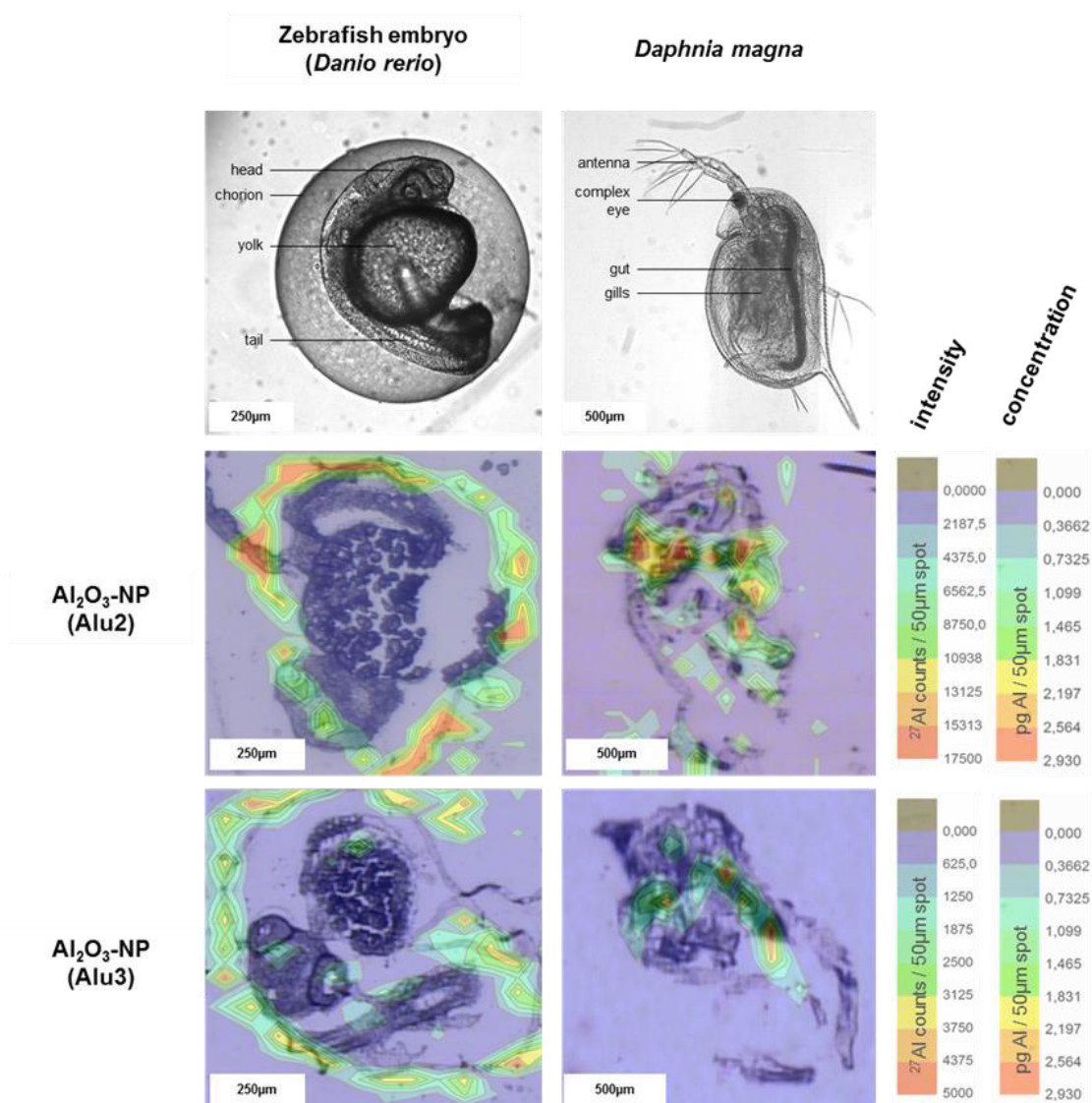


**Fig. S1** Overlay of visual images and the signal intensity for the respective element as recorded by LA-ICP-MS of ZFE (left) and *Daphnia magna* (right)

### 3. LA-ICP-MS as quantitative imaging technique

**Tab. S3** Limits of detection (LOD=Blank+3x standard deviation of the blank) for the different types of nanomaterials measured for the prepared matrix-matched standards

spot diameter	Al <sub>2</sub> O <sub>3</sub> (mean for all types of particles)	AgNP	AuNP
50 μm	500-1000 fg Al / 50μm spot	35.7 fg Ag / 50μm spot	12.5 fg Au / 50μm spot

#### MATRIX-MATCHED CALIBRATION APPROACH

To study a particle size-dependent effect in more detail, aerosol particles generated by LA-ICP-MS from Al<sub>2</sub>O<sub>3</sub>-NPs of different size from the agarose gels were collected approximately half the way between the ablation chamber and the plasma and investigated by SEM. The particle size distributions of the collected aerosols measured by SEM were in a comparable range as the initial sizes of the ENPs in suspension as determined by the BET method ( $x_{BET}$ ) what is shown in **Tab. S4**. Furthermore, particle agglomerates or aggregates in the aerosol were observed which even exceeded the size of the original particles.

**Tab. S4** Comparison of initial particle sizes and particle sizes determined with SEM after laser ablation

Nanomaterial	Initial primary particle size of the particle suspension (nm) <sup>[1]</sup>	Particle size detected after laser ablation (nm)	Size of agglomerates after laser ablation (nm)
Alu1	14	35 ± 11	239 ± 9
Alu2	111	48 ± 29	375 ± 130
Alu3	752	503 ± 367	3420 ± 1360

#### QUANTIFICATION OF ENP IN ZFE AND *DAPHNIA MAGNA* BY MATRIX-MATCHED CALIBRATION

For the comparison and validation of LA-ICP-MS results, the uptake concentrations were additionally determined by acid digestion and subsequent neb-ICP-MS analysis of whole organisms. The blank values of both methods are

listed in **Tab. S5** whereby no differences between the two organism species were observed.

**Tab. S5** Blank values of untreated organisms determined by neb-ICP-MS and LA-ICP-MS (n≥3)

Nanomaterial	µg element / L	ng element / organism
	neb-ICP-MS	LA-ICP-MS
AgNP	0.31 ± 0.09	0.32 ± 0.32
AuNP	0.36 ± 0.04	0.26 ± 0.06
Al <sub>2</sub> O <sub>3</sub> (Alu1)	1.01 ± 0.10	0.78 ± 0.11
Al <sub>2</sub> O <sub>3</sub> (Alu2)	1.00 ± 0.02	0.89 ± 0.12
Al <sub>2</sub> O <sub>3</sub> (Alu3)	1.37 ± 0.53	2.36 ± 0.30

## References

Böhme S., Stärk H.-J., Meißner T., et al. (2014). Quantification of Al<sub>2</sub>O<sub>3</sub> nanoparticles in human cell lines applying inductively coupled plasma mass spectrometry (neb-ICP-MS, LA-ICP-MS) and flow cytometry-based methods. *J Nanopart Res*, 16(9): 2592

## Chapter 4

### **THE CHORION OF THE ZEBRAFISH (*DANIO RERIO*) EMBRYO AS A BIOLOGICAL BARRIER FOR NANOPARTICLE UPTAKE?**

Submitted

Steffi Böhme<sup>1</sup>, Marta Baccaro<sup>2</sup>, Matthias Schmidt<sup>3</sup>, Annegret Potthoff<sup>4</sup>, Hans-Joachim Stärk<sup>5</sup>, Thorsten Reemtsma<sup>5</sup>, Dana Kühnel<sup>1</sup>,

<sup>1</sup> Helmholtz Centre for Environmental Research - UFZ, Department of Bioanalytical Ecotoxicology, Permoserstrasse 15, 04318 Leipzig (Germany)

<sup>2</sup> University of Siena, Department of Physical Science, Earth and Environment, Via Mattioli 4, 53100 Siena (Italy)

<sup>3</sup> Helmholtz Centre for Environmental Research - UFZ, Department Isotope Biogeochemistry, Permoserstrasse 15, 04318 Leipzig (Germany)

<sup>4</sup> Fraunhofer Institute for Ceramic Technologies and Systems - IKTS, Department of Powder and Suspension Characterization, Winterbergstrasse 28, 01277 Dresden (Germany)

<sup>5</sup> Helmholtz Centre for Environmental Research - UFZ, Department of Analytical Chemistry, Permoserstrasse 15, 04318 Leipzig (Germany)



### **ABSTRACT**

The zebrafish (*Danio rerio*) embryo (ZFE) is an established test organism to investigate the toxic potential of chemicals and can be adapted to test nanoparticles (NPs). However, there is little knowledge on the NP internalization by organisms and the underlying kinetic processes, which may differ substantially from chemicals. To shed light on this, the accumulation of metal-composed particles (Ag-, Au-, CuO-, ZnO-NP) with primary particle sizes in the range of 10-25 nm and the related metal cations was characterized in terms of temporal and spatial distribution within different ZFE compartments (egg, chorion, embryo). For ZFEs exposed to Ag-, Au-, and CuO-NPs a time-dependent adsorption of particles at the ZFE chorion structures (54-75 % of total uptake) was determined. In contrast, for ZFEs treated with ZnO-NPs lower concentrations were found to associate to the chorion (12 %) and a higher portion within the embryonic tissues (71 %). These observations were verified by the visualization of the particle distribution by LA-ICP-MS and electron microscopy. Furthermore, the percentage coverage of NPs at the chorion surface was calculated and ranged from 11 % (ZnO-NP) to 83 % (Au-NP) dependent on the agglomeration behavior of the NPs within the media. Finally, a mechanistic sorption scheme on the chemical and physical interactions of NPs and metal ions with the ZFE is presented. It is assumed that uptake of metals into the perivitelline space of ZFE is a consequence of the enrichment of NPs at the chorion surface by more than three orders of magnitude.

### **INTRODUCTION**

The zebrafish (*Danio rerio*) embryo (ZFE) toxicity test is a versatile in vitro model to assess hazard of chemicals and has been applied in several studies for the toxicological testing of nanoparticles (NPs) (e.g., Asharani et al. (2011), Brun et al. (2014), Chen et al. (2011)). The ZFE as vertebrate model species combines advantages such as a rapid development, easy maintenance in the laboratory, a large number of offspring, transparency of embryos and access to experimental manipulation to avoid extensive animal testing (Scholz et al. 2008). It allows the

observation of acute, lethal, and sublethal toxicological endpoints such as oedema, pigmentation, hatching (OECD 2013).

In order to allow estimations of the toxic potency of a substance, it is essential to determine the internal dose which triggers the occurrence of effects (Escher and Hermens 2004). The correlation between potential toxicological effects and internalized concentrations was already performed for ZFE exposed to different chemicals (Brox et al. 2014, El-Amrani et al. 2013, Kühnert et al. 2013). However, data for the association of NPs to the ZFE or specific compartments of the embryo are scarce either with regard to quantification of internalized amounts or related to the visualization of the particle distribution. For both, suitable analytical methods are needed which combine high sensitivity and high spatial resolution to detect NPs within biological tissues (Marquis et al. 2009). In recent studies mainly electron microscopy (SEM, TEM) (Asharani et al. 2008), fluorescence microscopy (Fent et al. 2010, Lin et al. 2011), and inductively coupled plasma mass spectrometry (ICP-MS) (Böhme et al. 2015, Brun et al. 2014, Chen et al. 2011) are used.

Especially, the influence of the chorion that protects the embryo until hatching on the internalization of NPs has to be systematically investigated. The complex structure of the ZFE chorion was characterized in detail by Rawson et al. (2000) and Hart and Donovan (1983). Both studies describe a three layered chorion structure which is divided in an outer zone with pore plugs, a middle fibrillar and an inner zone. In addition, the two latter zones are traversed by cone-shaped pore channels with a diameter of ~200 nm (Hart and Donovan 1983). The surface charge of the chorion is described as negative (Hart and Donovan 1983) attracting and binding positively charged metal ions (Henn 2011). The permeability of the chorion has been demonstrated and is essential for the gas supply of the embryo (Rawson et al. 2000). In addition, Bonsignorio et al. (1996) identified the molecular structure of the chorion mainly consisting of four polypeptides. In this context, the “chorion softening”, a process occurring during the first days of the embryo development can modify the composition and properties of the chorion (Kim et al. 2004). In theory, the semi-permeable chorion structure with pore channels should allow the passage of NPs into the internal parts of the ZFE, leading to the

accumulation of NPs within the perivitelline space (PVS) or at the surface of the embryo.

Previous studies on NP interaction with ZFEs were contradictory in the way that passage through the chorion as well as retention on its surface was reported. To our knowledge, only the studies of Browning et al. (2009) and Lee et al. (2013) directly showed the passage of Au-NPs (~12 nm) and stabilized Ag-NPs (5-20 nm) through the chorion pore channels. In the case of Browning et al. (2009), a dark-field optical microscopy and spectroscopy method was applied to study the transport of particles in real time.

In contrast, there are several studies describing the potential of the chorion to act as a particle barrier. For example, Osborne et al. (2013) observed a prevention of Ag-NP (10, 35 nm) and TiO<sub>2</sub>-NP (4, 10, 30, and 134 nm) internalization by the chorion. A barrier function of the chorion was additionally reported for several other NPs, namely Ru@SiO<sub>2</sub> particles (60, 200 nm) (Fent et al. 2010), as well as for CuO-, ZnO-, Co<sub>3</sub>O<sub>4</sub>-, and NiO-NPs (all NPs with primary particle size of 20-50 nm) (Lin et al. 2011). Furthermore, Auffan et al. (2014) assumed that the fish chorion acts as a protective membrane limiting the internalization of NPs or ions.

However, the NP-ZFE interaction needs to be elucidated in more detail in terms of time-dependency and the dependency on the chemical or physical properties of the particles. Therefore, in this study, the interaction of particles (Ag-, Au-, CuO-, and ZnO-NP) differing in chemical composition, particle size, and agglomeration behavior with the ZFE chorion was investigated. Specific objectives of this study were (1) the quantification of NP associated to or internalized in different compartments of the ZFE, (2) the visualization of NP distribution patterns, and (3) kinetic study of NP attachment at or within the ZFE chorion structures. By these investigations knowledge on NP-specific interaction with the model organism ZFE were gathered and points of accumulation in ZFE were identified. In addition, by the investigation of the respective metal cations the direct influence of the particulate fraction on the kinetic processes was evaluated.

## MATERIALS AND METHODS

### CHARACTERIZATION OF NANOPARTICLE POWDERS, SUSPENSIONS, AND EXPOSURE SOLUTIONS

The NPs were provided and characterized in detail by project partners of EU project NanoValid. The Ag-NPs and Au-NPs were delivered as water-based suspensions and the CuO-NPs and ZnO-NPs as powders. As coatings for the Ag-NPs polyvinyl pyrrolidone (PVP) and for Au-NPs sodium citrate was applied to prevent agglomeration processes within the suspension. The CuO-NPs were stabilized by the addition of 0.1 % tetrasodium pyrophosphate (NanoValid 2015). As for the ZnO-NPs no suitable stabilizer was found a stock suspension of 10 g/l was sonicated, abandoned to sediment for 24 h and the supernatant (~80 %) was taken as nanoscale fraction for the following characterization and biological experiments.

The exact measurement parameters for the determination of the NP primary particle size, the specific surface area (BET), the particle size distributions as well as the zeta potential in the stock suspensions can be found in the Supplemental Information. Furthermore, the stability and agglomeration behavior of particles in the exposure suspensions was investigated by dynamic light scattering (DLS). The dissolved ionic fraction within the NP exposure suspensions was measured prior to testing by ICP-MS in the supernatant after 30 min centrifugation at 16 000 g.

### ZEBRAFISH EMBRYO CULTURE, EXPOSURE, AND SAMPLE PREPARATION

Zebrafish (*Danio rerio*) embryos were exposed to the respective NPs according to the OECD test guideline 236 (OECD 2013). Fish were cultured at  $26 \pm 1$  °C at a 14 h:10 h light:dark cycle and fed daily with *Artemia spec.*. For the egg collection, spawn traps covered with a wire mesh were placed into the fish tanks on the day prior to spawning. After the selection of fertilized eggs, exposure experiments were started at 26 hours post fertilization (hpf) in ISO-water (294.0 mg/l  $\text{CaCl}_2 \cdot 2\text{H}_2\text{O}$ , 123.3 mg/l  $\text{MgSO}_4 \cdot 7\text{H}_2\text{O}$ , 63.0 mg/l  $\text{NaHCO}_3$ , and 5.5 mg/l KCl dissolved in

deionized water) for different time periods (0.5, 1, 2, 4, 8, and 24 h). The organisms were exposed to 60 µg element/l of NPs since this concentration reflects environmental relevant concentrations (Sun et al. 2014) and exerted no toxicological effects for any of the applied NPs. Elemental concentrations were measured by the collection of 1 ml of the exposure suspensions after preparation and prior to testing by ICP-MS (SI, **Tab. S1**). After exposure, only undamaged, living organisms were collected and washed in medium twice. Afterwards the NP concentration was determined in different ZFE compartments. The term “egg” refers to the embryo with intact chorion, the term “chorion” to the isolated chorion, and “embryo” to the embryonic tissue remaining after mechanical dechoriation with forceps. For the quantification of NP internalization, 4 of the respective organism compartments were pooled to obtain one sample and a minimum of 3 replicates were performed. For the visualization of the elemental distribution by LA-ICP-MS, exposed organisms were fixated, embedded in frozen section medium and cut in 40 µm sections by a microtome at -20 °C as described previously (Böhme et al. 2015). In parallel, all experiments were performed with the respective metal salt solutions (AgNO<sub>3</sub>, CuSO<sub>4</sub>\*5H<sub>2</sub>O, ZnSO<sub>4</sub>\*7H<sub>2</sub>O; 60 µg element/l) as positive controls and to assess the impact of the dissolved ionic fraction. The Au-NPs are inert and no dissolution is expected.

#### QUANTIFICATION OF TOTAL ELEMENT CONCENTRATIONS

In order to analyze the total elemental concentrations in exposed organisms, samples were subjected to an acid digestion system (DigiPrep, S-Prep) to generate homogeneous fluid samples. Therefore, the acid digestion was adjusted to the physico-chemical properties of the individual NPs. Samples exposed to Ag- and CuO-NPs were digested with nitric acid (65 %, suprapur, Merck) whereas those exposed to Au- and ZnO-NPs were digested with *aqua regia* (v/v HCl/HNO<sub>3</sub>, 3/1). The digested samples are subsequently analyzed by a quadrupole-based ICP-MS (ELAN DRCe, Perkin Elmer Sciex.) to determine the elemental concentrations. An external calibration was performed by analyzing elemental standard reference solutions. For all experiments untreated organisms were taken as negative controls (blank) (SI, **Tab. S2**) and the blank results were

subtracted from the ones measured for exposed organisms. The NP-percentage for the PVS was calculated by the subtraction of the chorion and embryo concentrations from the total amounts determined for the egg.

#### VISUALIZATION BY LASER ABLATION ICP-MS

The organism sections placed on glass slides were introduced into the ablation chamber and ablated by a Nd:YAG laser with a wavelength of 266 nm (LSX 500, CETAC). The laser energy was adjusted to 60 % to ensure a complete ablation of the organic layer. The spot ablation was performed with a 50 µm spot diameter for sufficient imaging. The generated particle aerosol is directly transported and introduced to the ICP-MS via an additional argon gas stream. The external calibration was performed by the ablation of individually particle spiked agarose gels according to an earlier protocol (Böhme et al. 2014). The transient intensity signals for the individual spots were collected in a data matrix, transformed to concentration values by the calibration curves and plotted as 2D-color images as described earlier (Böhme et al. 2015). For all experiments untreated organisms were measured as control (blank) (SI, **Fig. S1**). For Zn and Cu a higher natural abundance was observed and thus the blank intensities were subtracted from the sample intensities to obtain the final images.

#### ANALYSIS OF PARTICLE ACCUMULATION BY ELECTRON MICROSCOPY

In order to confirm the NP localization determined by LA-ICP-MS and to gain more detailed insights into whether particles attach at or within the chorion structure, organisms exposed for 24 h were subjected to electron microscopy. Organisms were washed and fixated as mentioned above, placed on SEM-stubs with an adhesive carbon foil and dried at room temperature for 2 h. In order to increase the conductivity, a 10 nm chromium layer was inductively sputtered onto the biological samples. Chromium was chosen instead of the commonly used Au/Pd, because its X-ray lines are well separated from those of Au, Ag, Cu, and Zn, respectively. The samples were subsequently investigated by a scanning electron microscope (SEM, Zeiss Merlin VP compact) equipped with an energy-dispersive

X-ray spectroscopy detector (EDX detecting unit, Bruker Quantax) for elemental analysis. With respect to the X-ray lines the following accelerating voltages were applied for the respective element: 2.5 (Au-, CuO-NP), 3.0 (ZnO-NP), 4.5 (Ag-NP), and 5 kV for controls.

#### CALCULATION OF CHORION SURFACE COVERAGE BY PARTICLES

In order to estimate the percentage of the chorion surface covered by NPs, the ratio between the theoretical and experimental number of particles covering the ZFE chorion surface was calculated.

The theoretical number was calculated assuming that the chorion surface area is the surface of a spherical egg of 700  $\mu\text{m}$  diameter (corresponds to 1.5  $\text{mm}^2$ ). The measured hydrodynamic particle size was then extrapolated to the minimal possible surface area of a square what represents the contact area. The total surface area of the chorion was subsequently divided through the surface area of the square area to obtain the theoretical particle number able to totally cover the chorion surface.

The experimental number of particles was determined by calculating the mass of one particle by the knowledge of the material density, the particle size, and the particle volume. The concentrations determined for the chorion compartment after different time periods were used as reference values. In the case of CuO and ZnO-NPs the elemental concentrations were converted into the respective metal oxide concentrations. By dividing the amount of the element at the chorion as determined by digestion and neb-ICP-MS by the mass of one particle the experimental number of particles was obtained.

For simplification, this calculation neither regarded the close-packing of spheres at the surface, nor the option that particles may be located inside the chorion pore channels. The time-dependent agglomeration of NPs within the media was included by the hydrodynamic particle size; however, the fractal structure of the formed agglomerates was not included in the calculation. This may lead to an overestimation of the mass for particle agglomerates and in turn results in an underestimation of the coverage.

## RESULTS

### CHARACTERIZATION OF NANOPARTICLE POWDERS, STOCK, AND EXPOSURE SUSPENSIONS

The Ag-, Au-, CuO-, and ZnO-NPs investigated in this study were provided and characterized in detail by partners within the EU project NanoValid ([www.nanovalid.eu](http://www.nanovalid.eu)) (SI, **Tab. S3**). The primary particle sizes of all NPs are in a range of 10-25 nm. The hydrodynamic particle sizes measured for the exposure suspensions in ISO-water differ in the following range:  $18 \pm 2$  nm (Au-NP) <  $80 \pm 1$  nm (ZnO-NP) <  $117 \pm 24$  nm (Ag-NP) <  $132 \pm 2$  nm (CuO-NP) at the start of the experiments. After 24 h of exposure, sizes of 204 nm (Ag-NP), 420 nm (CuO-NP), and  $>5 \mu\text{m}$  for Au- and ZnO-NPs were measured in the exposure suspensions, indicating a strong agglomeration of particles within the media. The dissolved fraction of the respective particle exposure suspensions was determined to be  $48.3 \pm 7.2$  % Ag (Ag-NP),  $9.8 \pm 5.5$  % Cu (CuO-NP), and  $58.1 \pm 2.6$  % Zn (ZnO-NP). For the majority of the NP exposure suspensions a significant difference between nominal and measured elemental concentrations prior to testing was observed (average recovery for all NPs: 68 %) (SI, **Tab. S1**).

### CALCULATION OF INTERNAL NANOPARTICLE CONCENTRATIONS

After exposure to  $60 \mu\text{g element/l}$ , the NP uptake into the egg as a whole, and its different compartments, namely the chorion, the perivitelline space (PVS) and the embryo was determined by neb-ICP-MS after acid digestion. The NP exposure suspensions used in these experiments contained metal (oxide) NPs but also dissolved metal cations as mentioned in the previous chapter. Therefore, metal concentrations determined inside exposed ZFEs may originate from the uptake of either NPs or dissolved metal cations. To distinguish between the two, a parallel experiment was performed in which ZFEs were exposed to the respective metal salts (SI, **Fig. S2**) and the amounts of metals inside the ZFEs were determined (SI, **Tab. S4**). The measured Au-NP concentrations were corrected by blank values. Assuming that the metal concentration determined in the different

compartments of the ZFE was linearly related to the external dissolved concentration these data were used to correct the internal concentrations determined in ZFEs exposed to NPs for the respective dissolved concentrations found in the NP suspensions (**Fig. 1**).

Furthermore, a time-dependent increase in the metal concentrations of NP treated ZFEs was solely observed up to 2 h of exposure. For exposure periods of 2-24 h no further increase in the determined concentrations for the egg, the chorion and the embryo were observed. Therefore, the concentrations and percentages for that exposure period (2-24 h) are calculated as time-averaged values. The exact elemental concentrations measured for the ZFEs exposed to different NPs at individual time periods are provided as Supplemental Material (SI, **Tab. S4**).

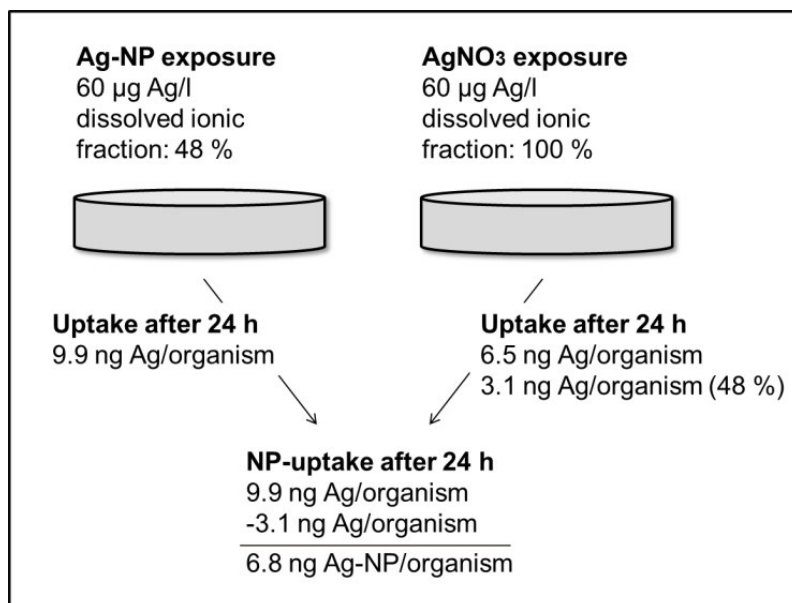


**Fig. 1:** Scheme on the calculation of NP-uptake concentrations by subtraction of the respective elemental amounts of the related dissolved ionic fraction measured for organisms exposed to metal salt solutions (exemplarily shown for Ag-NP treatment).

#### TIME-DEPENDENT NP INTERNALIZATION BY DIFFERENT ZFE COMPARTMENTS

For all particle types a time-dependent increase in the total concentrations measured for the eggs were observed up to 2 h of exposure. The mean over the exposure periods (2-24 h) ranged from 2.3 (CuO-NP), 2.4 (ZnO-NP), 6.2 (Ag-NP) to 11.9 (Au-NP) ng element/organism (**Fig. 2**).

#### 4. The zebrafish embryo chorion as potential biological barrier

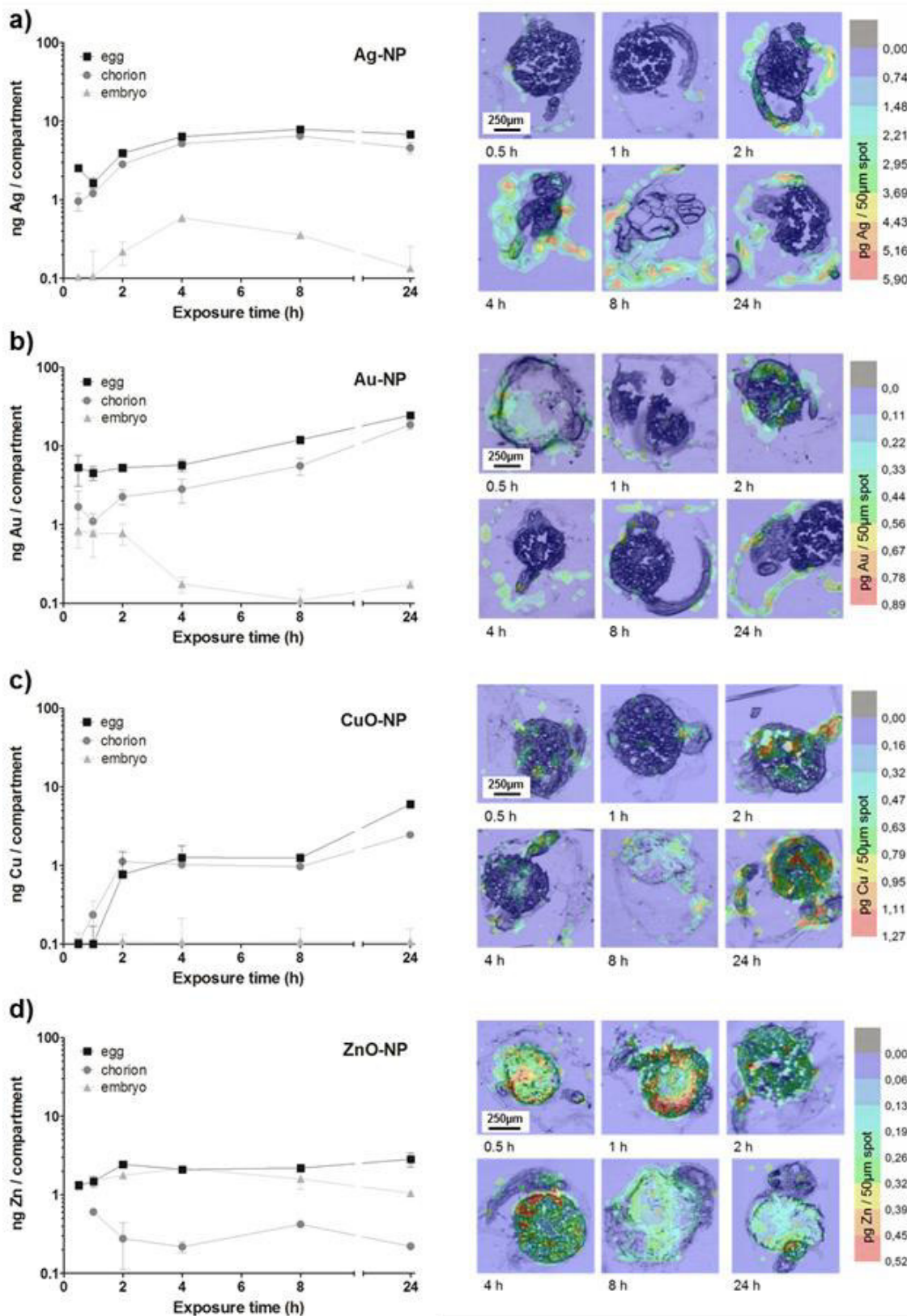


**Fig. 2:** Time resolved data for elemental concentrations in ZFE after exposure to 60 µg/l NPs ( $n \geq 3$ , shown as mean  $\pm$  SD) for a) Ag-, b) Au-, c) CuO-, and d) ZnO-NP. Concentrations determined after acid digestion by neb-ICP-MS (note the logarithmic y-axis) (left column) and visualization of the elemental concentrations by LA-ICP-MS (right column).

#### 4. The zebrafish embryo chorion as potential biological barrier

For Ag-, Au-, and CuO-NPs the chorion structure was identified as main compartment of accumulation attributing 54 % (Au-NP), 75 % (CuO-NP), and 76 % (Ag-NP) of the total concentration, respectively (**Tab. 1**). For ZFEs exposed to ZnO-NPs, however, only 12 % were associated to the chorion. Correspondingly, the relative metal amount determined in the embryo was low for Ag-, Au-, and CuO-NP treated organisms and ranged from 5 % (Au-NP) to 6 % (CuO-NP), while 71 % were measured for ZnO-NPs (**Tab. 1**). Finally, the metal content in the PVS was calculated as the difference between the total metal amount in the ZFE and the sum of chorion and embryo. For Ag-, CuO-, and ZnO-NPs (and all exposure times) the PVS contributed to about 20 % of the total internal concentration, while for Au-NP it was 42 % (**Tab. 1**).

**Tab. 1:** Time-averaged values (2-24 h) of the percentage concentrations of the chorion and embryo related to the total elemental amounts measured for the eggs exposed to 60 µg/l (n≥3). After subtraction of chorion and embryo concentrations from the amounts determined for the total egg, the remaining percentage is assigned to the perivitelline space.

Nanoparticle	Adsorption chorion (%)	Uptake embryo(%)	Uptake perivitelline space (%)
Ag-NP	75.7 ± 6.3	5.3 ± 2.6	19.0 ± 8.3
Au-NP	53.7 ± 13.1	4.8 ± 5.8	41.5 ± 11.0
CuO-NP	75.1 ± 21.5	6.1 ± 3.5	21.6 ± 20.4
ZnO-NP	12.2 ± 4.2	70.5 ± 22.3	19.9 ± 19.2

In addition, the elemental distribution in the ZFE after different exposure periods was visualized by LA-ICP-MS according to Böhme et al. (2015) (**Fig. 2**, right column). For Ag-NPs and Au-NPs (**Fig. 2a, b**) the same distribution patterns are observed, with the chorion structure being the main accumulation point (red colored areas). Furthermore, the time-dependent increase of NP amounts for the chorion structure is clearly visible. For ZnO-NPs, the embryonic tissue can be clearly identified as the area with the highest element concentrations (**Fig. 2d**). For CuO-NPs, however, neither an accumulation at the chorion nor a clear increase in metal concentrations for the embryonic tissues can be observed (**Fig. 2c**). In this case the imaging data obtained by LA-ICP-MS (right column) do not agree to the results. Since the LA-ICP-MS method applied is a semi-quantitative imaging

technique, recording concentrations for a thin section of the whole organism, a direct comparison to the quantitative amounts measured by neb-ICP-MS was not performed.

#### ELECTRON MICROSCOPY STUDIES ON THE ZFE CHORION

Scanning electron microscopy was applied to observe the sorption and agglomeration behavior of the NPs at the ZFE chorion structures in more detail. All types of NPs (Ag-, Au-, CuO-, ZnO-NPs) were detected at the chorion surface and their chemical identity was verified by EDX mapping and the measurement of EDX spectra for the respective elements (**Fig. 3**). In addition, for Au- and CuO-NPs a particle agglomeration was observed in selected regions of interest. However, the Ag- and ZnO-NPs were more difficult to identify in the particulate state, probably due to the high dissolution rates. Rather, these two elements were found to be homogeneously distributed over the chorion surface. However, the presence of NPs in the pore channels or the association of particles to other chorion structures is difficult to assess by this method.

#### CALCULATION OF ZFE CHORION COVERAGE BY NANOPARTICLES

In order to better understand the accumulation of NPs at the ZFE chorion the number of particles covering the chorion surface was calculated according to the measured NP concentrations for this compartment. In this context, we refer to a theoretical formation of a particle monolayer and the hydrodynamic diameter of particles within the exposure medium as it was determined over the experiment time. The detailed calculation procedure is described in the materials and methods part.

For example, for Ag-NPs a number of 62 million particles would result in a full surface coverage. A concentration of 4.6 ng/chorion after 24 h exposure was determined, corresponding to an experimental particle number of 12 million particles and 21 % chorion coverage (**Tab. 2**).

#### 4. The zebrafish embryo chorion as potential biological barrier

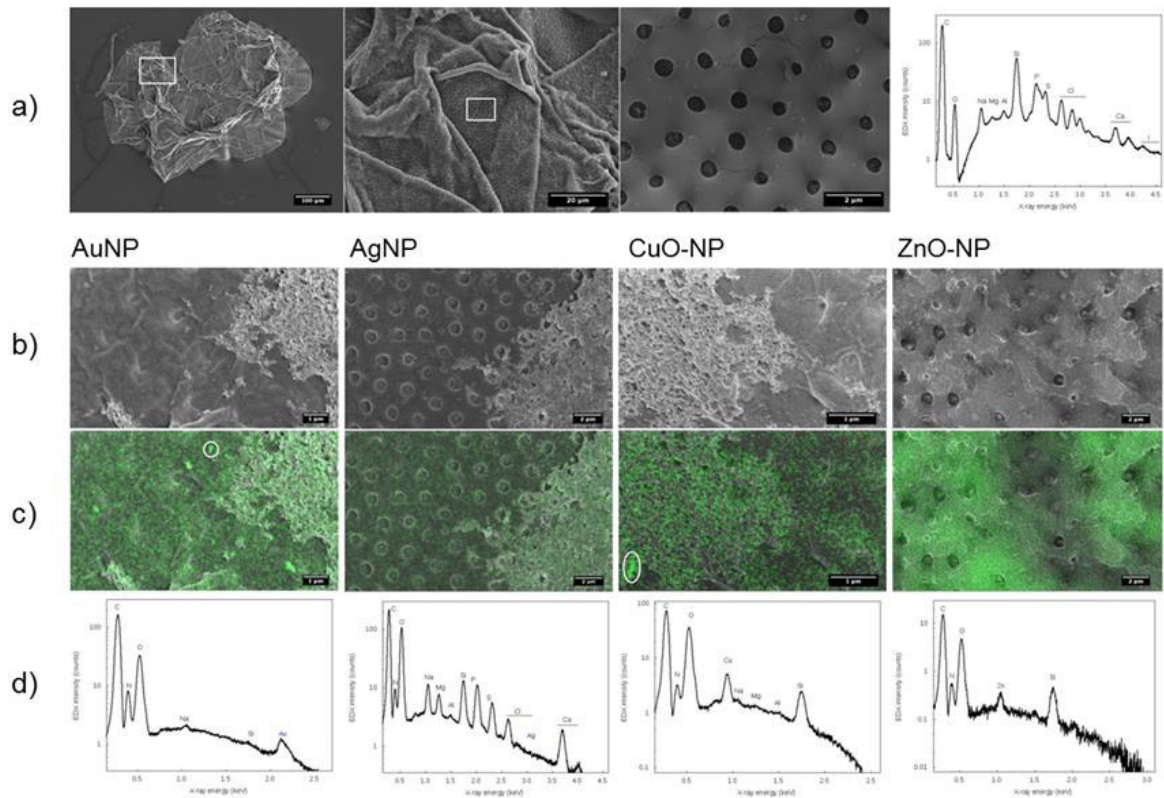


**Fig. 3:** SEM+EDX investigations at the ZFE chorion surface with a) representative images and spectra of the control (untreated chorion). Electron microscopic pictures for each NP (b), overlay with the EDX map of the respective element (c), and the EDX spectra (d) for the whole area (Ag-, ZnO-NP) or for selected regions of interest (Au-, CuO-NP) are shown.

The NPs show variations in percentage of surface coverage, in the order of ZnO-NP (11 %) < Ag-NP (21 %) < CuO-NP (32 %) < Au-NP (83 %) after 24 h of exposure. In general, the coverage of the ZFE chorion is time-dependent with trends towards increasing coverage for longer exposure periods (SI, **Tab. S5**). With knowledge on the thickness of the chorion (~2 μm), the chorion surface area (1.5 mm<sup>2</sup>), and the average NP concentration (~3 ng) determined for the chorion, the enrichment of NPs by adsorption to the chorion can be estimated with ~10 000-fold higher concentrations in comparison to the external NP exposure suspension.

#### 4. The zebrafish embryo chorion as potential biological barrier

**Tab. 2:** Coverage of the ZFE chorion surface by NPs according to the hydrodynamic particle sizes after exposure to 60 µg/l calculated as mean over 2-24 h exposure period values. The theoretical particle number refers to the calculated number of particles able to attach to the chorion surface. The experimental particle number was calculated by the determined elemental concentrations for the chorion and the respective hydrodynamic particle diameter.

Nanoparticle	Theoretical particle number	Experimental particle number	Coverage (%)
Ag-NP	61 800 000	11 700 000	21
Au-NP	2 700 000	8 550 000	83
CuO-NP	37 700 000	5 300 000	32
ZnO-NP	2 200 000	30 000	11

## DISCUSSION

In this study, zebrafish (*Danio rerio*) embryos were exposed to different types of nanoparticles and the corresponding metal salt solutions (except for Au) with the aim to (1) quantify the amount of the respective element associated to different ZFE compartments, (2) identify specific areas of accumulation for each material, and (3) gain information on the time-dependency of NP-ZFE interaction. Therefore, concentrations related to the NP-fraction were calculated by the measurement of both, ZFEs exposed to NPs and the respective metal salts. Distinct differences with regard to spatial and temporal distribution of the four NPs were observed.

Over the exposure period of 24 h, the formation of agglomerates in the exposure solution was especially observed for Au- and ZnO-NPs, leading to hydrodynamic particle sizes of >5 µm. The formation of large Au-NP agglomerates detected by DLS can be explained by a competition between the NP sodium citrate coating and ions within the exposure medium leading to a partly destruction of the capping and a subsequent formation of agglomerates. Furthermore, a high dissolved ionic fraction was detected for Ag-NPs ( $48.3 \pm 7.2$  %) and ZnO-NPs ( $58.1 \pm 2.6$  %). High dissolved ionic fractions within media were previously reported with values of 20-53 % for ZnO-NPs and 12-38 % for Ag-NPs (Brun et al. 2014, Wang and Wang 2014). This continuous release of ions from the NP surface can lead to a total NP dissolution as described for ZnO-NPs by Lopes et al. (2014).

The quantification of NP concentrations in the individual ZFE compartments revealed the ZFE chorion as main accumulation site with 54 % (Au-NP) to ~76 % (Ag- and CuO-NP) of the total internal concentrations in the whole egg (**Tab. 1**). The high sorption of NPs to the chorion structure was previously reported and quantified by Auffan et al. (2014) with a percentage of 58 to 85 % of Ag-NPs to be accumulated at the chorion after a 48 h exposure to 5 mg/l.

In contrast, low zinc concentrations were measured for the chorion of ZFEs, whereas higher concentrations were determined for the embryo comprising 71 % of the whole organism uptake (**Tab. 1**). These amounts are in agreement with the quantitative results of Brun et al. (2014), showing a dose-dependent zinc accumulation for the embryo (~80 %) after 48 and 96 h exposure with up to 5 mg/l ZnO-NPs. One reason for the high zinc concentrations determined for the embryo compartment can be an additional release of zinc ions by these NPs during the exposure period as observed by suppressed particle number events measured via DLS (data not shown). The dissolution of ZnO-NPs reflects the higher solubility of ZnO in comparison to the other applied materials, e.g. CuO (Chang et al. 2012).

Interestingly, the calculated percentage for each element in the PVS ranged around 20 % except for Au-NPs, for which 42 % of the total amounts were found in the PVS. This percentage is related to NPs, however, a subsequent release of dissolved metal cations from the NP surface is possible (Wang and Wang 2014), but cannot be distinguished with the applied methods. Related to the external element concentration of 60 µg/l and a theoretical PVS volume of 600 nl, the concentrations calculated for the PVS are approximately 20-times higher.

#### MECHANISTIC CHORION ADSORPTION SCHEME

By combining the information obtained on dose, distribution and the time-course of the NP and metal cation association to ZFEs, a mechanistic adsorption scheme of the interactions is proposed (**Fig. 4**). However, the scheme on mechanistic interactions presented here is not considered representative to all specific NP interactions with biological membranes. The model consists of three subsequent steps:

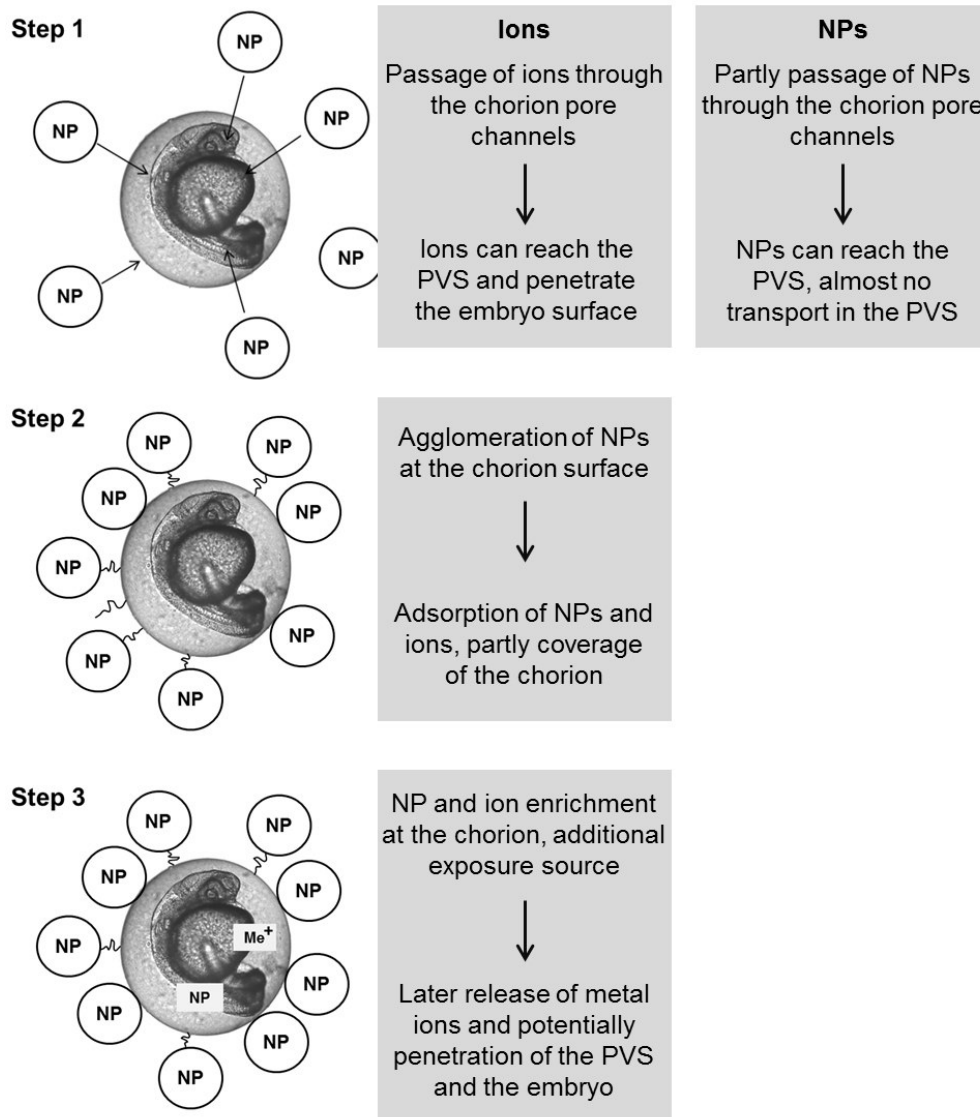


**Fig. 4:** Mechanistic NP-chorion sorption scheme showing individual mechanistic processes by exposure of ZFE to NP in a time-frame between 26-50 hpf (NP-nanoparticle, PVS-perivitelline space, Me<sup>+</sup>-metal ion).

(1) The passage of dissolved metal ions through the chorion pore channels into the PVS and the subsequent attachment to the embryo surface is possible via active ion transporters or passive diffusion with reported metal cation diffusion coefficients around  $6 \times 10^{-6} \text{ cm}^2 \text{ s}^{-1}$  (Scally et al. 2006). For NPs, the particle size, surface composition, and charge limit the passage through the chorion pore channels. As shown in this study, the particle size increases during exposure time in the exposure suspension. At the beginning of the experiments hydrodynamic particle sizes ranging between 20-130 nm were measured, theoretically matching the chorion pore size of  $\sim 200 \text{ nm}$  (Hart and Donovan 1983). However, even if NPs

pass the chorion and enter the PVS, the Brownian motion of NPs within the perivitelline fluid is reported to be 26-times slower than in the exposure media with an Ag-NP diffusion coefficient of  $3 \times 10^{-9} \text{ cm}^2 \text{ s}^{-1}$  (Lee et al. 2007). Therefore, it is highly unlikely that a large number of NPs reach the embryo and penetrate it. Even the low percentages of total elemental concentrations in the eggs that were determined in the embryo of Ag-, Au-, or CuO-NP treated ZFEs (**Fig. 2**) may well be due to dissolved ions (**Fig. 4**, top).

(2) An adsorption of NPs and dissolved metal cations at or within the chorion structure was shown by our quantification and visualization results (**Fig. 2** and **S2**). At longer exposure times (24 h) the agglomeration of NPs within the media (DLS measurements) as well as on the chorion (SEM+EDX measurements) was observed. The resulting particle sizes of 200 nm (Ag-NPs) to  $>5 \mu\text{m}$  (Au- and ZnO-NPs) are too large to pass the chorion pore channels. However, NPs physically attach or chemically bind to the chorion surface. Their adsorption to the chorion surface may be mediated by electrostatic interactions or van-der-Waals forces and is dependent on the thickness of the electric double layer at the surfaces of both, the chorion and the NP. Due to the high salt contents in the exposure medium, the double layers should be thin and electrostatic repulsion may be overcome by multivalent counter ions in the medium (Gimbel et al. 2004). These factors would support the attachment of NPs to the chorion surface. Besides that, Auffan et al. (2014) observed a complex formation between citrate-capped Ag-NPs and thiolated sites of proteins and enzymes of the chorion of Atlantic killifish embryos. However, the total blockage of chorion pore channels by the adsorption of NPs is only possible for a high surface loading of the chorion with particles.

In order to gain information on the number of NPs attached to the chorion surface the percentage NP-coverage was calculated (**Tab. 2**). For NPs with a low agglomeration potential and a high dissolved ionic fraction (ZnO-, Ag-NP) low coverages (11-21 %) were determined. In contrast, Au-NPs that form large agglomerates, showed the highest coverage of 83 %. For longer exposure periods (4-24 h) the calculated surface coverage of Au-NPs exceeds 100 %, suggesting the formation of NP double layers. While a complete coverage of the chorion surface has been reported for exposure experiments with silica particles

(Fent et al. 2010) it is also possible that, instead, the NPs form patches at the surface, as it has been observed before for Ag-NPs (Auffan et al. 2014).

(3) The adsorption of NPs at or within the ZFE chorion structures can lead to an enrichment of these materials as shown by an enrichment factor of ~10 000 compared to the external NP exposure concentration. Over the exposure time an additional release of NPs or dissolved metal cations from adsorbed and agglomerated NPs at the chorion may occur resulting in a higher exposure of the ZFE. This has been previously proposed by Misra et al. (2012). Especially, ions released from the particle surface may pass through the chorion pore channels if this transport is not hindered by electrostatic interactions. The thinning process of the chorion during the pre-hatching stage of the ZFE can further promote the described release processes due to changes in the biological structure (Kim et al. 2006).

The proposed mechanistic adsorption scheme improves the understanding of the mechanisms occurring during a NP-organism interaction.

## **CONCLUSIONS**

To date, little information on kinetics of NP uptake into ZFE is available. Within this study, the accumulation at the chorion surface was observed by the application of ICP-MS and electron microscopy based techniques. The embryo in its non-hatched stadium is protected by the chorion and the PVS against NP exposure. This is due to the small size of the chorion pores, electrostatic interactions between NPs and biological membranes as well as the low transport speed of NPs within the perivitelline fluid. Correspondingly, increased elemental concentrations at the ZFE chorion were detected in this study for Ag-, Au-, and CuO-NPs. For the highly soluble ZnO-NPs, however, highest concentrations were found within the embryonic tissues rather than at the chorion.

Indeed, the results of this study support the perception of the chorion of ZFE being a protective barrier against NP. However the chorion also attracts NPs so that the NP concentration at the chorion surface is orders of magnitude higher than in the free exposure medium. Due to this enrichment the chorion increases the exposure

of the embryo to the respective NP and may subsequently turn from a barrier into a source, of NP or of dissolved metal cations potentially released from the NPs. The protection of ZFEs at their early life stages by the chorion may eventually lead to elevated uptake into the PVS or the embryo.

In future, it would be important to correlate the amount of incorporated particles and their tissue distribution to toxicological effects occurring after NP exposure, with the aim to link these factors and to gain more knowledge on the interaction of nanoparticles and biological interfaces. Especially, concentrations necessary to trigger toxicological effects have to be determined.

#### **ACKNOWLEDGEMENT**

The authors thank Josefine Müller of the Department Bioanalytical Ecotoxicology (UFZ) for her help in the laboratory. This research was supported by “Europäischer Fonds für regionale Entwicklung (EFRE) und dem Freistaat Sachsen” within the ProVIS project. Furthermore, S.B. was kindly supported by the Helmholtz Impulse and Networking Fund through the Helmholtz Interdisciplinary Graduate School for Environmental Research (HIGRADE).

#### **DECLARATION OF INTEREST**

The authors report no conflicts of interest. This research was funded by the EU FP7 project NanoValid (Development of reference methods for hazard identification, risk assessment and LCA of engineered nanomaterials; grant no 263147). Any opinions, findings, or conclusions in this study are those of the author(s).

## REFERENCES

- Asharani P., Lianwu Y., Gong Z. and Valiyaveetil S. (2011). Comparison of the toxicity of silver, gold and platinum nanoparticles in developing zebrafish embryos. *Nanotoxicology*, 5(1): 43-54
- Asharani P., Wu Y. L., Gong Z. and Valiyaveetil S. (2008). Toxicity of silver nanoparticles in zebrafish models. *Nanotechnology*, 19(25): 1-8
- Auffan M., Matson C.W., Rose J., et al. (2014). Salinity-dependent silver nanoparticle uptake and transformation by Atlantic killifish (*Fundulus heteroclitus*) embryos. *Nanotoxicology*, 8: 167-176
- Böhme S., Stärk H.-J., Kühnel D. and Reemtsma T. (2015). Exploring LA-ICP-MS as a quantitative imaging technique to study nanoparticle uptake in *Daphnia magna* and zebrafish (*Danio rerio*) embryos. *Anal Bioanal Chem*, 407(18): 5477-5485
- Böhme S., Stärk H.-J., Meißner T., et al. (2014). Quantification of Al<sub>2</sub>O<sub>3</sub> nanoparticles in human cell lines applying inductively coupled plasma mass spectrometry (neb-ICP-MS, LA-ICP-MS) and flow cytometry-based methods. *J Nanopart Res*, 16(9): 2592
- Bonsignorio D., Perego L., Giacco L.D. and Cotelli F. (1996). Structure and macromolecular composition of the zebrafish egg chorion. *Zygote*, 4(2): 101-108
- Browning L.M., Lee K.J., Huang T., et al. (2009). Random walk of single gold nanoparticles in zebrafish embryos leading to stochastic toxic effects on embryonic developments. *Nanoscale*, 1: 138-152
- Brox S., Ritter A.P., Küster E. and Reemtsma T. (2014). A quantitative HPLC-MS/MS method for studying internal concentrations and toxicokinetics of 34 polar analytes in zebrafish (*Danio rerio*) embryos. *Anal Bioanal Chem*, 406(20): 4831-4840
- Brun N.R., Lenz M., Wehrli B. and Fent K. (2014). Comparative effects of zinc oxide nanoparticles and dissolved zinc on zebrafish embryos and eleuthero-embryos: Importance of zinc ions. *Sci Total Environ*, 476: 657-666
- Chang Y.-N., Zhang M., Xia L., et al. (2012). The toxic effects and mechanisms of CuO and ZnO nanoparticles. *Materials*, 5(12): 2850-2871
- Chen D., Zhang D., Jimmy C. Y. and Chan K.M. (2011). Effects of Cu<sub>2</sub>O nanoparticle and CuCl<sub>2</sub> on zebrafish larvae and a liver cell-line. *Aquat Toxicol*, 105(3): 344-354
- El-Amrani S., Sanz-Landaluze J., Guinea J. and Camara C. (2013). Rapid determination of polycyclic aromatic hydrocarbons (PAHs) in zebrafish eleutheroembryos as a model for the evaluation of PAH bioconcentration. *Talanta*, 104: 67-74
- Escher B.I. and Hermens J.L. (2004). Peer reviewed: internal exposure: linking bioavailability to effects. *Environ Sci Technol*, 38(23): 455A-462A
- Fent K., Weisbrod C.J., Wirth-Heller A. and Pielkes U. (2010). Assessment of uptake and toxicity of fluorescent silica nanoparticles in zebrafish (*Danio rerio*) early life stages. *Aquat Toxicol*, 100(2): 218-228
- Gimbel R., Jekel M. and Ließfeld R. (2004). Wasseraufbereitung: Grundlagen und Verfahren, Deutsche Vereinigung des Gas- und Wasserfaches DVGW, Oldenbourg Industrieverlag
- Hart N.H. and Donovan M. (1983). Fine structure of the chorion and site of sperm entry in the egg of Brachydanio. *J Exp Zool*, 227(2): 277-296

#### 4. The zebrafish embryo chorion as potential biological barrier

---

- Henn K. (2011). Limits of the fish embryo toxicity test with *Danio rerio* as an alternative to the acute fish toxicity test. *Dissertation*, Ruperto-Carola University of Heidelberg (Germany)
- Kim D.-H., Hwang C.N., Sun Y., et al. (2006). Mechanical analysis of chorion softening in prehatching stages of zebrafish embryos. *IEEE, Transactions on NanoBioscience*, 5: 89-94
- Kim D.-H., Sun Y., Yun S., et al. (2004). Mechanical property characterization of the zebrafish embryo chorion. *26th Annual International Conference of the IEEE*: 5061-5064
- Kühnert A., Vogts C., Altenburger R. and Küster E. (2013). The internal concentration of organic substances in fish embryos - a toxicokinetic approach. *Environ Toxicol Chem*, 32(8): 1819-1827
- Lee K.J., Browning L.M., Nallathamby P.D. and Xu X.-H.N. (2013). Study of charge-dependent transport and toxicity of peptide-functionalized silver nanoparticles using zebrafish embryos and single nanoparticle plasmonic spectroscopy. *Chem Res Toxicol*, 26(6): 904-917
- Lee K.J., Nallathamby P.D., Browning L.M., et al. (2007). *In vivo* imaging of transport and biocompatibility of single silver nanoparticles in early development of zebrafish embryos. *ACS nano*, 1(2): 133-143
- Lin S., Zhao Y., Xia T., et al. (2011). High content screening in zebrafish speeds up hazard ranking of transition metal oxide nanoparticles. *ACS nano*, 5(9): 7284-7295
- Lopes S., Ribeiro F., Wojnarowicz J., et al. (2014). Zinc oxide nanoparticles toxicity to *Daphnia magna*: size-dependent effects and dissolution. *Environ Toxicol Chem*, 33(1): 190-198
- Marquis B.J., Love S.A., Braun K.L. and Haynes C.L. (2009). Analytical methods to assess nanoparticle toxicity. *Analyst*, 134(3): 425-439
- Misra S.K., Dybowska A., Berhanu D., et al. (2012). The complexity of nanoparticle dissolution and its importance in nanotoxicological studies. *Sci Total Environ*, 438: 225-232
- Nanovaid, EU-Project (2015). Dispersion of NNV-011 (CuO) nanoparticle suspensions for toxicological testing. *Internal Draft*
- OECD (2013). Test No. 236: Fish Embryo Acute Toxicity (FET) Test, [www.oecd.org](http://www.oecd.org).
- Osborne O.J., Johnston B.D., Moger J., et al. (2013). Effects of particle size and coating on nanoscale Ag and TiO<sub>2</sub> exposure in zebrafish (*Danio rerio*) embryos. *Nanotoxicology*, 7(8): 1315-1324
- Rawson D.M., Zhang T., Kalicharan D., Jongebloed W.L. (2000). Field emission scanning electron microscopy and transmission electron microscopy studies of the chorion, plasma membrane and syncytial layers of the gastrula-stage embryo of the zebrafish *Brachydanio rerio*. *Aquac Res*, 31(3): 325-336
- Scally S., Davison W. and Zhang H. (2006). Diffusion coefficients of metals and metal complexes in hydrogels used in diffusive gradients in thin films. *Anal Chim Acta*, 558(1): 222-229
- Scholz S., Fischer S., Gündel U., et al. (2008). The zebrafish embryo model in environmental risk Assessment - applications beyond acute toxicity testing. *Environ Sci Pollut Res*, 15(5): 394-404
- Sun T.Y., Gottschalk F., Hungerbühler K. and Nowack B. (2014). Comprehensive probabilistic modelling of environmental emissions of engineered nanomaterials. *Environ Pollut*, 185: 69-76
- Wang J. and Wang W.-x. (2014). Significance of physicochemical and uptake kinetics in controlling the toxicity of metallic nanomaterials to aquatic organisms. *J Zhejiang Univ-Sc A*, 15(8): 573-592

## SUPPLEMENTARY INFORMATION

### Materials and methods

#### CHARACTERIZATION OF NANOPARTICLE POWDERS, SUSPENSIONS, AND EXPOSURE SOLUTIONS

The NPs were provided and characterized in detail by project partners of EU project NanoValid ([www.nanovalid.eu](http://www.nanovalid.eu)). The Ag-NPs and Au-NPs were delivered as water-based suspensions and the CuO-NPs and ZnO-NPs as powders. As coatings for the Ag-NPs polyvinyl pyrrolidone (PVP) and for Au-NPs sodium citrate was applied to prevent agglomeration processes within the suspension. The CuO-NPs were stabilized by the addition of 0.1 % tetrasodium pyrophosphate and sonicated for 5 min with an energy input of  $3.25 \times 10^5 \text{ kJ/m}^3$  (NanoValid 2015). As for the ZnO-NPs no suitable stabilizer was found an alternative approach was chosen: a stock suspension of 10 g/l was sonicated according to the CuO-NP protocol and abandoned to sediment for 24 h. The supernatant (~80 %) was taken as nanoscale fraction for the following characterization and biological experiments.

The primary particle sizes of the NPs were obtained by transmission electron microscopy (TEM) measurements. The specific surface area according to Brunauer, Emmet and Teller (BET) was calculated from the adsorbed nitrogen volume within a pressure range of  $p/p_0$  0.05 to 0.20 (ASAP 2010 Physisorption Analyzer, Micromeritics GmbH). Dynamic light scattering (DLS, Zetasizer Nano ZS, Malvern Instruments Ltd.) was applied to determine the particle size distribution and the zeta potential of the NPs in the stock suspensions. Furthermore, the stability and agglomeration behavior of particles in the exposure solutions was investigated by DLS after 24 h. DLS calculations were performed based on Smoluchowski equations. The dissolved ionic fraction within the NP exposure solutions was measured prior to testing by ICP-MS for the supernatant after centrifugation.

A comparison between nominal and real exposure concentrations measured by neb-ICP-MS is shown in **Tab. S1**. Loss of substance from the exposure solutions

#### 4. The zebrafish embryo chorion as potential biological barrier

may result from adsorption, agglomeration and degradation of particles taking place during handling and storage of suspensions. Furthermore the precipitation of NP-salts and complexes not ascertainable with the analytical techniques applied is possible.

**Tab. S1:** Comparison between nominal and real nanoparticle exposure concentrations.

Nominal NP exposure concentrations	Real NP exposure concentrations	Recovery
60 µg Ag/L	16.2 µg Ag/L	27 %
60 µg Au/L	34.2 µg Au/L	57 %
60 µg Cu/L	52 µg Cu/L	87 %
60 µg Zn/L	55.5 µg Zn/L	93 %

#### QUANTIFICATION OF TOTAL ELEMENT CONCENTRATIONS VISUALIZATION BY LASER ABLATION ICP-MS

Prior to the testing of the NPs, untreated organisms were investigated to obtain information on the natural background of the respective elements after digestion (SI, **Tab. S2**) and for LA-ICP-MS (SI, **Fig. S1**). For all following results, the background was already subtracted.

**Tab. S2:** Natural background of respective elements obtained by neb-ICP-MS measurement of untreated organisms (control) after digestion.

Nanomaterial	Concentration egg (ng/organism)	Concentration chorion (ng/chorion)	Concentration embryo (ng/embryo)
Ag-NP	0.12 ± 0.01	0.12 ± 0.01	0.11 ± 0.01
Au-NP	0.20 ± 0.01	0.18 ± 0.02	0.11 ± 0.01
CuO-NP	1.81 ± 0.23	1.06 ± 0.17	0.54 ± 0.18
ZnO-NP	2.73 ± 0.84	2.88 ± 0.94	2.65 ± 0.31

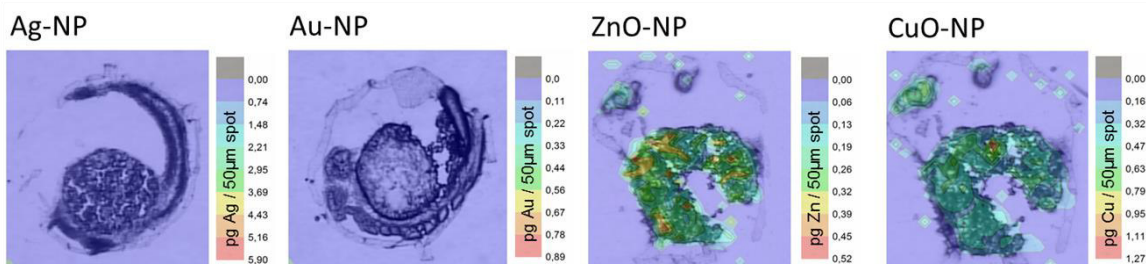


**Fig. S1:** Natural background of respective elements obtained by LA-ICP-MS measurement of untreated organisms (control).

## Results

### CHARACTERIZATION OF NANOPARTICLE POWDERS, SUSPENSIONS, AND EXPOSURE SOLUTIONS

The hydrodynamic particle sizes measured for the exposure solutions in ISO-WATER differ in the following range:  $18 \pm 2$  nm (Au-NP) <  $80 \pm 1$  nm (ZnO-NP) <  $117 \pm 24$  nm (Ag-NP) <  $132 \pm 2$  nm (CuO-NP) at the start of the experiments. After 24 h exposure, sizes of 204 nm (Ag-NP), 420 nm (CuO-NP), and >5 000 nm for Au and ZnO-NPs were measured in the exposure solutions, indicating a high agglomeration of particles within the media. The dissolved fraction of the respective particle solutions was determined to be  $48.3 \pm 7.2$  % Ag (Ag-NP),  $9.8 \pm 5.5$  % Cu (CuO-NP), and  $58.1 \pm 2.6$  % Zn (ZnO-NP) (SI, **Tab. S3**).

Within this study, a LA-ICP-MS method to visualize the nanoparticle uptake and the distribution in the biological tissues of environmental organisms, like the zebrafish (*Danio rerio*) embryo and *Daphnia magna* was developed. The 2D-color plots for Alu2 and Alu3 are shown in **Fig. S1**. For ZFE most of the particles were accumulated at the chorion. On the contrary, the ENP distribution in *Daphnia magna* clearly indicates active uptake, since metal signals are elevated in the gut of the organisms and minor amounts are visualized to be accumulated in the gill and eye tissues. The limit of detection (LOD) depends on the type of the introduced particle and the spot diameter which is used for the laser ablation itself (**Tab. S3**). In this context, an increasing spot diameter leads to an increase in the ablated area, a larger produced and evaporated volume and thus a higher detection limit. The LODs for silver and gold are lower when comparing them with

the ones for aluminum, what is a result of the natural abundance of these elements which is higher for aluminum.

#### CALCULATION OF NANO-IMPACT CONCENTRATIONS

After exposure to 60 µg element/l, the particle uptake into the egg, the chorion, and the embryo was measured by neb-ICP-MS after acid digestion. In order to present the internalized NP amounts, the determined concentrations after NP exposure were corrected by the elemental amounts measured for ZFE treated with the respective ionic substances whereby solely the concentration corresponding to the dissolved ionic fraction in the NP exposure solutions were subtracted. The values measured for ZFE treated with Au-NP were solely corrected by the controls. The exact elemental concentrations measured for the ZFE after exposure to individual time periods, NPs, and ionic substances were collected in **Tab. S4**.

#### IMPACT OF THE CHEMICAL IDENTITY OF NANOPARTICLES WITH RESPECT TO IONIC FRACTIONS

In addition to the exposure with nanomaterials, also the respective ionic substances ( $\text{AgNO}_3$ ,  $\text{CuSO}_4 \cdot 5\text{H}_2\text{O}$ ,  $\text{ZnSO}_4 \cdot 7\text{H}_2\text{O}$ ) were tested as positive controls for Ag-NP, CuO-NP, and ZnO-NP. The obtained concentrations after an exposure to 60 µg element/l for 24 h are  $6.4 \pm 1.8$  ng/organism,  $2.1 \pm 0.4$  ng/organism, and  $0.4 \pm 0.1$  ng/organism for  $\text{AgNO}_3$ ,  $\text{CuSO}_4 \cdot 5\text{H}_2\text{O}$ , and  $\text{ZnSO}_4 \cdot 7\text{H}_2\text{O}$ , respectively (SI, **Fig. S2**).

**Tab. S3:** Chemical and physical properties of investigated nanomaterials (powder, suspension, exposure solution).

Nanomaterial	Characterization of powders		Characterization of suspensions				Characterization of exposure solutions (ISO-WATER)		
	X <sub>TEM</sub> (nm)	BET (m <sup>2</sup> /g)	Concentration (g/l)	Coating (c) / stabilizer (s)	Smoluchovski Zeta potential (mV)	X <sub>DLS</sub> (nm)	Dissolved fraction (%)	X <sub>DLS</sub> (nm) t <sub>0</sub>	X <sub>DLS</sub> (nm) t <sub>24</sub>
AgNP	21 ± 8	-	4.0	PVP (c)	-19	117 ± 24	48.3 ± 7.2	135	204
AuNP	13 ± 1	-	0.06	Sodium citrate (s)	-38	18 ± 2	-	22	> 5 000
CuO-NP	22-25	28	0.09	Tetrasodium pyrophosphate (s)	-64	132 ± 2	9.8 ± 5.5	131	420
ZnO-NP	10-15	60	5.6	-	+34	80 ± 1	58.1 ± 2.6	81	> 5 000

**Tab. S4:** Percentage distribution and concentrations measured for the zebrafish embryo and chorion structures for a 60 µg element/l exposure.**RESULTS OF NP-EXPOSURE WITHOUT SUBTRACTION OF THE RESPECTIVE IONIC FRACTION**

Exposure period (h)	Ag-NP		Concentration chorion		Concentration embryo		Time-average 2-24 h	
	Concentration egg (ng/organism)	Concentration chorion (ng/chorion)	Concentration chorion (ng/chorion)	Concentration embryo (ng/embryo)	Time-average 2-24 h (ng/organism)	Time-average 2-24 h (ng/chorion)	Time-average 2-24 h (ng/embryo)	Time-average 2-24 h (ng/embryo)
0.5	3.07 ± 0.34	1.36 ± 0.73	1.36 ± 0.73	0.13 ± 0.07	8.46 ± 1.78	5.63 ± 1.38	0.43 ± 0.14	0.43 ± 0.14
1	2.37 ± 0.64	1.91 ± 0.49	1.91 ± 0.49	0.20 ± 0.07				
2	5.64 ± 0.58	3.59 ± 0.81	3.59 ± 0.81	0.33 ± 0.22				
4	8.22 ± 1.33	5.82 ± 1.15	5.82 ± 1.15	0.65 ± 0.19				
8	10.01 ± 1.27	7.49 ± 2.43	7.49 ± 2.43	0.44 ± 0.21				
24	9.95 ± 0.80	5.64 ± 2.83	5.64 ± 2.83	0.31 ± 0.05				

#### 4. The zebrafish embryo chorion as potential biological barrier

Au-NP							
Exposure period (h)	Concentration egg (ng/organism)	Concentration chorion (ng/chorion)	Concentration embryo (ng/embryo)	Time-average 2-24 h (ng/organism)	Time-average 2-24 h (ng/chorion)	Time-average 2-24 h (ng/embryo)	
0.5	5.46 ± 4.63	1.87 ± 2.12	1.05 ± 0.89	12.04 ± 7.82	7.54 ± 6.69	0.51 ± 0.28	
1	4.66 ± 1.91	1.28 ± 0.73	0.98 ± 0.98				
2	5.43 ± 1.35	2.44 ± 1.13	0.98 ± 0.67				
4	5.84 ± 2.01	3.00 ± 2.09	0.38 ± 0.28				
8	12.10 ± 1.84	5.80 ± 2.95	0.30 ± 0.12				
24	24.79 ± 0.68	18.91 ± 5.11	0.38 ± 0.24				
CuO-NP							
Exposure period (h)	Concentration egg (ng/organism)	Concentration chorion (ng/chorion)	Concentration embryo (ng/embryo)	Time-average 2-24 h (ng/organism)	Time-average 2-24 h (ng/chorion)	Time-average 2-24 h (ng/embryo)	
0.5	0.17 ± 0.08	0.19 ± 0.17	0.11 ± 0.10	2.59 ± 2.18	1.61 ± 0.64	0.10 ± 0.01	
1	0.11 ± 0.02	0.37 ± 0.24	0.10 ± 0.16				
2	0.96 ± 1.49	1.26 ± 0.29	0.10 ± 0.05				
4	1.54 ± 1.48	1.24 ± 0.77	0.10 ± 0.13				
8	1.53 ± 0.57	1.22 ± 0.93	0.11 ± 0.19				
24	6.35 ± 0.76	2.72 ± 0.15	0.10 ± 0.18				

#### 4. The zebrafish embryo chorion as potential biological barrier

ZnO-NP						
Exposure period (h)	Concentration egg (ng/organism)	Concentration chorion (ng/chorion)	Concentration embryo (ng/embryo)	Time-average 2-24 h (ng/organism)	Time-average 2-24 h (ng/chorion)	Time-average 2-24 h (ng/embryo)
0.5	3.19 ± 0.15	0.28 ± 0.03	2.71 ± 0.17	3.75 ± 0.13	0.51 ± 0.14	2.78 ± 0.36
1	3.34 ± 0.09	1.06 ± 0.23	2.90 ± 0.18			
2	3.76 ± 0.30	0.63 ± 0.09	2.79 ± 0.15			
4	3.57 ± 0.13	0.37 ± 0.08	3.36 ± 0.08			
8	3.75 ± 0.82	0.69 ± 0.13	2.55 ± 0.91			
24	3.94 ± 1.22	0.38 ± 0.07	2.42 ± 0.71			

#### RESULTS OF EXPOSURE WITH IONIC SUBSTANCES

AgNO <sub>3</sub>						
Exposure period (h)	Concentration egg (ng/organism)	Concentration chorion (ng/chorion)	Concentration embryo (ng/embryo)	Time-average 2-24 h (ng/organism)	Time-average 2-24 h (ng/chorion)	Time-average 2-24 h (ng/embryo)
0.5	1.13 ± 0.28	0.82 ± 0.24	0.12 ± 0.05	1.80 ± 0.36	0.22 ± 0.09	0.55
1	1.54 ± 0.13	1.46 ± 0.41	0.31 ± 0.30			0.74
2	3.55 ± 0.83	1.58 ± 0.93	0.23 ± 0.07			1.72
4	3.81 ± 0.51	1.33 ± 0.54	0.12 ± 0.05			1.84
8	4.41 ± 1.37	2.08 ± 1.91	0.18 ± 0.19			2.13
24	6.52 ± 1.76	2.22 ± 1.42	0.36 ± 0.29			3.15
						48.3 % Concentration egg
						48.3 % Concentration chorion
						48.3 % Concentration embryo

4. The zebrafish embryo chorion as potential biological barrier

CuSO <sub>4</sub> *5H <sub>2</sub> O									
Exposure period (h)	Concentration egg (ng/organism)	Concentration chorion (ng/chorion)	Concentration embryo (ng/embryo)	Time-average 2-24 h (ng/organism)	Time-average 2-24 h (ng/chorion)	Time-average 2-24 h (ng/embryo)	9.8 % Concentration egg	9.8 % Concentration chorion	9.8 % Concentration embryo
0.5	1.77 ± 0.11	1.42 ± 0.20	0.50 ± 0.04	2.74 ± 0.50	2.20 ± 0.50	0.25 ± 0.09	0.17	0.14	0.05
1	1.67 ± 0.16	1.32 ± 0.22	0.44 ± 0.66				0.16	0.13	0.04
2	1.93 ± 0.04	1.39 ± 0.19	0.16 ± 0.09				0.19	0.14	0.02
4	2.81 ± 0.43	2.20 ± 0.13	0.40 ± 0.34				0.28	0.22	0.04
8	2.89 ± 0.21	2.51 ± 0.46	0.24 ± 0.09				0.28	0.25	0.02
24	3.32 ± 0.42	2.69 ± 0.67	0.21 ± 0.09				0.32	0.26	0.02

ZnSO <sub>4</sub> *7H <sub>2</sub> O									
Exposure period (h)	Concentration egg (ng/organism)	Concentration chorion (ng/chorion)	Concentration embryo (ng/embryo)	Time-average 2-24 h (ng/organism)	Time-average 2-24 h (ng/chorion)	Time-average 2-24 h (ng/embryo)	58.1 % Concentration egg	58.1 % Concentration chorion	58.1 % Concentration embryo
0.5	3.20 ± 0.29	0.87 ± 0.10	2.47 ± 0.23	2.35 ± 0.28	0.40 ± 0.14	1.95 ± 0.28	1.86	0.50	1.43
1	3.20 ± 0.54	0.78 ± 0.26	2.37 ± 0.50				1.86	0.46	1.38
2	2.27 ± 0.16	0.61 ± 0.41	1.75 ± 0.26				1.32	0.35	1.02
4	2.53 ± 0.34	0.26 ± 0.01	2.06 ± 0.26				1.47	0.15	1.20
8	2.67 ± 0.32	0.45 ± 0.18	1.64 ± 0.10				1.55	0.26	0.95
24	1.92 ± 0.10	0.27 ± 0.03	2.35 ± 0.78				1.12	0.16	1.37

## RESULTS OF NP-EXPOSURE WITH SUBTRACTION OF THE RESPECTIVE IONIC FRACTION

Ag-NP												
Exposure period (h)	Concentration egg (ng/organism)		Concentration chorion (ng/chorion)		Concentration embryo (ng/embryo)		Time-average 2-24 h (ng/organism)		Time-average 2-24 h (ng/chorion)		Time-average 2-24 h (ng/embryo)	
0.5	2.53 ± 0.03		0.96 ± 0.24		0.07 ± 0.01		6.25 ± 1.45	4.76 ± 1.32	0.32 ± 0.17	38.0	2.9	59.1
1	1.63 ± 0.25		1.21 ± 0.04		0.05 ± 0.12					74.2	3.0	22.8
2	3.92 ± 0.12		2.83 ± 0.06		0.22 ± 0.07					72.0	5.5	22.5
4	6.38 ± 0.41		5.18 ± 0.31		0.59 ± 0.07					81.1	9.3	9.6
8	7.88 ± 0.05		6.48 ± 0.26		0.36 ± 0.01					82.3	4.5	13.2
24	6.80 ± 0.48		4.57 ± 0.70		0.13 ± 0.12					67.2	2.0	30.8
Au-NP												
Exposure period (h)	Concentration egg (ng/organism)		Concentration chorion (ng/chorion)		Concentration embryo (ng/embryo)		Time-average 2-24 h (ng/organism)		Time-average 2-24 h (ng/chorion)		Time-average 2-24 h (ng/embryo)	
0.5	5.35 ± 2.26		1.69 ± 0.97		0.84 ± 0.34		11.93 ± 7.82	7.36 ± 6.69	0.31 ± 0.27	31.6	15.8	52.6
1	4.55 ± 0.90		1.10 ± 0.28		0.77 ± 0.39					24.2	17.0	58.8
2	5.33 ± 0.62		2.26 ± 0.48		0.78 ± 0.24					42.5	14.7	42.8
4	5.73 ± 0.95		2.83 ± 0.96		0.18 ± 0.04					49.3	3.1	47.6
8	11.99 ± 0.86		5.63 ± 1.39		0.10 ± 0.04					47.0	0.8	52.2
24	24.68 ± 0.29		18.74 ± 2.47		0.17 ± 0.02					75.9	0.7	23.4

4. The zebrafish embryo chorion as potential biological barrier

CuO-NP										
Exposure period (h)	Concentration egg (ng/organism)	Concentration chorion (ng/chorion)	Concentration embryo (ng/embryo)	Time-average 2-24 h (ng/organism)	Time-average 2-24 h (ng/chorion)	Time-average 2-24 h (ng/embryo)	Chorion (%)	Embryo (%)	PVS (%)	
0.5	0.10 ± 0.02	0.05 ± 0.01	0.06 ± 0.03	2.33 ± 2.14	1.40 ± 0.62	0.08 ± 0.01	45.8	60.2	0	
1	0.10 ± 0.07	0.24 ± 0.01	0.06 ± 0.25				> 100	58.7	0	
2	0.77 ± 0.72	1.13 ± 0.05	0.09 ± 0.02				> 100	11.2	0	
4	1.26 ± 0.53	1.03 ± 0.32	0.06 ± 0.11				81.2	5.0	13.8	
8	1.24 ± 0.18	0.97 ± 0.24	0.08 ± 0.05				78.2	6.8	15.0	
24	6.02 ± 0.17	2.46 ± 0.26	0.08 ± 0.05				40.8	1.4	57.8	
ZnO-NP										
Exposure period (h)	Concentration egg (ng/organism)	Concentration chorion (ng/chorion)	Concentration embryo (ng/embryo)	Time-average 2-24 h (ng/organism)	Time-average 2-24 h (ng/chorion)	Time-average 2-24 h (ng/embryo)	Chorion (%)	Embryo (%)	PVS (%)	
0.5	1.33 ± 0.07	0.01 ± 0.03	1.27 ± 0.03	2.39 ± 0.28	0.28 ± 0.08	1.64 ± 0.40	0	95.8	4.2	
1	1.48 ± 0.23	0.61 ± 0.01	1.52 ± 0.16				> 100	> 100	0	
2	2.44 ± 0.07	0.28 ± 0.16	1.77 ± 0.06				11.3	72.4	16.3	
4	2.10 ± 0.10	0.22 ± 0.03	2.16 ± 0.09				10.4	> 100	0	
8	2.19 ± 0.25	0.42 ± 0.03	1.59 ± 0.41				19.2	72.6	8.2	
24	2.83 ± 0.56	0.22 ± 0.02	1.05 ± 0.03				7.8	37.1	55.1	

#### 4. The zebrafish embryo chorion as potential biological barrier

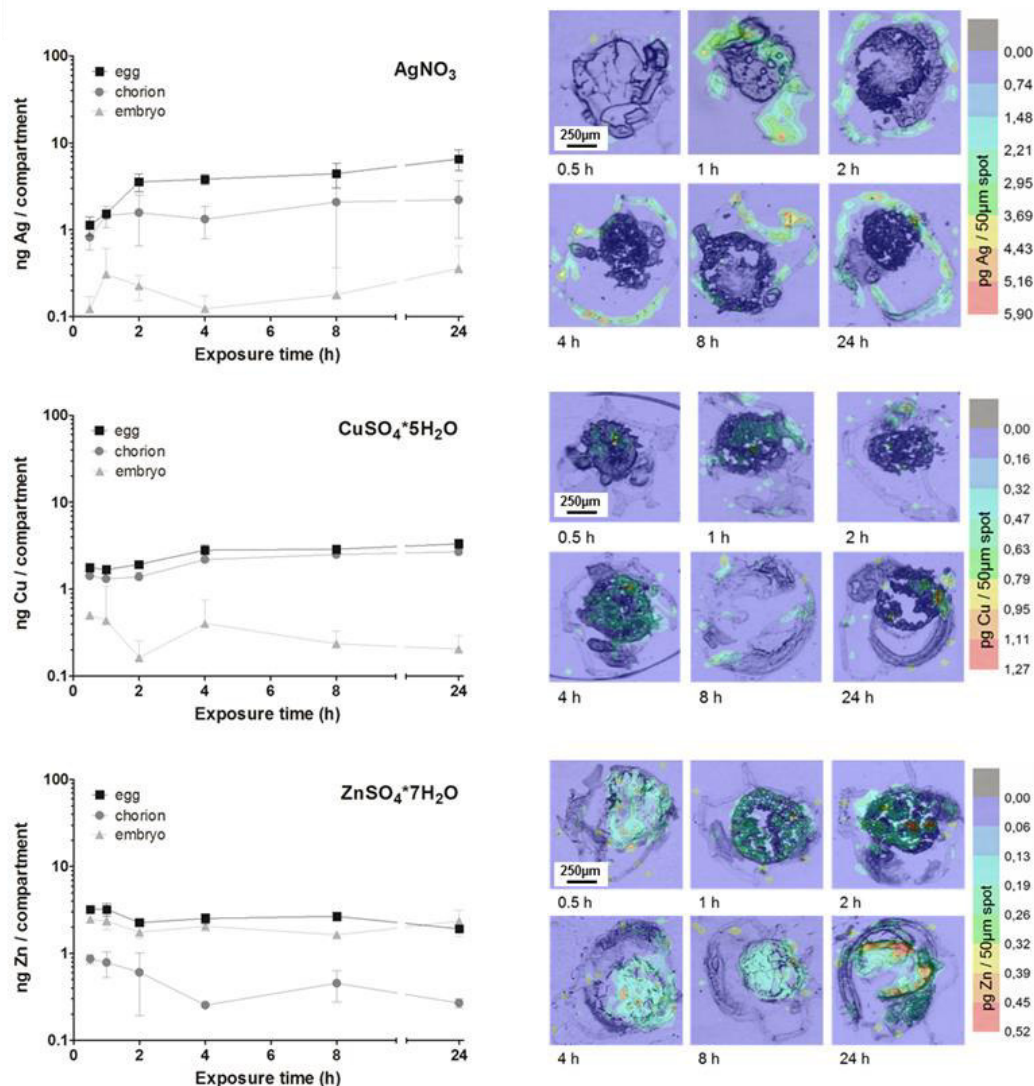


**Fig. S2:** Time resolved data for elemental concentrations in ZFE after exposure to 60 µg/l of  $\text{AgNO}_3$ ,  $\text{CuSO}_4 \cdot 5\text{H}_2\text{O}$ , and  $\text{ZnSO}_4 \cdot 7\text{H}_2\text{O}$  ( $n \geq 3$ , shown as mean  $\pm$  SD). Concentrations determined after acid digestion by neb-ICP-MS (note the logarithmic y-axis) (left column) and visualization of the elemental concentrations by LA-ICP-MS (right column).

#### CALCULATION OF ZFE CHORION COVERAGE BY NPs

In order to gain a better understanding of the accumulation of particles at the chorion surface the number of particles covering the chorion surface was calculated according to the measured NP concentrations for this compartment. For the calculation itself the time-dependent increase in hydrodynamic particle size was included. The coverage of the ZFE chorion is time-dependent with trends towards increasing coverage for longer exposure times (**Tab. S5**).

#### 4. The zebrafish embryo chorion as potential biological barrier

**Tab. S5:** Percentage cover of the ZFE chorion surface by NPs according to the hydrodynamic particle sizes after 24 h exposure to 60 µg/l.

Theoretical particle number to totally cover the chorion surface				
Time (h)	AgNP	AuNP	CuO-NP	ZnO-NP
0.5	83 200 000	96 950 000	82 000 000	46 000 000
1	80 800 000	29 350 000	75 300 000	18 800 000
2	77 400 000	8 000 000	64 100 000	6 400 000
4	71 200 000	2 100 000	48 000 000	1 900 000
8	61 650 000	500 000	29 900 000	500 000
24	37 000 000	60 000	8 700 000	60 000
Average 2-24 h	61 800 000	2 700 000	37 700 000	2 200 000
Experimental particle number related to measured chorion concentrations				
Time (h)	AgNP	AuNP	CuO-NP	ZnO-NP
0.5	2 350 000	1 950 000	200 000	0
1	2 950 000	1 300 000	900 000	60 000
2	6 950 000	2 600 000	4 300 000	30 000
4	12 700 000	3 300 000	3 900 000	20 000
8	15 900 000	6 500 000	3 700 000	40 000
24	11 200 000	21 750 000	9 300 000	20 000
Average 2-24 h	11 700 000	8 550 000	5 300 000	30 000
Ratio theoretic against experimental (% coverage)				
Time (h)	AgNP	AuNP	CuO-NP	ZnO-NP
0.5	2.8	2.0	0.2	0
1	3.7	4.4	1.2	0.3
2	9.0	32.6	6.7	0.4
4	17.9	> 100	8.1	1.1
8	25.8	> 100	12.3	8.0
24	30.4	> 100	> 100	35.7
Average 2-24 h	20.8 ± 8.1	83.2 ± 29.2	31.8 ± 19.5	11.3 ± 14.4

## References

NanoValid, EU-Project (2015). Dispersion of NNV-011 (CuO) nanoparticle suspensions for toxicological testing. *Internal Draft*



## Chapter 5

### **EFFECT PROPAGATION AFTER SILVER NANOPARTICLE EXPOSURE IN ZEBRAFISH (*DANIO RERIO*) EMBRYOS: A CORRELATION TO INTERNAL CONCENTRATION AND DISTRIBUTION PATTERNS**

Environmental Science: Nano (2015), published online, DOI: 10.1039/c5en00118h

Steffi Böhme<sup>1</sup>, Hans-Joachim Stärk<sup>2</sup>, Thorsten Reemtsma<sup>2</sup>, Dana Kühnel<sup>1</sup>

<sup>1</sup> Helmholtz Centre for Environmental Research - UFZ, Department of Bioanalytical Ecotoxicology, Permoserstrasse 15, 04318 Leipzig (Germany)

<sup>2</sup> Helmholtz Centre for Environmental Research - UFZ, Department of Analytical Chemistry, Permoserstrasse 15, 04318 Leipzig (Germany)



## **NANO IMPACT**

The zebrafish (*Danio rerio*) embryo (ZFE) is an established in vitro test model and can be adjusted towards the toxicity testing of nanoparticles (NPs). However, the chorion represents an effective barrier for particles and therefore, toxic effects may be underestimated. Accordingly, the correlation between the observed adverse effects and internal concentrations was investigated in ZFEs exposed to AgNPs and AgNO<sub>3</sub>. Internal silver concentrations were determined and combined with the toxicological information to obtain critical internal effect concentrations triggering biological responses. Furthermore, toxicological points of action were visualised and morphological changes during the occurrence of toxic effects were observed.

## **ABSTRACT**

The zebrafish (*Danio rerio*) embryo (ZFE) is an established ecotoxicological test organism used to investigate the hazardous potential of chemicals. It has been frequently used to test nanoparticles (NPs) for adverse effects. Beyond the assessment of the effects, information on real exposure concentrations, particle uptake and distribution patterns as well as the determination of internal effect concentrations contributes to a deeper understanding of NP-organism interactions. The AgNP and AgNO<sub>3</sub> dose-response curves recorded for different ZFE developmental stages were corrected to real exposure concentrations measured by ICP-MS within this study. Effective concentrations of silver exerting toxic effects were determined by this approach. Organisms showing no effects and individuals with sublethal or lethal effects were compared with regard to silver distribution patterns and internal uptake concentrations in order to allow a more exact correlation. As a result, the internal silver dose per organism differs around 0.5-1 ng Ag per organism irrespective of the developmental stage. However, for earlier developmental stages (2 hours post fertilisation) the ZFE chorion was found to effectively adsorb silver, leading to an up to 20-fold increase in total silver concentrations compared to the later chorion-free stages of the ZFE. Finally, a correlation between increased internal silver (particulate and ionic) concentrations and the occurrence of sublethal and lethal effects was observed.

### INTRODUCTION

In general, the observation of biological effects at certain concentrations is used to calculate dose-response curves, delivering effect concentrations (e.g., EC<sub>50</sub>-values) and thus allowing the estimation of the toxic potential of a substance. However, by applying nominal concentrations for the calculation of effect concentrations, toxicity is underestimated in case of a substance loss from exposure solutions. Indeed, for some nanoparticles (NPs), the real exposure concentrations are reported to be lower compared to the amounts of nominal exposure.<sup>1,2</sup> As a consequence, the analytical measurement of exposure concentrations, especially for NPs, is necessary to correctly determine the toxicity of a substance and to perform an appropriate risk assessment.<sup>3</sup>

The zebrafish (*Danio rerio*) embryo (ZFE) toxicity test is a versatile in vitro model used to assess the hazardous potential of chemicals. It has been applied in several studies for the toxicological testing of NPs.<sup>4-6</sup> The ZFE, as a vertebrate model species, combines advantages such as rapid development, easy maintenance in the laboratory, a large number of offspring, transparency of embryos and access to experimental manipulation to avoid expensive animal testing.<sup>7</sup> It allows the observation of acute lethal and sublethal (e.g. oedema, pigmentation, hatching) toxicological endpoints.

In addition, the ZFE test allows complementing the effect-based toxicity data with internal concentrations obtained by accumulation studies. The correlation between potential toxicological effects and internalised concentrations was already performed for ZFEs exposed to different organic chemicals.<sup>8,9</sup> However, data for the accumulation of NPs in the ZFE are required with regard to the quantification of internal concentrations and the visualisation of the particle distribution. Suitable analytical methods are needed which cover the requirements of high (elemental) sensitivity and spatial resolution to detect NPs within biological tissues.<sup>10</sup> Mainly electron microscopy (SEM, TEM)<sup>11</sup>, fluorescence microscopy<sup>12,13</sup>, and inductively coupled plasma mass spectrometry (ICP-MS)<sup>5,6</sup> were applied in recent studies.

The NP accumulation at or within the ZFE chorion structures has been observed assuming a particle barrier function of the chorion.<sup>12,13</sup> The yolk syncytial layer

was described as target structure for AgNPs indicating that the particle interaction with this structure is inducing toxicity.<sup>1</sup> Furthermore, the embryo surface is suggested as an accumulation point potentially leading to an uptake of particles or ions *via* the skin. However, there is no evidence of NP or ion incorporation within the embryo tissues.<sup>1, 13</sup> As a consequence, it is not fully clear, how the interaction of NPs with the whole embryo leads to the propagation of toxic effects.

In order to improve the analytical detection of NPs associated with environmental organisms, we optimised ICPMS-based techniques in order to determine the internal concentrations and gain information on the elemental distribution within the organism. Therefore, neb-ICP-MS was adopted for the quantification of metal-based NPs. Laser Ablation ICP-MS (LA-ICP-MS), a 2D imaging technique, was developed to visualise the NP distribution within organisms.<sup>14, 15</sup>

Different developmental stages of ZFEs (e.g. to be concise, stages with and without chorion) were exposed to AgNPs to address the gap between the information based on observed toxicological effects and quantitative internal NP concentrations. Subsequently, (1) dose-response curves obtained for the different stages were corrected for real exposure concentrations, (2) internal concentrations were determined, and (3) the distribution of silver in embryos which showed no damage, sublethal or lethal effects were compared. Furthermore, recent studies reported a high impact on toxicity by the dissolved silver ion fraction, released from the particle surface.<sup>16, 17</sup> Hence, in addition to AgNPs, AgNO<sub>3</sub> exposures were included in the study to demonstrate whether substantial differences in AgNP and silver ion uptake and distribution exist. The aim of this study was to identify toxicological points of action and gain information on the propagation of toxic effects related to an AgNP exposure.

## MATERIALS AND METHODS

### ZEBRAFISH CULTIVATION AND SELECTION

Zebrafish (*Danio rerio*) embryos were exposed to AgNPs and AgNO<sub>3</sub> according to the OECD test guideline 236.<sup>18</sup> The organisms were cultured at 26 ± 1 °C at a 14:10 h light:dark cycle. The fishes were fed with *Artemia spec.* on a daily basis. For the egg collection, spawn traps covered with a wire mesh were placed into fish tanks on the day prior to spawning. After the selection, the fertilised eggs were transferred to ISO-water (294.0 mg/l CaCl<sub>2</sub>\*2H<sub>2</sub>O, 123.3 mg/l MgSO<sub>4</sub>\*7H<sub>2</sub>O, 63.0 mg/l NaHCO<sub>3</sub>, and 5.5 mg/l KCl dissolved in deionised water) and different developmental stages of the ZFE were used for the toxicity and accumulation studies (**Tab. 1**). The 26 hours post fertilisation (hpf) ZFEs were dechorionated prior to testing by a mechanical dechorionation with forceps. All experiments involving zebrafish embryos were performed in compliance with the relevant laws and institutional guidelines, and the institution has all relevant permissions to breed zebrafish.

**Tab. 1:** Developmental stages (stadium) of the ZFE chosen for experiments. The age at the onset of exposure is given.

	Stadium	Description	Characteristics
	2 hpf	Whole organism	Organism including embryo and chorion
	26 hpf	Dechorionated embryo	Mechanical dechorionation at 24 hpf, no chorion
	71 hpf	Hatched embryo	Naturally hatched embryos, no chorion

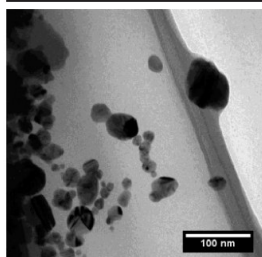
### NANOPARTICLE CHARACTERISATION

The AgNPs used in this study were provided and characterised in detail by the partners of the EU project NanoValid ([www.nanovalid.eu](http://www.nanovalid.eu), internal draft).<sup>19</sup> The main characteristics are summarised in **Tab. 2**. Briefly, the AgNPs are characterised by a primary particle size of 10 - 21 nm, a hydrodynamic particle

size of  $117 \pm 24$  nm, and a polyvinyl pyrrolidone (PVP) coating. The primary particle sizes were obtained by means of electron microscopy techniques (SEM, TEM) and nanoparticle tracking analysis (NTA). Furthermore, dynamic light scattering (DLS) was applied to determine the particle size distribution and the zeta potential of the AgNPs in the stock suspension.

**Tab. 2:** Chemical and physical properties of AgNP stock suspension and exposure suspensions.<sup>19</sup>

Parameters	Stock suspension	Exposure suspension ( $100 \mu\text{g l}^{-1}$ )
Shape	Spheres	Spheres
$X_{\text{TEM}}$	$21 \pm 8$ nm	—
$X_{\text{AFM}}$	$13 \pm 9$ nm	—
$X_{\text{NTA}}$	10-150 nm	—
Coating	PVP	PVP
$X_{\text{DLS}}$	$117 \pm 24$ nm	135 nm
Zeta potential	$-19 \pm 9$ mV	—
Dissolved fraction	$48.3 \pm 7.2\%$	$44.3 \pm 5.3\%$



$\text{AgNO}_3$  (ICP-MS standard, 1g/l, Merck) was used as positive control to assess the influence of ionic silver on toxicity and uptake. The silver exposure solutions for toxicity and accumulation studies were prepared in ISO-water just before testing. The dissolved silver ion fraction was determined for the stock suspension as well as for the different concentrations of the exposure suspensions in ISO-water (for AgNPs). Therefore, the samples were centrifuged for 30 min at 16 000 g. After centrifugation, the amount of dissolved silver in the supernatant was measured by ICP-MS and the residue was digested and analysed for the total silver concentration.

## EXPOSURE OF ZFE FOR EFFECT ASSESSMENT

The AgNP and  $\text{AgNO}_3$  exposure solutions in a concentration range of 1-1000  $\mu\text{g l}^{-1}$  were freshly prepared by dilution in ISO-water prior to testing. The exposure experiment was conducted in 24-well plates with one individual and 2 ml exposure media per well. In total 10 individuals per concentration were investigated and a minimum of 3 replicates was performed. Samples of the

exposure solutions were taken prior to testing in order to analyse the silver concentrations by ICP-MS measurements. The toxicological effects were assessed after exposure periods of 24 h and 48 h according to the OECD guideline 236.<sup>18</sup> In this context, sublethal effects are defined as edema (yolk, pericard), change of pigmentation or heart frequency, a missing blastula, epiboly, or adverse eye formation. Coagulation, missing formation of somites, no detachment of tail and no heartbeat are indicators for lethality. The dose-response curves representing the percentage of lethality against the exposure concentrations and the EC<sub>50</sub>-values were calculated using GraphPad Prism 5.

### EXPOSURE OF ZFE FOR ACCUMULATION STUDIES

Nominal AgNP and AgNO<sub>3</sub> concentrations up to 150 µg l<sup>-1</sup> were used for the exposure in the accumulation studies. Exposure concentrations of 100 µg l<sup>-1</sup> AgNPs or AgNO<sub>3</sub> were applied for the determination of the silver distribution in the ZFE of different developmental stages by LA-ICP-MS. Five individuals were exposed in glass petri dishes with a total exposure media volume of 10 ml. In parallel, samples of the exposure solutions were taken prior to exposure in order to analyse the concentrations by ICP-MS. The Ag speciation was calculated for both AgNP and AgNO<sub>3</sub> exposures by using Visual MINTEQ (Visual MINTEQ, ver. 3.1, 2013, KTH, Sweden).<sup>20</sup> The calculation was based on the measured dissolved Ag in the respective exposure suspension. The pH was set to 7.6 and temperature to 26 °C.

For the subsequent correlation of observed effects to the internal concentrations, ZFE showing either no toxic effects, sublethal, or lethal effects were selected and collected for the elemental analysis. In order to obtain a sufficient amount of sample material, three individuals per concentration were pooled for one sample. The organisms were washed twice with the medium after 24 h exposure, shock frozen and digested for the neb-ICP-MS measurements. The washed organisms were fixated with a paraformaldehyde phosphate buffered solution, embedded with frozen section medium (Neg-50, Richard Allen Scientific) and cut in 40 µm sections by a microtome (MICROM Cryo Star, HM560, Thermo Scientific) at

-20 °C. The sections were placed on glass slides and were introduced to the laser ablation system for the imaging by LA-ICP-MS.

### ICP-MS MEASUREMENTS

A quadrupole-based ICP-MS (ELAN DRGe, Perkin Elmer Sclex) was applied to quantify the silver concentrations within the exposed organisms. The AgNP- or AgNO<sub>3</sub>-exposed ZFEs were digested with 30% nitric acid (65%, suprapur, Merck) in an open digestion system (DigiPrep, S-Prep). The homogeneous samples obtained after digestion were analysed for their silver concentrations by neb-ICP-MS. An external calibration was performed by analysing an AgNO<sub>3</sub> standard reference solution (1 g l<sup>-1</sup>, Merck).

The sections were ablated by a Nd : YAG laser (LSX 500, CETAC, USA) with a wavelength of 266 nm for the visualisation of the silver distributions within the embryos by LA-ICP-MS. The laser energy was adjusted to 60% to ensure a complete ablation of the organic layer. The generated particle aerosol was directly transported and introduced to the ICP-MS via an additional argon gas stream. A 50 µm spot diameter for the spot ablation was chosen to avoid measurement times above 4 h for one organism section. An external calibration was performed by applying individual particle-spiked agarose gels in accordance with an earlier protocol.<sup>15</sup> The transient intensity signals for the individual spots were collected in a data matrix and converted to concentrations using the calibration curves. Both the exact parameters for the transformation into a 2D-color plot and the LOD of the applied semi-quantitative LA-ICP-MS technique (35.7 fg Ag/50 µm spot) were reported earlier.<sup>14</sup>

## RESULTS AND DISCUSSION

In order to gain insight into the propagation of toxic effects exerted by NPs in ZFEs, systematic exposure experiments of the developmental stages (**Tab. 2**) with and without chorion, and a range of AgNP and AgNO<sub>3</sub> concentrations were performed. As knowledge on external and internal silver concentrations is vital, classical concentration response testing was complemented by analytical determination of silver concentrations and distribution in the experimental system.

### EXTERNAL EXPOSURE CONDITIONS

The silver concentrations determined in the prepared exposure solutions differ significantly from the nominal ones with a recovery of  $63 \pm 12\%$  and  $55 \pm 11\%$  for AgNO<sub>3</sub> and AgNPs, respectively. This is in line with previous studies on AgNPs, describing similar differences between nominal and measured concentrations.<sup>1,2</sup> The loss of silver from the exposure system may be accounted to the adsorption to the surroundings such as the walls of the exposure vessels, pipette tips, or the agglomeration and sedimentation of particles.<sup>3</sup> The precipitation of silver as AgCl and a subsequent concentration loss is another phenomenon described in the literature.<sup>21</sup> As a consequence, the bioavailable silver fraction is reduced which might reduce the efficiency of the digestion and subsequent ICP-MS analysis. As indicated by the saturation index calculated for the Ag species distribution within the exposure suspensions, no precipitation of AgCl(s) can be expected.

The OECD guidance document on the handling of difficult substances recommends that the difference between nominal and real concentrations should not exceed  $\pm 20\%$ ,<sup>22</sup> otherwise corrective actions concerning exposure design or calculation of results are needed. Whether this recommendation is also applicable to NPs is currently under debate.<sup>23</sup> Usually, effect concentrations are expressed as nominal concentrations which can result in high variabilities between studies<sup>3</sup> as reported by Escher and Hermens.<sup>21</sup> Toxicity and quantitative data were corrected to measured concentrations as a consequence.

In addition, a large dissolved silver ion fraction (44–48%) was detected within the AgNP stock and exposure suspensions, which is constant over time. This is in agreement with the literature data on silver dissolution in PVP-coated AgNP suspensions showing that up to 40% of the silver is present in the ionic form.<sup>17</sup> Hence, only small differences in the toxicity of AgNPs and AgNO<sub>3</sub> are to be expected, as the dissolved silver dominates in both exposures. The comparability of both exposures was demonstrated by the calculation of the identical shares of the different silver species for both exposures, with 66% AgCl (aq), 23% AgCl<sup>2-</sup>, and 10% dissolved Ag<sup>+</sup>. The observed effects and measured uptake concentrations were directly compared as a consequence.

### TOXICITY ASSESSMENT AND CORRECTION TO REAL EXPOSURE CONCENTRATIONS

The following steps were performed for a complete toxicity assessment: (1) ZFE toxicity testing of AgNPs and AgNO<sub>3</sub> according to the OECD test guideline 236, (2) correction of calculated dose-response curves and the LC<sub>50</sub>-values using measured, real silver concentrations, and (3) comparison of the obtained results based on nominal and corrected exposure concentrations. The corrected effect concentrations compared to the nominal effect concentrations were shown in **Fig. 1**. A concentration-dependent toxicity was observed for AgNP and AgNO<sub>3</sub> treated ZFEs.

The most sensitive developmental ZFE stage was 26 hpf, followed by 2 hpf and 71 hpf, for both AgNPs and AgNO<sub>3</sub> exposures based on nominal concentrations. On the contrary, the LC<sub>50</sub>-values corrected for the measured silver concentrations were comparable with the different ZFE developmental stages (**Fig. 1**). One exception was the corrected LC<sub>50</sub>-value of the AgNO<sub>3</sub> of ZFEs exposed at 71 hpf, indicating a lower sensitivity of the later developmental stage towards ionic silver. However, the corrected LC<sub>50</sub>-values of AgNPs and AgNO<sub>3</sub> were in the same concentration range of 30–40 µg l<sup>-1</sup> (corresponding to 0.28–0.38 µM), indicating that the toxicity is independent of the ZFE stadium upon the start of the exposure experiment. After 48 h exposure, the LC<sub>50</sub>-values were comparable to the 24 h

effect values as reported in the ESI, **Fig. S1**. Based on the amount of dissolved silver (**Fig. 1**), the differences in LC<sub>50</sub>-values of 71 hpf ZFEs were confirmed. In this case, the higher toxicity of AgNPs can be related to an enhanced dissolution of particles at the contact site of the organism after an increased exposure to AgNPs of this ZFE stadium due to the higher mobility of the organisms.

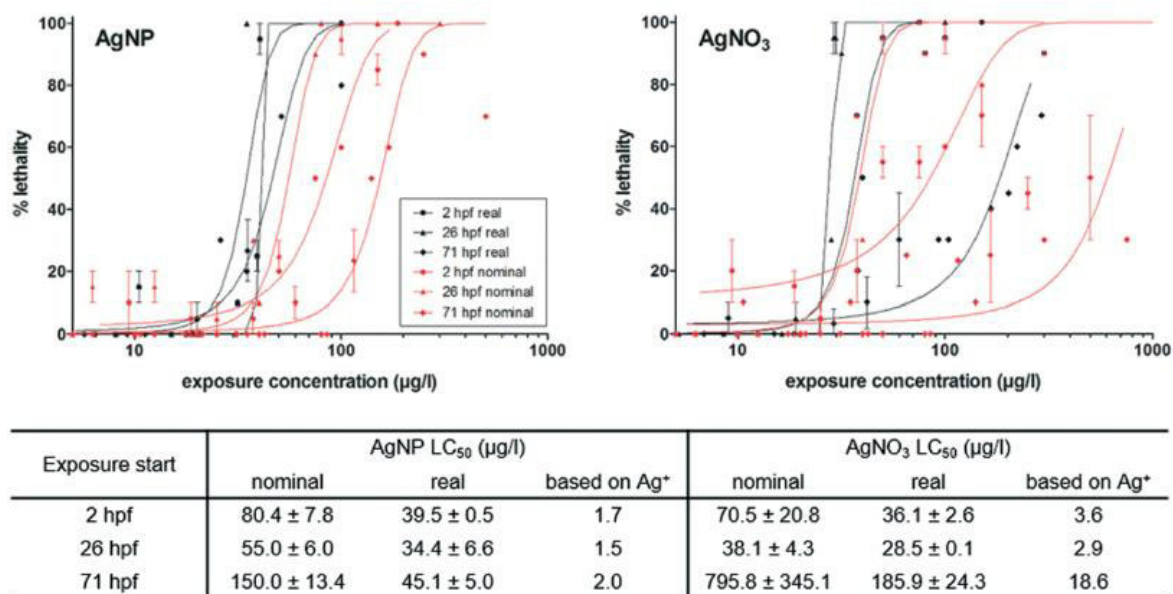


**Fig. 1:** Dose–response curves based on nominal (red) and corrected real exposure concentrations (black) for the respective developmental stages of the ZFE. The calculated nominal and real LC<sub>50</sub>-values of the respective AgNP or AgNO<sub>3</sub> exposure as well as the developmental stage are listed in the table below. The LC<sub>50</sub>-values based on the dissolved Ag<sup>+</sup> were calculated according to the ionic silver content in the exposure solution.

Groh *et al.*<sup>21</sup> described toxicity to be dependent on the developmental stage of the ZFE, with a higher sensitivity during the earlier stages. On the contrary, Asharani *et al.*<sup>11</sup> reported ZFEs in the 4–6 hpf stages as more resistant. However, both studies applied nominal concentrations for their dose–response modelling and the calculation of LC<sub>50</sub>-values. The results of our study showed that the presence or absence of the chorion around the embryo did not significantly influence the toxic potency of the silver. That is in agreement with Cunningham *et al.*<sup>17</sup> observing similar toxicological results for both ZFE with and without chorion.

Groh *et al.*<sup>21</sup> collected and reported LC<sub>50</sub>-values for silver exposed ZFEs ranging from 0.1 nM–820 µM for AgNPs and around 0.75 µM for AgNO<sub>3</sub>. The LC<sub>50</sub>-values obtained in this study are well within this range. With regard to the reported LC<sub>50</sub>-

value of AgNO<sub>3</sub>, our results for AgNPs and AgNO<sub>3</sub> (LC<sub>50</sub> ~0.33 µM) corrected for real concentrations match quite well. The LC<sub>50</sub>-values for AgNPs and AgNO<sub>3</sub> were comparable. Hence, the toxicity may be attributed to dissolved silver alone, as both the AgNPs and AgNO<sub>3</sub> exposure contained the same share of dissolved silver. A major impact of the bioavailable ionic fraction on the acute toxicity of AgNPs towards zebrafish embryos was reported by previous studies.<sup>1,20,24</sup> Furthermore, the study of Bar-Ilan *et al.*<sup>25</sup> stated that the sequence and type of events leading to the death of zebrafish embryos are similar for AgNPs and ionic silver. In contrast, Yue *et al.*<sup>26</sup> demonstrated a particle-specific effect on RTgill-W1 cells with higher toxicity of cit-AgNP in comparison to AgNO<sub>3</sub> exposures if related to the dissolved silver fraction.

### QUANTIFICATION AND VISUALIZATION OF SILVER ACCUMULATION IN ZFEs IN ABSENCE OF TOXICOLOGICAL EFFECTS

The ZFEs of different developmental stages were exposed to concentrations up to 150 µg l<sup>-1</sup> for 24 h. Only living and intact organisms were selected to be analysed by ICP-MS in order to obtain the internal concentrations. In addition, ZFEs exposed to 100 µg l<sup>-1</sup> were sectioned and the elemental distribution was visualised by LA-ICP-MS.

The ZFEs exposed at 2 hpf are characterised by the chorion structure surrounding the embryo.<sup>27</sup> Silver concentrations of 15 ng Ag per organism for AgNPs and 8 ng Ag per organism for AgNO<sub>3</sub> were measured for 2 hpf ZFEs after 24 h exposure (**Fig. 2**). Furthermore, a clear concentration dependent increase in internal silver concentrations was observed for ZFEs exposed to AgNO<sub>3</sub> at 2 hpf whereby a higher variability between the exposure concentrations and the internal concentrations was observed for AgNPs. The differences between the measured silver concentrations of AgNP- and AgNO<sub>3</sub>-exposed ZFEs may be attributed to the presence of the chorion. The adsorption and binding processes of the particulate and ionic silver to the chorion's structure were expected to be different and may lead to the observed differences in the silver concentrations for ZFEs exposed at 2 hpf. Auffan *et al.*<sup>28</sup> observed a complex formation between citrate-capped Ag-

## 5. Correlation of internal concentration and toxicological effects

NPs and thiolated sites of proteins and enzymes of the chorion of Atlantic killifish embryos.

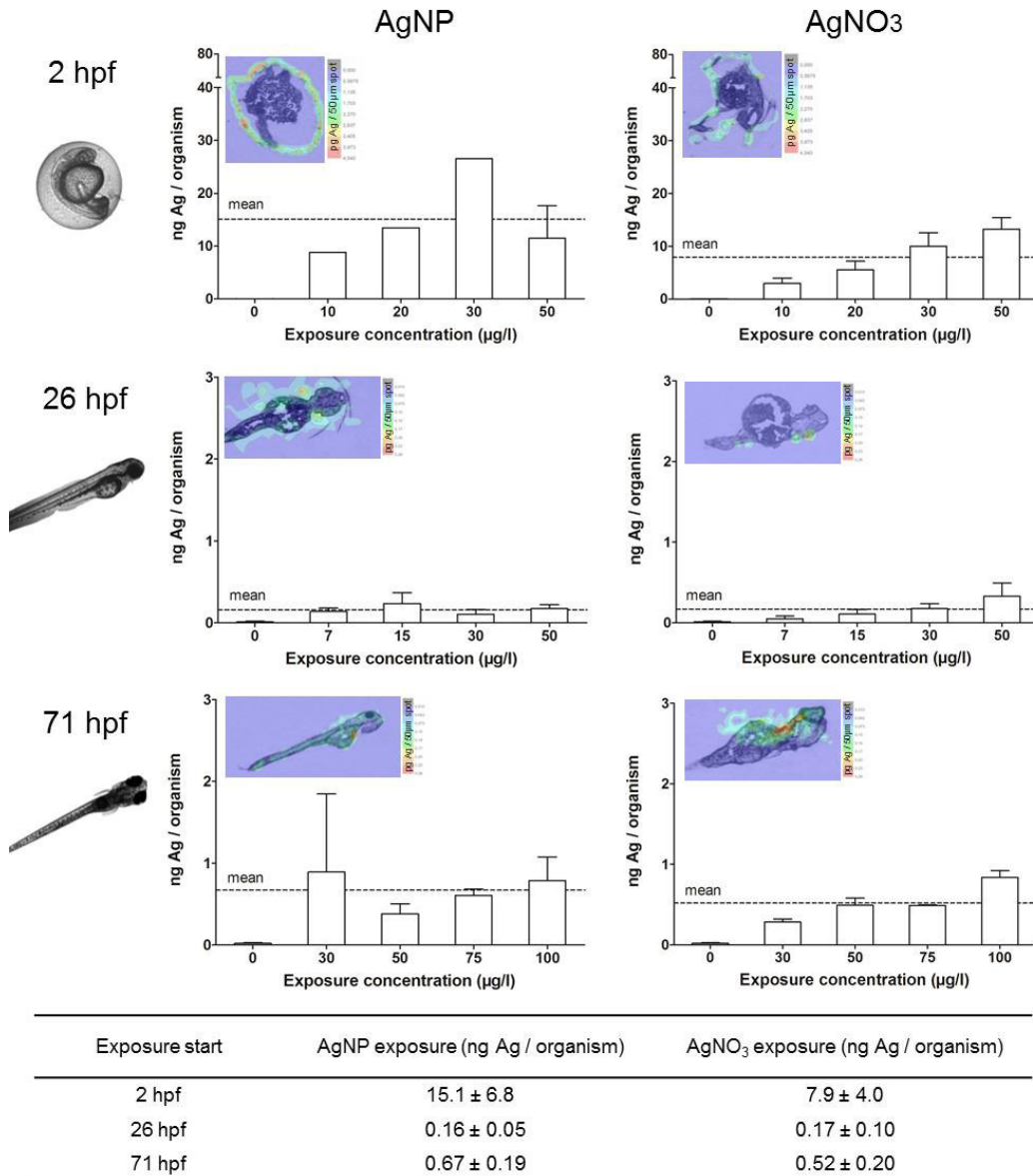


**Fig. 2:** Silver concentrations measured for ZFE exposed at different developmental stages (2, 26, and 71 hpf) in absence of toxicological effects. Quantification results obtained by neb-ICP-MS and respective LA-ICP-MS images after 24 h of exposure are shown. The color scale bar of LA-ICP-MS measurements represent silver concentrations from highest (red) to lowest value (blue). The table below shows the calculated means over the exposure concentrations (dotted lines in graphs).

ZFEs without chorion (26, 71 hpf) showed lower silver concentrations for both AgNP and AgNO<sub>3</sub> exposures compared to the ZFEs exposed at 2 hpf. In detail, concentration means of 0.2 and 0.7 ng Ag per organism were measured for 26 hpf and 71 hpf ZFEs treated with AgNPs, respectively (**Fig. 2**). The internal uptake

concentration for chorion-free development stages was independent of the exposure concentration. These findings indicated that the ZFE chorion played a crucial role in the adsorption of silver irrespective of the type (particular or ionic), resulting in up to 20-fold higher silver concentrations in the organisms compared to the chorion free stages. By the visualisation via LA-ICP-MS, the accumulation of silver at or within the chorion structures for ZFEs of the 2 hpf developmental stage became obvious (**Fig. 2**).

The association of AgNPs or Ag-nanoplates to the chorion structure without a direct uptake of particles by the embryo was previously observed by George *et al.*<sup>29</sup> and Osborne *et al.*<sup>1</sup> In contrast, Asharani *et al.*<sup>11</sup> and Lee *et al.*<sup>30</sup> detected an incorporation of single AgNPs within the perivitelline space (PVS) located between the chorion and the embryo or even within the embryonic tissues. These contrasting findings may be caused by the influence of the particle properties such as the coating and size of the particles<sup>31</sup> and the exposure duration on the internalisation process. For example, Asharani *et al.*<sup>11</sup> applied small and stabilised AgNPs (5–20 nm) which were able to pass through the chorion pore channels and reach the embryo. The transport of 12 nm AgNPs through the chorion pore channels into the inter ZFE compartments was examined after short exposure durations of 0–2 h in the study of Lee *et al.*<sup>30</sup>

The above mentioned studies determined either (1) the real NP concentrations in exposure suspensions, (2) the measured quantitative AgNP uptake concentrations or (3) they visualised the silver distribution within the organisms. However, a combination of the three parameters is needed. Furthermore, the influence of the developmental stage of the ZFE on the uptake and distribution of silver was not examined so far. Two studies reported quantification results for ZFEs with intact chorion. The study of George *et al.*<sup>29</sup> on Ag nanoplates reported silver concentrations of 400–450 ppb per ZFE for 4 hpf ZFE treated with 5 mg l<sup>-1</sup> for 48 h corresponding to an uptake of 0.3–0.4 ng per ZFE, assuming an organism volume of 800 nl. In addition, Auffan *et al.*<sup>28</sup> measured a total AgNP concentration of 60–140 ng per organism for Atlantic killifish (*Fundulus heteroclitus*) embryos exposed to 5 mg l<sup>-1</sup> and 48 h.

## SILVER PARTICLE AND ION DISTRIBUTION PATTERNS FOR ZEFs SHOWING SUBLETHAL EFFECTS

In order to investigate the silver accumulation during the occurrence of toxicological effects, individual ZFEs showing sublethal effects such as edema (yolk, pericard), change of pigmentation or heart frequency were selected and collected. Especially the occurrence of edema was prominent during the exposure with AgNPs and AgNO<sub>3</sub>. The observed sublethal effects are in accordance with other studies which reported interruptions in the cardiac cycle, edema, or hatching delays.<sup>11,16</sup> The quantification and visualisation results were presented in **Fig. 3**. No individuals showing effects could be collected (n.d.-not determined) or solely single individuals were analysed (no error bar) for some exposure concentrations.

All individuals showing sublethal effects accumulated increased silver concentrations compared to ZFEs showing no effects. The following silver concentrations were measured after a 24 h AgNP exposure for ZFEs exposed at 2, 26, and 71 hpf: 17.4, 1.0, and 1.3 ng Ag per organism, respectively. A concentration-dependent uptake was observed for the 2 hpf (both for AgNP and AgNO<sub>3</sub> treatment) and the 71 hpf ZFE stage (only for the exposure with AgNPs). Differences between the uptake concentrations of AgNPs and AgNO<sub>3</sub> were only measured for ZFEs exposed at 71 hpf with higher silver concentrations for organisms exposed to AgNPs. Probably, the enrichment of particles at the embryo surface leads to a subsequent release of silver ions into the embryonic tissues for this later developmental stage. Furthermore, the ZFE of this developmental stage is more mobile, implying a potentially higher exposure to AgNPs.

The silver distribution for 2 hpf ZFEs showing sublethal effects was different compared to the silver distribution within ZFEs lacking toxicological effects. As visible via the LA-ICP-MS imaging, silver was not only detected at the chorion, but also in the perivitelline space (PVS). This compartment is hard to sample individually but the silver accumulation in the PVS can be easily detected by LA-ICP-MS. However, it was not possible to distinguish between silver particles or the silver ion fraction by using this method. Since we detected a high fraction of ionic silver in the AgNP suspensions, the main proportion detected in the PVS might be

## 5. Correlation of internal concentration and toxicological effects

attributed to dissolved silver ions. The NP–chorion interaction seems to result in a higher permeability of the chorion, and therefore more silver was detected within the PVS. Once silver is accumulated in the PVS, the translocation of silver to the embryo surface is likely. This was indeed observed for the later developmental stages (26, 71 hpf) (**Fig. 3**).

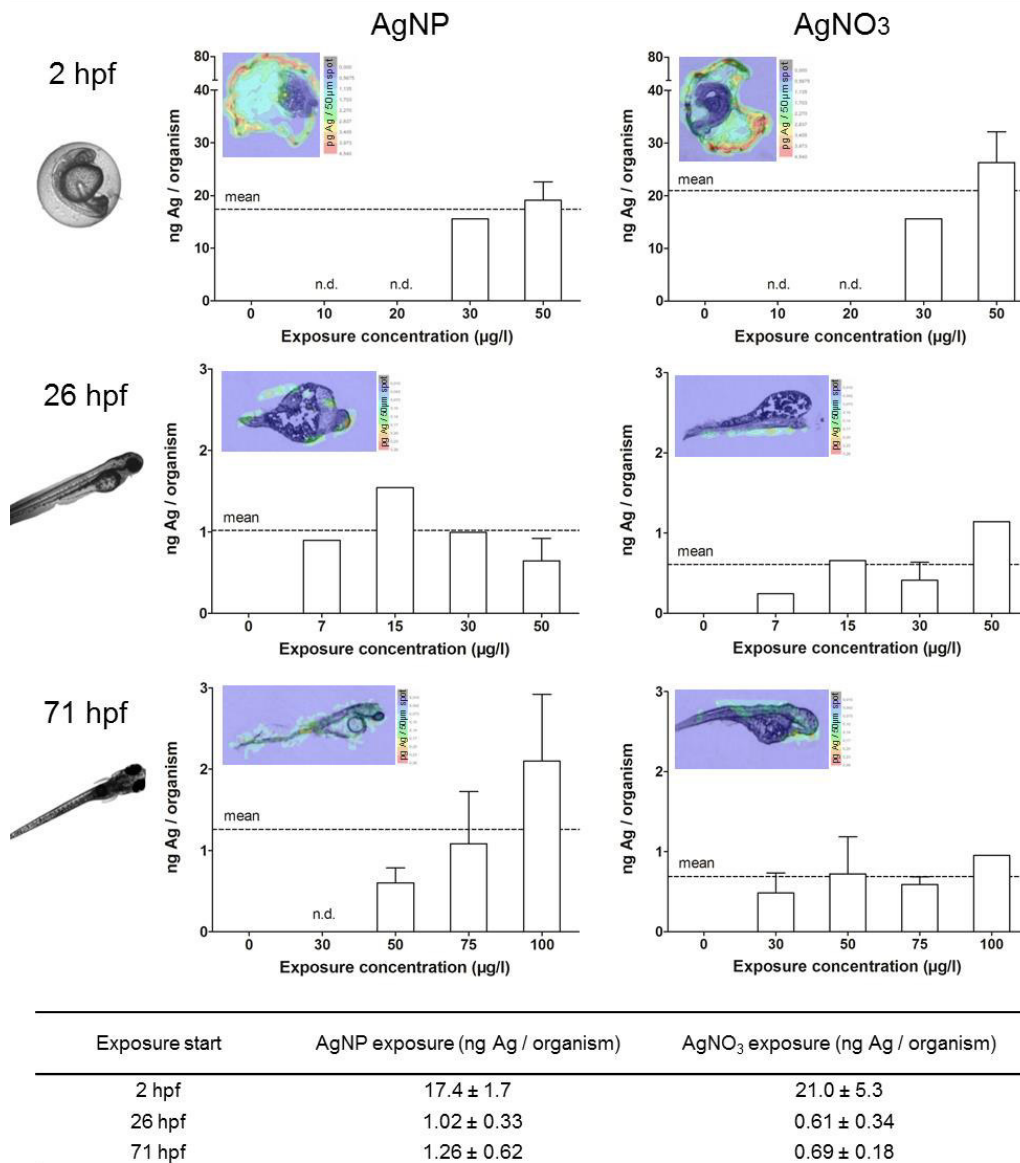


**Fig. 3:** Silver concentrations measured for ZFE exposed at different developmental stages (2, 26, and 71 hpf) in presence of sublethal effects. Quantification results obtained by neb-ICP-MS and respective LA-ICP-MS images after 24 h of exposure are shown. The color scale bar of LA-ICP-MS measurements represent silver concentrations from highest (red) to lowest value (blue). The table below shows the calculated means over the exposure concentrations (dotted line in graphs).

Concerning the number and sizes of particles, Lee *et al.*<sup>32</sup> qualitatively showed that deformed ZFEs internalised larger and a higher number of AgNPs compared to normally developed embryos of 120 hpf. The potential of metal oxide NPs to reach the embryo surface and to penetrate the skin triggering toxic effects was described previously by Lin *et al.*<sup>13</sup> and Zhu *et al.*<sup>33</sup> In this context, Osborne *et al.*<sup>1</sup> described the yolk syncytial layer as the target tissue for AgNPs resulting in the passage of particles into the yolk, an uptake by the embryo, and subsequently the occurrence of adverse effects or lethality. Furthermore, the release of silver ions from AgNPs accumulated in the ZFE due to a particle destabilisation was theoretically described by Bar-Ilan *et al.*<sup>25</sup> and van Aerle *et al.*<sup>24</sup>.

### SILVER ACCUMULATION ASSESSMENT IN LETHAL ZFEs

In order to determine the silver accumulation in dead embryos, we selected and collected individual ZFEs showing one of the following parameters according to the OECD test guideline 236:<sup>18</sup> coagulation, missing formation of somites, no detachment of tail or no heartbeat. No individuals showing effects could be collected (n.d.-not determined) or solely single individuals were analysed (no error bar) for some exposure concentrations. For all we know, this is the first study quantifying NP uptake within dead ZFEs.

As described for ZFEs with sublethal effects, dead ZFEs also showed higher internal silver concentrations compared to intact, living organisms. In general, no differences between AgNP or AgNO<sub>3</sub> exposure were observed for dead ZFEs. The silver concentrations determined for the chorion-free stages were comparable to those of ZFEs showing sublethal effects, with 0.9 (26 hpf) and 1.2 ng Ag per organism (71 hpf) for a 24 h AgNP exposure. Only for ZFEs exposed at 2 hpf, probably due to the presence of the chorion, a two-fold increase in accumulation compared to ZFEs showing sublethal effects was observed, e.g., 33 ng Ag per organism for AgNP exposed organisms.

However, the denaturation of the ZFEs upon death results in physically defect organisms. This leads to huge standard deviations of the silver concentrations

measured for 2 hpf ZFEs, indicating technical constraints when sampling and analysing silver concentrations of dead ZFEs with chorion.

In addition, the silver distribution in ZFEs changed over time. The highest silver concentrations at 2 hpf are located in the dead embryo tissue as shown by LA-ICP-MS measurements (**Fig. 4**). The enrichment in this specific ZFE compartment is similar for both particulate and ionic silver. Silver accumulation at the surface of the embryo (26 hpf) and silver distribution within the embryo tissue (71 hpf) are again observed for the later ZFE stages. However, it remains unclear, whether the increase in internal silver concentrations in damaged embryos is a cause of toxicity or its consequence.

### CORRELATION BETWEEN TOXICOLOGICAL EFFECTS AND INTERNAL CONCENTRATIONS

The toxicological testing of AgNPs and AgNO<sub>3</sub> revealed comparable LC<sub>50</sub>-values for the different developmental ZFE stages related to the measured exposure concentrations. As a consequence, the presence of the chorion alone seems to have no mitigating effect on silver toxicity.

In contrast, the quantification and visualisation data obtained for AgNP and AgNO<sub>3</sub> exposed ZFEs differ with respect to the developmental stage. The chorion has a tremendous impact on the amount of silver detected based on the measurement of silver associated to the ZFE. Especially, distinct differences in the internal silver concentrations and distribution patterns were detected for the first developmental stage (2 hpf) due to the presence of the chorion. This phenomenon was compared in 26 hpf ZFEs, with and without chorion, but no differences in the internal silver concentrations of the embryos were measured (data not shown). The structure of the chorion adsorbed substantial amounts of silver, which, however, did not influence the toxicity effects. Likewise, the presence of the chorion influenced the silver distribution upon occurrence of sublethal and lethal effects. The internal silver concentrations and distribution patterns were comparable for chorion-free stages (26 hpf, 71 hpf) even for ZFEs showing adverse effects.

## 5. Correlation of internal concentration and toxicological effects

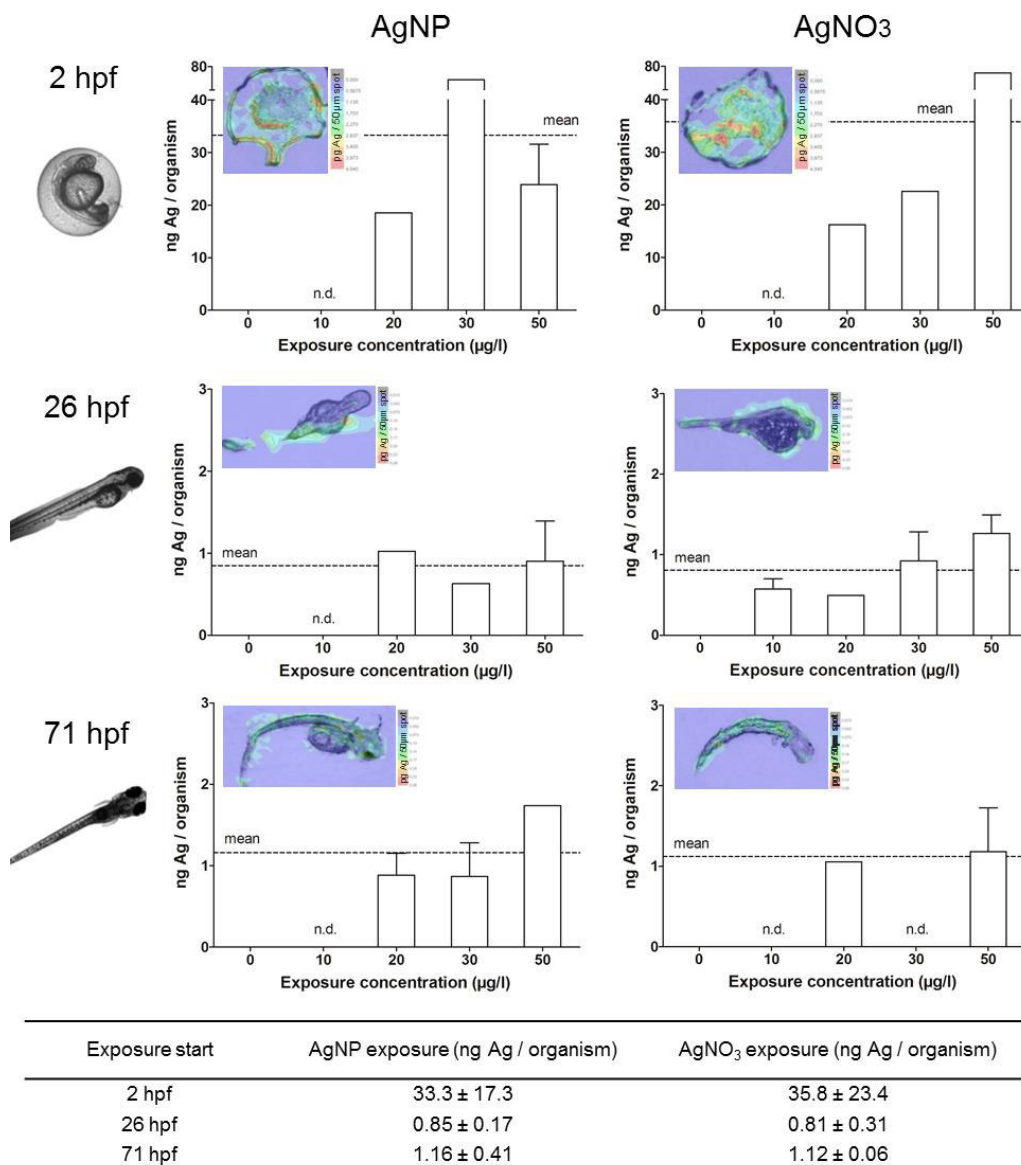


**Fig. 4:** Silver concentrations measured for dead ZFE exposed at different developmental stages (2, 26, and 71 hpf). Quantification results obtained by neb-ICP-MS and respective LA-ICP-MS images after 24 h of exposure are shown. The color scale bar of LA-ICP-MS measurements represent silver concentrations from highest (red) to lowest value (blue). The table below shows the calculated means over the exposure concentrations (dotted line in graphs).

The toxicological effects at different developmental stages were correlated with the respective internal concentrations (**Fig. 5**). The 2 hpf stage enclosed by the chorion was excluded from the correlation since the chorion was identified as the major adsorption site for AgNPs and would hence disturb the correlation. Thus, we referred to the internal concentration measured for the embryo since the attachment to the outer surface and the direct internalisation of silver in the embryonic tissues were described as the main mechanism leading to toxicity.<sup>1,11</sup>

The correlation revealed an effect-related increase in internal ZFE concentrations (**Fig. 5**) as a higher percentage of effect (sublethal or lethal) is linked to a slight increase in the internal silver concentration. In general, the silver concentrations obtained for ZFEs showing adverse effects vary between 0.5–1 ng Ag per organism for both AgNPs and AgNO<sub>3</sub>. This further indicates that the results are independent of the silver entity introduced to the organism. However, the progression of the effects over time is still not fully resolved, and it remains unclear, whether the increase in silver uptake is the cause or the result of damage to ZFE tissues.

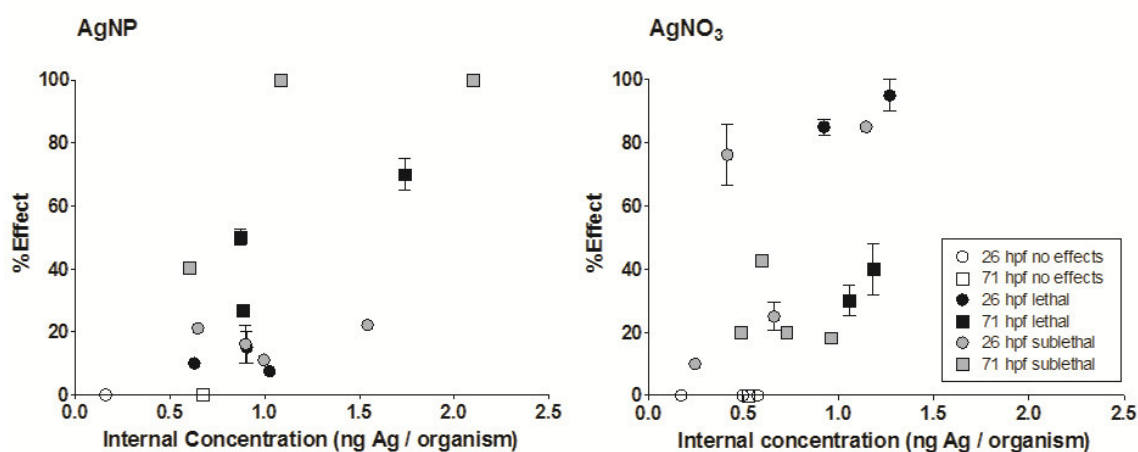


**Fig. 5:** Correlation between observed toxicological effects and internal silver concentrations. The measured uptake concentrations and effects for chorion-free developmental stages (26 hpf, 71 hpf) for ZFE showing no effects (empty symbols), sublethal (grey filled symbols), and dead ZFE (black filled symbols) are shown.

To our knowledge, this is the first direct correlation of the effect values and internal concentrations based on AgNP exposure. Lee *et al.*<sup>30</sup> reported a dependency of toxicity on the exposure concentration with a critical concentration of 0.19 nM AgNPs (~21 ng), which matches our results. However, we extended the observation of toxicity by determining the critical internal dose (0.5–1 ng Ag per organism) directly affecting the embryo. Nevertheless, further measurements are necessary to validate the presented internal effect concentrations.

We assume that sublethal and lethal effects occur upon accumulation of a critical silver dose within the embryo. This is in agreement with Escher and Hermens<sup>3</sup> describing this relationship for substances leading to an irreversible biological effect. Furthermore, this is in line with the assumption that NPs behave differently

from chemicals, which penetrate the chorion and build an equilibrium of internal and external concentration by simple diffusion. In the case of NPs, the particle uptake is driven by kinetically controlled particle attachment and deposition processes and hence no thermodynamic equilibrium as for organic substances is formed.<sup>34</sup> Thus, the NP accumulation can be considered as an irreversible step and the deposition of a critical mass of particles can trigger the occurrence of biological effects. Importantly, this effect interferes with the partitioning behaviour of silver ions which simultaneously interact with the ZFE.

### IMPLICATIONS FOR THE ZFE AS MODEL FOR NP TESTING

From our point of view, the ZFE is a suitable biological model for the testing of NPs when certain aspects specific to these materials are considered.

For example, the impact of the ionic fraction released from NP surfaces has to be regarded since ions are actually the chemical component mainly triggering the toxicological effects. However, as described by Cunningham *et al.*<sup>17</sup> all NP test solutions should be regarded as a mixture of AgNPs, aggregates, silver complexes, and dissolved silver ions, which is relevant for both analytical and toxicity studies. Moreover, analytically measured exposure concentrations should be the basis for reliable and comparable dose–response calculations.

The complex influence of the ZFE chorion on the amount of substance taken up needs further attention with regard to accumulation studies. Indeed, the determination of internal concentrations often refers to the whole organism including the chorion. This does not reflect real internal concentrations as the chorion acts as a biological barrier, resulting in concentration overestimation.<sup>35</sup> Therefore, we recommend a dechoriation before performing accumulation studies or prior to the analytical measurement. Especially, for the correlation of toxicological effects and uptake amounts, it is favourable to refer to the internal silver concentrations measured for the isolated embryo.

## **CONCLUSION**

We analysed embryos of different developmental stages and compared the internal concentration and distribution of silver after exposure to AgNPs and AgNO<sub>3</sub> by applying a suite of ICP-MS-based techniques optimised for measuring NPs. Small differences in silver toxicity were observed between the different developmental stages and particulate and ionic silver, respectively by correcting the exposure concentrations for measured concentrations. On the basis of internal silver concentrations, the embryo stage with chorion accumulated substantially more silver compared to the later stages without the chorion, assuming the adsorption of silver to the chorion structures. However, substantial differences in silver distribution were observed when the embryos affected by silver exposure were compared to unaffected ones.

Analytical techniques allowing the differentiation of particle and ionic fractions in one organism would highly contribute to our understanding of especially silver particle toxicity in future studies. Further, the inclusion of more time points would help to gain deeper insight into the toxicological effect progression. The PVS as a ZFE compartment neglected in this study needs consideration which requires improved sampling procedures.

This study is of general relevance, as the procedure is applicable to other test organisms (e.g. daphnids) and NPs. In addition, new insights into the mechanisms and processes on NP–organism interactions were provided which are essential to further improve the risk assessment of such materials.

## **ACKNOWLEDGMENTS**

This research was funded by the EU FP7 project NanoValid (Development of reference methods for hazard identification, risk assessment and LCA of engineered nanomaterials; grant no 263147). Additionally, S. B. was kindly supported by the Helmholtz Impulse and Networking Fund through the Helmholtz Interdisciplinary Graduate School for Environmental Research (HIGRADE).

## REFERENCES

1. Osborne O.J., Johnston B.D., Moger J., et al. (2013). Effects of particle size and coating on nanoscale Ag and TiO<sub>2</sub> exposure in zebrafish (*Danio rerio*) embryos. *Nanotoxicology*, 7(8): 1315-1324
2. Völker C., Gräf T., Schneider I., et al. (2014). Combined effects of silver nanoparticles and 17 $\alpha$ -ethinylestradiol on the freshwater mudsnail *Potamopyrgus antipodarum*. *Environ Sci Pollut Res*, 21(18): 1-10
3. Escher B.I. and Hermens J.L. (2004). Peer reviewed: internal exposure: linking bioavailability to effects. *Environ Sci Technol*, 38(23): 455A-462A
4. Asharani P., Lianwu Y., Gong Z., Valiyaveetil S. (2011). Comparison of the toxicity of silver, gold and platinum nanoparticles in developing zebrafish embryos. *Nanotoxicology*, 5(1): 43-54
5. Brun N.R., Lenz M., Wehrli B. and Fent K. (2014). Comparative effects of zinc oxide nanoparticles and dissolved zinc on zebrafish embryos and eleuthero-embryos: Importance of zinc ions. *Sci Total Environ*, 476: 657-666
6. Chen D., Zhang D., Jimmy C.Y. and Chan K.M. (2011). Effects of Cu<sub>2</sub>O nanoparticle and CuCl<sub>2</sub> on zebrafish larvae and a liver cell-line. *Aquat Toxicol*, 105(3): 344-354
7. Scholz S., Fischer S., Gündel U. (2008). The zebrafish embryo model in environmental risk assessment - applications beyond acute toxicity testing. *Environ Sci Pollut Res*, 15(5): 394-404
8. El-Amrani S., Sanz-Landaluze J., Guinea J. and Camara C. (2013). Rapid determination of polycyclic aromatic hydrocarbons (PAHs) in zebrafish eleutheroembryos as a model for the evaluation of PAH bioconcentration. *Talanta*, 104: 67-74
9. Kühnert A., Vogts C., Altenburger R. and Küster E. (2013). The internal concentration of organic substances in fish embryos - a toxicokinetic approach. *Environ Toxicol Chem*, 32(8): 1819-1827
10. Marquis B.J., Love S.A., Braun K.L. and Haynes C.L. (2009). Analytical methods to assess nanoparticle toxicity. *Analyst*, 134(3): 425-439
11. Asharani P., Wu Y.L., Gong Z. and Valiyaveetil S. (2008). Toxicity of silver nanoparticles in zebrafish models. *Nanotechnology*, 19(25): 1-8
12. Fent K., Weisbrod C.J., Wirth-Heller A. and Pielkes U. (2010). Assessment of uptake and toxicity of fluorescent silica nanoparticles in zebrafish (*Danio rerio*) early life stages. *Aquat Toxicol*, 100(2): 218-228
13. Lin S., Zhao Y., Xia T., et al. (2011). High content screening in zebrafish speeds up hazard ranking of transition metal oxide nanoparticles. *ACS nano*, 5(9): 7284-7295
14. Böhme S., Stärk H.-J., Kühnel D. and Reemtsma T. (2015). Exploring LA-ICP-MS as a quantitative imaging technique to study nanoparticle uptake in *Daphnia magna* and zebrafish (*Danio rerio*) embryos. *Anal Bioanal Chem*, 407(18): 5477-5485
15. Böhme S., Stärk H.-J., Meißner T., et al. (2014). Quantification of Al<sub>2</sub>O<sub>3</sub> nanoparticles in human cell lines applying inductively coupled plasma mass spectrometry (neb-ICP-MS, LA-ICP-MS) and flow cytometry-based methods. *J Nanopart Res*, 16(9): 2592

16. Bowman C.R., Bailey F.C., Elrod-Erickson M., Neigh A.M., et al. (2012). Effects of silver nanoparticles on zebrafish (*Danio rerio*) and *Escherichia coli* (ATCC 25922): A comparison of toxicity based on total surface area versus mass concentration of particles in a model eukaryotic and prokaryotic system. *Environ Toxicol Chem*, 31(8): 1793-1800
17. Cunningham S., Brennan-Fournet M.E., Ledwith D., Byrnes L., et al. (2013). Effect of nanoparticle stabilization and physicochemical properties on exposure outcome: acute toxicity of silver nanoparticle preparations in zebrafish (*Danio rerio*). *Environ Sci Technol*, 47(8): 3883-3892
18. OECD (2013). Test No. 236: Fish Embryo Acute Toxicity (FET) Test. [www.oecd.org](http://www.oecd.org).
19. NanoValid, EU-Project (2014). ENP Specification Form Silver Nanoparticles (NNV-003). *Internal Draft*
20. Visual MINTEQ, Version 3.1, 2013, Department of Land and Water Resources Engineering, KTH, Sweden, Available at: <http://vminteq.lwr.kth.se/>.
21. Groh K.J., Dalkvist T., Piccapietra F., Behra R., et al. (2015). Critical influence of chloride ions on silver ion-mediated acute toxicity of silver nanoparticles to zebrafish embryos. *Nanotoxicology*, (9): 81-91
22. OECD (2000). Guidance Document on Aquatic Toxicity Testing of Difficult Substances and Mixtures. [www.oecd.org](http://www.oecd.org).
23. Kühnel D. and Nickel C. (2014). The OECD expert meeting on ecotoxicology and environmental fate - Towards the development of improved OECD guidelines for the testing of nanomaterials. *Sci Total Environ*, 472: 347-353
24. Bar-Ilan O., Albrecht R.M., Fako V.E. and Furgeson D.Y. (2009). Toxicity assessments of multisized gold and silver nanoparticles in zebrafish embryos. *Small*, 5(16): 1897-1910
25. van Aerle R., Lange A., Moorhouse A., Paszkiewicz K., et al. (2013). Molecular mechanisms of toxicity of silver nanoparticles in zebrafish embryos. *Environ Sci Technol*, 47(14): 8005-8014
26. Yue Y., Behra R., Sigg L., Freire P. F., et al. (2015). Toxicity of silver nanoparticles to a fish gill cell line: Role of medium composition. *Nanotoxicology*, 9: 54-63.
27. Kimmel C.B., Ballard W.W., Kimmel S.R., et al. (1995). Stages of embryonic development of the zebrafish. *Dev Dynam*, 203(3): 253-310
28. George S., Lin S., Ji Z., et al. (2012). Surface defects on plate-shaped silver nanoparticles contribute to its hazard potential in a fish gill cell line and zebrafish embryos. *ACS nano*, 6(5): 3745-3759
29. Lee K.J., Nallathamby P.D., Browning L.M., et al. (2007). *In vivo* imaging of transport and biocompatibility of single silver nanoparticles in early development of zebrafish embryos. *ACS nano*, 1(2): 133-143
30. Powers C.M., Slotkin T.A., Seidler F.J., et al. (2011). Silver nanoparticles alter zebrafish development and larval behavior: distinct roles for particle size, coating and composition. *Neurotoxicology and teratology*, 33(6): 708-714
31. Auffan M., Matson C.W., Rose J., et al. (2014). Salinity-dependent silver nanoparticle uptake and transformation by Atlantic killifish (*Fundulus heteroclitus*) embryos. *Nanotoxicology*, (8): 167-176

## 5. Correlation of internal concentration and toxicological effects

---

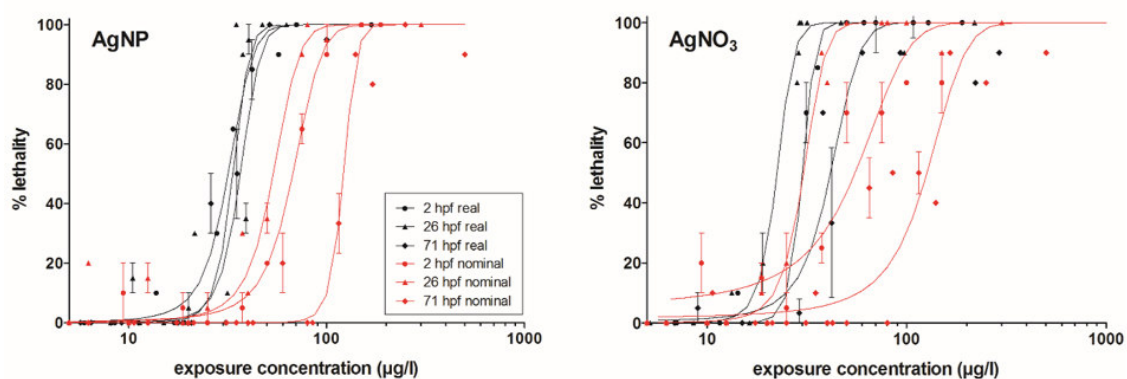
32. Lee K.J., Browning L.M., Nallathamby P.D., et al. (2012). *In vivo* quantitative study of sized-dependent transport and toxicity of single silver nanoparticles using zebrafish embryos. *Chem Res Toxicol*, 25(5): 1029-1046
33. Zhu X., Zhu L., Duan Z., et al. (2008). Comparative toxicity of several metal oxide nanoparticle aqueous suspensions to Zebrafish (*Danio rerio*) early developmental stage. *J Environ Sci Heal A*, 43(3): 278-284
34. Praetorius A., Tufenkji N., Goss K.-U., et al. (2014). The road to nowhere: equilibrium partition coefficients for nanoparticles. *Environ Sci: Nano*, 1(4): 317-323
35. Brox S., Ritter A.P., Küster E. and Reemtsma T. (2014). Influence of the perivitelline space on the quantification of internal concentrations of chemicals in eggs of zebrafish embryos (*Danio rerio*). *Aquat Toxicol*, 157: 134-140

## ELECTRONIC SUPPLEMENTARY INFORMATION

### Results and discussion

#### TOXICITY ASSESSMENT AND CORRECTION TO REAL EXPOSURE CONCENTRATIONS

The following steps for a complete toxicity assessment were performed: (1) ZFE toxicity testing of AgNPs and AgNO<sub>3</sub> according to the OECD test guideline 236, (2) correction of calculated dose-response curves and the LC<sub>50</sub>-values using measured, real silver concentrations, and (3) comparison of the results obtained based on nominal and corrected exposure concentrations. The corrected compared to the nominal effect concentrations after 48 h of exposure are shown in **Fig. S1**. In general, for both, AgNP and AgNO<sub>3</sub> treated ZFEs, a concentration-dependent toxicity was observed.



Exposure start	AgNP LC <sub>50</sub> (µg/l)			AgNO <sub>3</sub> LC <sub>50</sub> (µg/l)		
	nominal	real	based on Ag <sup>+</sup>	nominal	real	based on Ag <sup>+</sup>
2 hpf	66.0 ± 3.7	31.3 ± 1.4	1.4	49.9 ± 12.8	29.8 ± 0.8	3.0
26 hpf	52.8 ± 5.7	33.4 ± 4.3	1.5	30.1 ± 1.7	22.2 ± 1.3	2.2
71 hpf	121.1 ± 5.3	36.3 ± 3.4	1.6	118.8 ± 22.8	40.6 ± 4.9	4.1

**Fig. S1:** Dose-response curves based on nominal (red) and corrected real exposure concentrations (black) for the respective developmental stages of the ZFE. The calculated nominal and real LC<sub>50</sub> values of the respective AgNP or AgNO<sub>3</sub> exposure as well as the developmental stage are listed in the table below. The LC<sub>50</sub> values based on the dissolved Ag<sup>+</sup> were calculated according to the ionic silver content in the exposure solution.



## **Chapter 6**

### **FIRST QUALITATIVE RESULTS OF A NOVEL LASER ABLATION AND SINGLE PARTICLE ICP-MS (LA-SP-ICP-MS) METHOD COMBINATION**

In preparation

Steffi Böhme<sup>1</sup>, Hans-Joachim Stärk<sup>2</sup>, Thorsten Reemtsma<sup>2</sup>

<sup>1</sup> Helmholtz Centre for Environmental Research - UFZ, Department of Bioanalytical Ecotoxicology, Permoserstrasse 15, 04318 Leipzig (Germany)

<sup>2</sup> Helmholtz Centre for Environmental Research - UFZ, Department of Analytical Chemistry, Permoserstrasse 15, 04318 Leipzig (Germany)



### ABSTRACT

For the detection, quantification and visualization of nanoparticles (NPs) within biological and environmental samples, established analytical methods for the measurement of chemicals have to be improved. ICP-MS allows the (elemental) sensitive detection and quantification of NP concentrations. In recent years, both LA-ICP-MS for the visualization as well as SP-ICP-MS for the quantification of single particle events were applied. However, a combination of a visualization of NP internalization with information on the NP size in parallel is missing. In this study, LA-ICP-MS as semi-quantitative imaging technique was applied for the visualization of the AgNP distribution within *Daphnia magna*. Therefore, individually NP-spiked agarose gels were ablated for an external calibration. As element sensitive detector, SP-ICP-MS analysis was used to distinguish between internalized particle and dissolved ionic fractions. By the adjustment of the gas flows, laser ablation spot diameter and energy a combination of both methods was realized on a qualitative basis. This study presents first measurements on the combination of LA-ICP-MS with SP-ICP-MS. The obtained results show the first qualitative detection of single NPs after the ablation of a biological sample with SP-ICP-MS. The improvement of instrumentation and data evaluation parameters would further move this novel method combination towards a reliable, quantitative single particle visualization technique matching the upcoming requirements of analytical methods for advanced NP-analysis.

### INTRODUCTION

Nanoparticle (NP) research is a rapid developing and growing field due to the numerous applications of engineered nanomaterials, e.g. as ingredients of cosmetics, food, packaging material, electronics, or in medicine (Lowry et al. 2012). Since 2011, the European Commission defines nanomaterials (NM) as “(...) a material containing particles (...) where, for 50 % or more of the particles in the number size distribution, one or more external dimensions is in the size range 1 nm-100 nm.” (Commission 2011).

The above mentioned EU-definition requires adequate analytical methods to detect and quantify NPs within consumer products, biological tissues or environmental samples. Available analytical methods and techniques are often established for the analysis of chemical substances with known properties. NPs can behave completely different due to their unique chemical and physical characteristics and therefore an improvement of existing or the development of new analytical measurement tools is required (Marquis et al. 2009). Especially, techniques able to analyze the internalization, modification, and localization of NPs with high (elemental) sensitivity and able to distinguish between particle and dissolved ionic fractions are needed.

Laser Ablation ICP-MS (LA-ICP-MS) was firstly established for the elemental analysis of solid samples, e.g. rocks or archeological samples (Russo et al. 2002). During the last years the tendency to develop LA-ICP-MS further into the direction of an imaging technique for biological samples grown (Pozebon et al. 2014). Especially, improvements in the spatial resolution and the elemental detection within cell layers or organism sections were performed. For example, Drescher et al. (2012) and Wang et al. (2013) visualized the NP and a metal-tagged biomarker uptake and distribution on a cellular level by LA-ICP-MS down to a spatial resolution of 1  $\mu\text{m}$ , respectively. Recently, a particle size effect by the laser ablation was detected resulting in an incomplete ablation and evaporation of NPs embedded in a soft organic matrix (Böhme et al. 2015). This effect leads to the transport of almost unchanged NPs to the ICP-MS and an incomplete ionization within the plasma. Therefore, a signal intensity suppression can be observed what can distort the overall analysis and quantification. Since this effect is dependent on the particle size, concentration underestimations can be expected for particles  $>150$  nm (Böhme et al. 2015). The detected particle size effect is a limitation of LA-ICP-MS and has to be compensated, e.g. by a matrix-matched calibration with individually NP-spiked standards such as agarose gels (Böhme et al. 2014).

In recent years, Single Particle ICP-MS (SP-ICP-MS) as a promising technique able to detect single particle events and to determine different particle size fractions was introduced (Pace et al. 2011; Lee et al. 2014) and has been applied for routine analysis (Peters et al. 2015). First, SP-ICP-MS was established for the

analysis of colloids e.g. in water samples (Degueldre and Favarger 2003; Degueldre et al. 2006). The main advantages of this technique are the rapid analysis time within seconds, the high elemental sensitivity, and the possibility to combine it with other techniques such as Field Flow Fractionation (FFF) or chromatographic separation methods (Hassellöv et al. 2008). The distinction of different composed NPs, of NPs and natural occurring particles or of NPs and dissolved ions is another benefit of this technique (Pace et al. 2011). For example, the distinction of Ag-NPs and dissolved silver ions in water samples using SP-ICP-MS was reported recently by Mitrano et al. (2014).

The aim of this study is to present a novel method combination of both, LA-ICP-MS for imaging and SP-ICP-MS for specific single particle detection. Preliminary experiments on a qualitative detection basis should highlight the suitability of the technique to improve the analysis and detection of NPs in a broad range of samples. Therefore, *Daphnia magna* exposed to AgNPs were applied for the first investigations. The possible applications of this combination as well as the limitations and necessary improvements are illustrated.

### **Experimental**

#### NANOPARTICLE CHARACTERIZATION

The AgNPs used in this study were provided and characterized in detail by partners of the EU-project NanoValid ([www.nanovalid.eu](http://www.nanovalid.eu)). Briefly, the AgNPs have a primary particle size of 10 - 21 nm, a hydrodynamic particle size of  $117 \pm 24$  nm, and a polyvinyl pyrrolidone (PVP) coating. The dissolved silver ionic fraction was determined for the stock suspension after centrifugation and subsequent measurement of the supernatant with ICP-MS showing that up to 48 % of the silver is present in the ionic form.

### SAMPLE PREPARATION

The exposure of *Daphnia magna* was performed according to the OECD test guideline 202 (OECD 2004). The crustaceans were cultivated under controlled conditions at 20 °C at a 16:8 h light/dark cycle. Daphnids were fed three times a week with algae and individuals aged less than 24 h (neonates) were exposed to AgNPs in ADaM (Aachener Daphnienmedium) for 24 h with an ENP-concentration of 10 µg element/l (non-toxic). After exposure, only living, healthy organisms were collected, washed, fixated and embedded with frozen section medium. Afterwards, the organisms were cut into 40 µm sections by a microtome (MICROM Cryo Star, HM560, Thermo Scientific) at -20 °C. The sections were placed on glass slides and were subsequently introduced to the laser ablation chamber.

### PARAMETERS FOR LA-SP-ICP-MS MEASUREMENTS

A high resolution double-focusing sector field ICP-MS (Element XR, Thermo Fisher Inc.) was applied for concentration analysis and SP-ICP-MS measurements (**Tab. 1**). For SP-ICP-MS analysis the Element XR was operated in low resolution (R=300). Sampling time of 3 ms (3 x 1 ms) was applied with enough replicates to achieve a total analysis time of 60 or respectively 120 s. For data evaluation, the background/dissolved signal was subtracted from the NP signals and the particle size distributions were enumerated by excel using a modified calculation tool based on the sheet provided by the RIKILT institute (RIKILT 2014).

The exposed organism sections were ablated using a Nd:YAG laser with a wavelength of 213 nm (LSX-213, CETAC) (**Tab. 1**). For imaging, the laser energy was adjusted to 60 % to ensure a complete ablation of the organic layer. A 50 µm diameter as spot size was used for the ablation and the respective element signal was recorded in the transient measurement mode. The nebulizer was used in parallel to mix the laser aerosol with a blank solution and to have constant wet plasma conditions. An external calibration was performed with individually NP-spiked agarose gels of 40 µm in thickness. The maximum intensities of the peak highs obtained by the ablation of the individual spots were collected in a data

matrix transformed to concentration values as described previously (Böhme et al. 2015).

For the combination of LA- and SP-ICP-MS a series of different laser energies for the ablation, spot diameters and intensities of the gas streams (nebulizer, additional) were tested. These parameters are adjusted in order to adequately “dilute” the ablated organic material and to obtain maximum signal intensity.

**Tab. 1:** Measurement parameters of LA-SP-ICP-MS combination.

---

ICP-MS: Element XR, Thermo Fisher Inc.

Laser: LSX-213, CETAC Nd:YAG laser 213 nm

Element: Ag<sup>107</sup>, density: 10.49 g/cm<sup>3</sup>

---

SP-ICP-MS parameters	1.25 kV RV power
	3 ms dwell time
	120 s acquisition time
	1.1 l/min argon auxiliary gas flow
	0.61 l/min argon shield gas flow
	0.45 l/min argon nebulizer gas flow

---

LA-ICP-MS parameters	50 µm spot diameter
	60 % laser energy
	0.1 l/min laser argon gas flow

---

### TEM ANALYSIS

For the investigations of the initial NP size and particles formed after laser ablation, transmission electron microscopy (TEM) (Zeiss Merlin VP compact) was applied. In order to ensure a statistic reliable number of particles, the particle aerosol formed by the laser ablation process was collected and concentrated. Therefore, first experiments on passing the aerosol by the additional argon gas stream into a hexane solution and subsequently deposit it on a TEM mesh for drying were performed (results are not shown).

## RESULTS AND DISCUSSION

In order to combine LA- and SP-ICP-MS measurements, the previously reported particle size effect (Böhme et al. 2015) which occurs during the laser ablation of soft organic matrices has to be verified. Therefore, the by the laser ablation process formed particle aerosol was collected, concentrated and investigated by TEM. At the beginning of the experiments, a primary particle size of 20 - 50 nm was observed for the prepared NP suspensions prior (**Fig. 1**). With the obtained results the particle size effect occurring during LA-ICP-MS measurements was validated. This limitation of LA-ICP-MS is the basis for the here presented method combination of LA- and SP-ICP-MS analysis since it allows to detect single particle events.

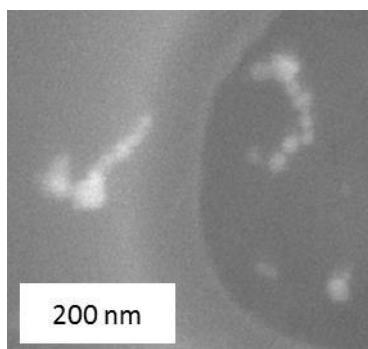


**Fig. 1:** SEM/TEM images prior to the laser ablation of the soft organic matrix of the sample.

The first LA-SP-ICP-MS measurements show the detection of single particle events after the ablation of organism sections of *Daphnia magna* exposed to AgNPs (**Fig. 2**). For the SP-ICP-MS measurements a small region of interest (e.g., an area of the gut of *Daphnia magna*) was chosen for a single spot ablation and the subsequent ICP-MS detection. These qualitative results correspond to our expectations and the described particle size effect. However, it is not clear whether the NPs may change during the laser ablation process or whether they are completely, unchanged transported to the ICP.

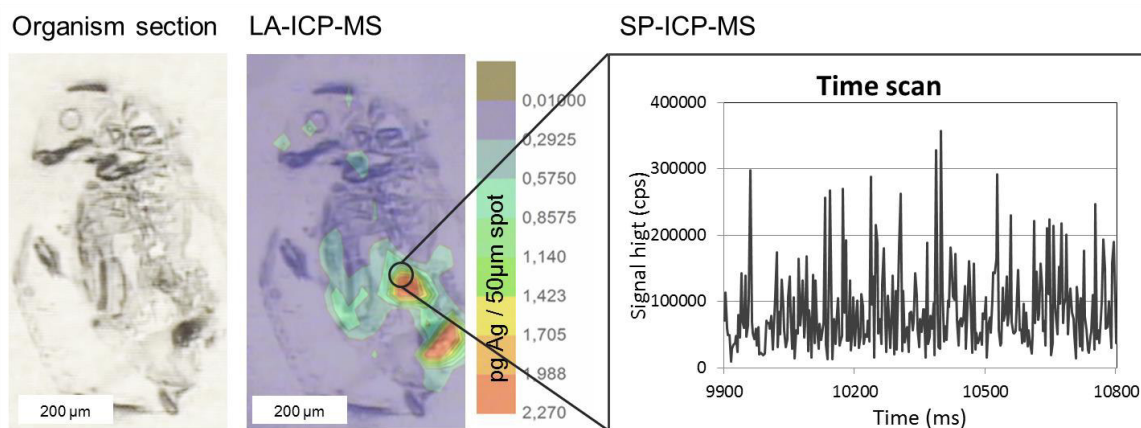


**Fig. 2:** LA-SP-ICP-MS measurement results on AgNP exposed *Daphnia magna* with elemental imaging by LA-ICP-MS and particle information by SP-ICP-MS detection.

In addition, a huge influence of the chosen spot diameter for the ablation was observed. For smaller spot diameters less material is ablated and the transport speed is drastically reduced. Therefore, future investigations will focus on the dependencies of the spot diameter, the ablated material and transportation speed on the final transport efficiency of the particle aerosol. For these reasons the presented method combination is first applied for qualitative measurements.

With regard to the collected SP-ICP-MS data, a mixture of AgNP signals and an increased background signal which can be attributed to an additional detection of dissolved silver ions was observed (**Fig. 3**). The NP characterization results obtained before the performance of the exposure experiments already showed that the AgNP suspension contains a large dissolved silver ion fraction (~48 %). The high silver ion background measured by SP-ICP-MS can be either referred to the initial fraction of dissolved ionic silver within the suspensions, to a NP modification within the organism such as a silver ion release from the NP surface, or to a fragmentary destruction of AgNPs during the ablation process. In order to investigate these circumstances, the instrument parameters (e.g., transport efficiency, laser energy) have to be optimized and additional investigations on the NP internalization, distribution and modifications possibly occurring once being in the organism have to be performed, e.g., by electron microscopy.

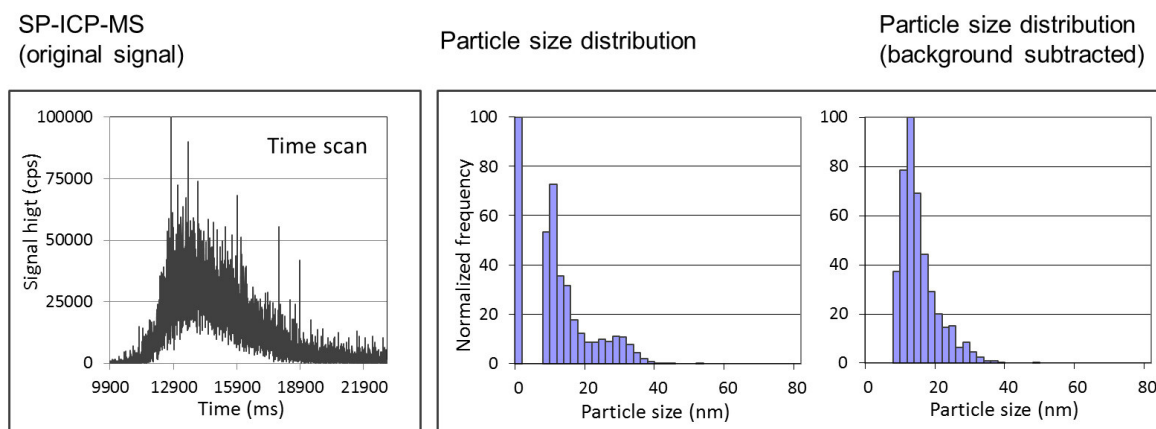


**Fig. 3:** SP-ICP-MS data evaluation procedure including statistical evaluation, background (ionic fraction) subtraction and calculation of the particle size distribution.

In the presented experiments small regions of interest were ablated by single spots in order to “dilute” the sample and to avoid a data overload. Theoretically, the method combination is designed to visualize the elemental distribution (LA-ICP-MS information) and to measure the single particle events (SP-ICP-MS information) in parallel.

The SP-ICP-MS data evaluation was improved with respect to the statistical equations and algorithms to obtain a reliable particle distribution histogram. Especially, the interpretation of the here presented results with a high ionic background is limited with the usual applied analysis software tool developed by RIKILT Wageningen UR. Furthermore, due to limitations in the ICP-MS software and the subsequent data evaluation of large data volumes, solely the measurement of specific areas is possible up to now. The measurement procedure and the specific information which can be obtained by this novel method combination are summarized in **Fig. 4**.

## CONCLUSION

This study presents first qualitative results on the combination of LA-ICP-MS with SP-ICP-MS. Therefore, *Daphnia magna* as established ecotoxicological test organisms were exposed to AgNPs, sectioned and analyzed by the application of the developed method protocol. Next to visualization information on the elemental distribution, the distinction of internalized NPs and the respective dissolved silver

ions is possible without a complex sample preparation. The improvement of instrumentation and data evaluation parameters would further move this combination towards a reliable, quantitative single particle visualization technique. With LA-SP-ICP-MS the upcoming requirements of analytical methods for advanced NP-analysis within biological and environmental samples can be covered resulting in an improved toxicological risk assessment of these materials.

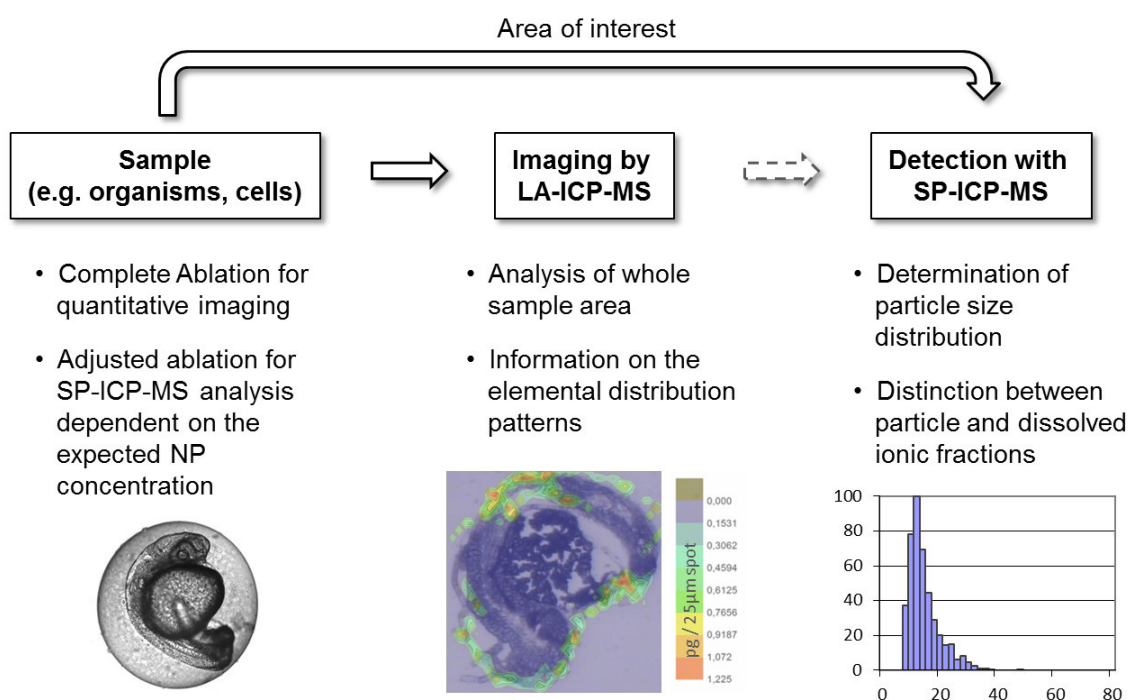


**Fig. 4:** Scheme on the applied procedure and parameters of the method combination of LA- and SP-ICP-MS.

## ACKNOWLEDGMENTS

The authors thank Matthias Schmidt of the Department Isotope Biogeochemistry (UFZ) for the help with the performance of SEM and TEM measurements. This research was funded by the EU-project NanoValid (Development of reference methods for hazard identification, risk assessment and LCA of engineered nanomaterials; grant no 263147) and was supported by “Europäischer Fonds für regionale Entwicklung (EFRE) und dem Freistaat Sachsen” within the ProVIS project.

## REFERENCES

- Böhme S., Stärk H.-J., Kühnel D. and Reemtsma T. (2015). Exploring LA-ICP-MS as a quantitative imaging technique to study nanoparticle uptake in *Daphnia magna* and zebrafish (*Danio rerio*) embryos. *Anal Bioanal Chem*, 407(18): 5477-5485
- Böhme S., Stärk H.-J., Meißner T., et al. (2014). Quantification of Al<sub>2</sub>O<sub>3</sub> nanoparticles in human cell lines applying inductively coupled plasma mass spectrometry (neb-ICP-MS, LA-ICP-MS) and flow cytometry-based methods. *J Nanopart Res*, 16(9): 2592
- European Commission (2011). Commission Recommendation of 18 October 2011 on the definition of nanomaterial. *Official J Eur Union*, 50: 38-40
- Degueldre C. and Favarger P.-Y. (2003). Colloid analysis by single particle inductively coupled plasma-mass spectroscopy: a feasibility study. *Colloid Surface A*, 217(1): 137-142
- Degueldre, C., Favarger P.-Y. and Wold S. (2006). Gold colloid analysis by inductively coupled plasma-mass spectrometry in a single particle mode. *Anal Chim Acta*, 555(2): 263-268
- Drescher D., Giesen C., Traub H., et al. (2012). Quantitative imaging of gold and silver nanoparticles in single eukaryotic cells by laser ablation ICP-MS. *Anal Chem*, 84(22): 9684-9688
- Hassellöv M., Readman J.W., Ranville J.F. and Tiede K. (2008). Nanoparticle analysis and characterization methodologies in environmental risk assessment of engineered nanoparticles. *Ecotoxicology*, 17(5): 344-361
- Lee S., Bi X., Reed R.B., et al. (2014). Nanoparticle size detection limits by single particle ICP-MS for 40 elements. *Environ Sci Technol*, 48(17): 10291-10300
- Lowry G.V., Gregory K.B., Apte S.C. and Lead J.R. (2012). Transformations of nanomaterials in the environment. *Environ Sci Technol*, 46(13): 6893-6899
- Marquis B.J., Love S.A., Braun K.L. and Haynes C.L. (2009). Analytical methods to assess nanoparticle toxicity. *Analyst*, 134(3): 425-439
- Mitrano D., Ranville J., Bednar A., et al. (2014). Tracking dissolution of silver nanoparticles at environmentally relevant concentrations in laboratory, natural, and processed waters using single particle ICP-MS (spICP-MS). *Environ Sci: Nano*, 1(3): 248-259
- OECD (2004). Test No. 202: *Daphnia sp.* Acute Immobilisation Test. [www.oecd.org](http://www.oecd.org).
- Pace H.E., Rogers N.J., Jarolimek C., et al. (2011). Determining transport efficiency for the purpose of counting and sizing nanoparticles via single particle inductively coupled plasma mass spectrometry. *Anal Chem*, 83(24): 9361-9369
- Peters R., Herrera-Rivera Z., Undas A., et al. (2015). Single particle ICP-MS combined with a data evaluation tool as a routine technique for the analysis of nanoparticles in complex matrices. *J Anal At Spectrom*, 30(6): 1274-1285
- Pozebon D., Scheffler G.L., Dressler V.L. and Nunes M.A. (2014). Review of the applications of laser ablation inductively coupled plasma mass spectrometry (LA-ICP-MS) to the analysis of biological samples. *J Anal At Spectrom*, 29(12): 2204-2228
- RIKILT, Wageningen UR (2014). Single Particle Calculation Tool. *Software tool*
- Russo R.E., Mao X., Liu H., et al. (2002). Laser ablation in analytical chemistry - a review. *Talanta*, 57(3): 425-451

Wang H.A.O., Grolimund D., Giesen C., et al. (2013). Fast Chemical Imaging at High Spatial Resolution by Laser Ablation Inductively Coupled Plasma Mass Spectrometry. *Anal Chem*, 85(21): 10107-10116



## **ACKNOWLEDGEMENT**

Mein größter Dank gilt Dr. Dana Kühnel, die es mir ermöglicht hat dieses Thema zu bearbeiten, mich im Department für Bioanalytische Ökotoxikologie einzubringen und mir dabei alle Freiheiten gelassen hat und immer offen für Diskussionen war.

Weiterhin möchte ich Prof. Dr. Thorsten Reemtsma (Professor an der Universität Leipzig) für die Betreuung von universitärer Seite her danken. Einige Besprechungen mit vielen analytischen Denkanstößen und Anmerkungen zu den Manuskripten haben die Kooperation mit dem analytischen Department sehr bereichernd gemacht.

Außerdem danke ich Dr. Hans-Joachim Stärk, der mich bei meiner Arbeit von Beginn an sehr gut betreut hat und immer offen für meine analytischen Ideen war und diese unterstützt hat.

Ebenso möchte ich hier Prof. Dr. Rolf Altenburger für die hilfreichen und motivierenden Diskussionen sowie für die Begutachtung meiner Arbeit danken.

Weiterhin vielen Dank die Studenten die ich betreuen durfte und die mich in meiner Arbeit sehr unterstützt haben: Marta, Sarah, Sylvia und Mona.

Allen Projektpartnern, insbesondere meinen Co-Autoren gilt besonderer Dank. Durch die Projekttreffen war immer ein reger Gedanken- und Ideenaustausch auch über die Doktorarbeit hinaus möglich, die mich auch persönlich geprägt hat. Großer Dank auch an Wibke, die mich ans UFZ gebracht hat.

Großer Dank gilt auch meinen täglichen Leidensgenossen, sowie übergreifenden Departmentkollegen: Wolle, Sarah, Josefine, Jule, Nils, Patrick, Eva und Stephan. Ich danke euch für eure Unterstützung, Motivation und ablenkenden Worte in der Mittagspause!

Zu guter Letzt danke ich meiner Familie, die immer ein offenes Ohr für meine Probleme hatten und mich auch in schwierigen Zeiten unterstützt haben und für mich da waren.

Vielen Dank euch allen für diese tolle und spannende Zeit!

## CURRICULUM VITAE

Name	Steffi Böhme
Date of Birth	30.12.1988
Place of Birth	Schkeuditz
2012-2015	PhD student Helmholtz Centre for Environmental Research, Leipzig Department Bioanalytical Ecotoxicology
2014	ECETOC Young Scientist Award
Since 2012	Postgraduate Study: "Toxikologie und Umweltschutz", University Leipzig
2012	Diploma Thesis: "Isolierung, Charakterisierung und Reaktivität von Hopfenbittersäuren in Bier"
2011-2012	Grant of the Barth Haas Group, Nürnberg
2009-2011	Student Assistant, Smart Membranes GmbH, Halle (Saale)
2007-2012	Study of Food Chemistry, Martin-Luther-University Halle-Wittenberg, Halle (Saale)
1999-2007	Abitur, Gymnasium Delitzsch

## SCIENTIFIC CONTRIBUTIONS

### Peer-reviewed publications

“An interlaboratory comparison of nanosilver characterisation and hazard identification: harmonising techniques for high quality data” *Environ Int*, 2015, accepted.

Jemec A., Kahru A., Potthoff A., Drobne D., Heinlaan M., Böhme S., Geppert M., Novak S., Schirmer K., R R., Singh S., Aruoja V., Sihtmäe M., Juganson K., Käkinen A., Kühnel D.

“Effect propagation after silver nanoparticle exposure in zebrafish (*Danio rerio*) embryos: a correlation to internal concentration and distribution patterns” *Environ Sci: Nano*, 2015, published online, DOI: 10.1039/c5en00118h.

Böhme S., Stärk H.-J., Reemtsma T., Kühnel D.

“Exploring LA-ICP-MS as a quantitative imaging technique to study nanoparticle uptake in *Daphnia magna* and zebrafish (*Danio rerio*) embryos.” *Anal Bioanal Chem*, 2015, 407(18): 5477-5485.

Böhme S., Stärk H.-J., Kühnel D., Reemtsma T.

„Quantification of Al<sub>2</sub>O<sub>3</sub> nanoparticles in human cell lines applying inductively coupled plasma mass spectrometry (neb-ICP-MS, LA-ICP-MS) and flow cytometry-based methods” *J Nanopart Res*, 2014, 16(9): 2592

Böhme S., Stärk H.-J., Meißner T., Springer A., Reemtsma T., Kühnel D., Busch W.

“Oxidation of Isohumulones Induces the Formation of Carboxylic Acids by Hydrolytic Cleavage” *J Agric Food Chem*, 2014, 62 (30), 7541–7549

Rakete S., Berger R., Böhme S., Glomb M. A.

### Platform presentations

SETAC Europe 25<sup>th</sup> Annual Meeting 05/2015 (Barcelona/Spain)

“The zebrafish embryo chorion as a biological barrier for nanoparticle uptake?!”

Invitation Guest Presentation EAWAG 03/2015 (Zurich/Switzerland)

„Quantification and visualization of nanoparticle uptake in environmental organisms by means of ICP-MS“

CANAS 03/2015 (Leipzig/Germany)

“New developments in the field of the visualization of nanoparticle uptake by environmental organisms with LA-ICP-MS”

Higrade Fall Conference 10/2014 (Leipzig/Germany)

„Nanoparticles: the big small enemies?! - An analytical detection story“

NanoSafetyCluster Forum for Young Scientists 10/2014 (Siracusa/Italy)

“Quantification and visualization of nanoparticle uptake in different environmental organisms by ICP-MS”

24. ICP-MS Anwendertreffen 09/2014 (Geesthacht/Germany)

“Visualisierung der Aufnahme von Nanopartikeln mittels LA-ICP-MS”

SETAC Europe 24th Annual Meeting 05/2014 (Basel/Switzerland)

„Visualisation of silver nanoparticle uptake by Laser Ablation – Inductively Coupled Plasma Mass Spectrometry“

CANAS 03/2013 (Freiberg/Germany)

„Quantification of nanoparticle uptake in complex biological matrices using ICP-MS“

## **Poster presentations**

13th Research Festival 12/2014 (Leipzig/Germany)

“The visualization of nanoparticle uptake by Laser Ablation – Inductively Coupled Plasma Mass Spectrometry (LA-ICP-MS)“

7th Nanotox 04/2014 (Antalya/Turkey)

„The zebrafish embryo chorion as a biological barrier for nanoparticle uptake?!“

8th ICEEN 07/2013 (Aix-en-Provence/France)

„Quantification of the silver nanoparticle and silver ion uptake by zebrafish embryos using ICP/MS“

nanoSAFE 11/2012 (Grenoble/France)

„Internalisation of aluminium oxide nanoparticles into human cells: impact of particle size on the quantitative uptake“

SETAC GLB + GDCh meeting 09/2012 (Leipzig/Germany)

„Influence of grain size effects on the analysis of nanoparticle treated human cells by ICP-MS“



## **EIDESSTATTLICHE ERKLÄRUNG**

Hiermit erkläre ich, Steffi Böhme, an Eides statt, dass ich die vorgelegte Arbeit „Development and application of quantification and visualization techniques to investigate the uptake of nanoparticles by cells and ecotoxicological test organisms“ selbstständig angefertigt habe.

Ich versichere, dass die vorliegende Arbeit ohne unzulässige Hilfe und ohne Benutzung anderer als der angegebenen Hilfsmittel angefertigt wurde und dass die aus fremden Quellen direkt oder indirekt übernommenen Gedanken in der Arbeit als solche kenntlich gemacht worden sind.

Die Personen, von denen ich bei der Erstellung, Auswahl und Auswertung des Materials sowie bei der Herstellung der Manuskripte Unterstützungsleistungen erhalten habe, wurden unter „author contributions“ genannt. Dabei versichere ich, dass außer den genannten keine weiteren Personen bei der geistigen Herstellung der vorliegenden Arbeit beteiligt waren, insbesondere auch nicht die Hilfe eines Promotionsberaters in Anspruch genommen wurde, und dass Dritte weder unmittelbar noch mittelbar geldwerte Leistungen für Arbeiten erhalten haben, die im Zusammenhang mit dem Inhalt der vorgelegten Dissertation stehen.

Die Arbeit wurde an keiner weiteren nationalen oder internationalen Einrichtung zum Zwecke einer Promotion oder eines anderen Prüfungsverfahrens vorgelegt.

Steffi Böhme

Leipzig, 08. Juli 2015

